

COMPARISON OF A THEORETICAL ANALYSIS WITH AN  
EXPERIMENTAL STRESS ANALYSIS OF AN FRP  
THIN-WALL COMPOSITE BOX BEAM

by

CLARK TIMOTHY HARBAUGH

B.S., Kansas State University, 1972

---

A THESIS

submitted in partial fulfillment of the

requirements for the degree

MASTER OF SCIENCE

Department of Mechanical Engineering

KANSAS STATE UNIVERSITY  
Manhattan, Kansas

1989

Approved by:

  
Major Professor

## PREFACE

An oft used purpose of experimental methods and experimental analyses is to verify whether the theory based calculations, along with any assumptions made, can be substantiated experimentally. It was with this intention that this project was undertaken. Although the methods of analyzing stress and strain in isotropic materials are well documented, the analysis of nonisotropic materials is not so well established.

This work examines the theoretically predicted stress in a thin-wall box beam which was fabricated from a nonisotropic composite material. The elastic constants of this composite material were unknown, and so had to be determined using experimental methods. From these and other intermediate steps, the stress and corresponding strain were predicted in the box beam due to a known loading condition. These were then compared to the results found by experimental methods.

One difficulty which was encountered involved finding the modulus of elasticity of the composite material in compression. The experimentally determined value was deemed invalid and so another method had to be used to find its value.

As with most projects, many others contributed to the successful completion of this work. Appreciation is hereby expressed to Dr. Hugh S. Walker for his help and guidance in completing this project. In addition, I am grateful to Dr. K. K. Hu and Dr. Chi L. Huang for their encouragement and stimulation in preparatory coursework. In addition, the assistance of Gary Thornton and Brian Bramel was invaluable in cutting and machining the test specimens and in making test fixtures. Gratitude is also due to the Mechanical Engineering Department for furnishing the material and test equipment for use in this project, and to the Civil Engineering Department for the use of their Riehle test machine. Finally, I am indebted to my wife Olinda and our two children for their enduring patience while I labored on this project.

TABLE OF CONTENTS

	Page
PREFACE . . . . .	ii
LIST OF TABLES . . . . .	v
LIST OF FIGURES . . . . .	vii
Chapter	
I. INTRODUCTION . . . . .	1
II. METHODS AND PROCEDURES . . . . .	4
Description of FRP Composite . . . . .	4
Experimental Determination of FRP Composite Properties . . . . .	10
Transformation of Properties . . . . .	59
Experimental Determination of Beam Deflections . . . . .	62
Theoretical Determination of Compressive Modulus of Elasticity . . . . .	67
Theoretical Beam Stresses and Strains . . . . .	69
Experimental Beam Strain . . . . .	70
Shear Lag Effect on Beam Strain Measurements . . . . .	79
III. RESULTS AND CONCLUSIONS . . . . .	86
Results . . . . .	86
Conclusions . . . . .	87
IV. SELECTED BIBLIOGRAPHY . . . . .	89
V. APPENDIX . . . . .	90

## LIST OF TABLES

Table	Page
1. Theoretical Beam Stresses . . . . .	69
2. Theoretical Beam Strains . . . . .	70
3. Strain Gage Multiplying Factors . . . . .	72
4. Strains for Position "A" . . . . .	79
5. Strains for Position "B" . . . . .	79
6. Comparison of Strain Values . . . . .	86
7. X Axis Tension Test, Specimen No. 1 . . . . .	90
8. X Axis Tension Test, Specimen No. 2 . . . . .	90
9. X Axis Tension Test, Specimen No. 3 . . . . .	91
10. Y Axis Tension Test, Specimen No. 4 . . . . .	91
11. Y Axis Tension Test, Specimen No. 5 . . . . .	92
12. Y Axis Tension Test, Specimen No. 6 . . . . .	92
13. X Axis Flexure Test, Specimen No. 7 . . . . .	93
14. X Axis Flexure Test, Specimen No. 8 . . . . .	93
15. X Axis Flexure Test, Specimen No. 9 . . . . .	93
16. X Axis Flexure Test, Specimen No. 10 . . . . .	94
17. X Axis Flexure Test, Specimen No. 11 . . . . .	94
18. Y Axis Flexure Test, Specimen No. 12 . . . . .	94
19. Y Axis Flexure Test, Specimen No. 13 . . . . .	95
20. Y Axis Flexure Test, Specimen No. 14 . . . . .	95

LIST OF TABLES, continued

Table	Page
21. X Axis Compression Test, Specimen No. 15 .	95
22. X Axis Compression Test, Specimen No. 16 .	96
23. X Axis Compression Test, Specimen No. 17 .	96
24. X Axis Compression Test, Specimen No. 18 .	96
25. X Axis Compression Test, Specimen No. 19 .	97
26. Y Axis Compression Test, Specimen No. 20 .	97
27. Y Axis Compression Test, Specimen No. 21 .	98
28. Y Axis Compression Test, Specimen No. 22 .	98
29. Y Axis Compression Test, Specimen No. 23 .	99
30. Y Axis Compression Test, Specimen No. 24 .	99
31. On-Axis Shear Test . . . . .	100
32. Off-Axis Shear Test . . . . .	100
33. Box Beam Load vs. Deflection . . . . .	101
34. Box Beam Strains, Position "A" . . . . .	101
35. Box Beam Strains, Position "B" . . . . .	101
36. Test Specimen Dimensions . . . . .	102

## LIST OF FIGURES

Figure	Page
1. Detail of Plain Weave . . . . .	5
2. Original Fiberglass Reinforcing Cloth . . .	5
3. Box Beam Fabrication Details . . . . .	8
4. X Axis Tensile Test Specimen Dimensions . .	11
5. Tensile Test Specimen No. 1, Load vs. Longitudinal Strain . . . . .	13
6. Tensile Test Specimen No. 1, Load vs. Transverse Strain . . . . .	14
7. Tensile Test Specimen No. 2, Load vs. Longitudinal Strain . . . . .	15
8. Tensile Test Specimen No. 2, Load vs. Transverse Strain . . . . .	16
9. Tensile Test Specimen No. 3, Load vs. Longitudinal Strain . . . . .	17
10. Tensile Test Specimen No. 3, Load vs. Transverse Strain . . . . .	18
11. Y Axis Tensile Test Specimen Dimensions . .	21
12. Tensile Test Specimen No. 4, Load vs. Longitudinal Strain . . . . .	22
13. Tensile Test Specimen No. 4, Load vs. Transverse Strain . . . . .	23
14. Tensile Test Specimen No. 5, Load vs. Longitudinal Strain . . . . .	24
15. Tensile Test Specimen No. 5, Load vs. Transverse Strain . . . . .	25
16. Tensile Test Specimen No. 6, Load vs. Longitudinal Strain . . . . .	26

LIST OF FIGURES, continued

Figure	Page
17. Tensile Test Specimen No. 6, Load vs. Transverse Strain . . . . .	27
18. Flexure Test Specimen Dimensions . . . . .	28
19. Flexure Test Fixture Details . . . . .	29
20. Flexure Test Specimen No. 7, Load vs. Deflection . . . . .	30
21. Flexure Test Specimen No. 8, Load vs. Deflection . . . . .	31
22. Flexure Test Specimen No. 9, Load vs. Deflection . . . . .	32
23. Flexure Test Specimen No. 10, Load vs. Deflection . . . . .	33
24. Flexure Test Specimen No. 11, Load vs. Deflection . . . . .	34
25. Flexure Test Specimen No. 12, Load vs. Deflection . . . . .	36
26. Flexure Test Specimen No. 13, Load vs. Deflection . . . . .	37
27. Flexure Test Specimen No. 14, Load vs. Deflection . . . . .	38
28. Compression Test Specimen Dimensions . . . . .	39
29. Compression Test Specimen No. 15, Load vs. Strain . . . . .	41
30. Compression Test Specimen No. 16, Load vs. Strain . . . . .	42
31. Compression Test Specimen No. 17, Load vs. Strain . . . . .	43
32. Compression Test Specimen No. 18, Load vs. Strain . . . . .	44

LIST OF FIGURES, continued

Figure	Page
33. Compression Test Specimen No. 19, Load vs. Strain . . . . .	45
34. Compression Test Specimen No. 20, Load vs. Strain . . . . .	46
35. Compression Test Specimen No. 21, Load vs. Strain . . . . .	47
36. Compression Test Specimen No. 22, Load vs. Strain . . . . .	48
37. Compression Test Specimen No. 23, Load vs. Strain . . . . .	49
38. Compression Test Specimen No. 24, Load vs. Strain . . . . .	50
39. Shear Test Specimen Dimensions . . . . .	52
40. Shear Test Fixture . . . . .	53
41. On-axis Shear Test, Load vs. Strain, Gages #1, #3 . . . . .	55
42. On-axis Shear Test, Load vs. Strain, Axial Gage . . . . .	56
43. Off-axis Shear Test, Load vs. Strain, Gage #1 . . . . .	57
44. Off-axis Shear Test, Load vs. Strain, Gage #3 . . . . .	58
45. Fiberglass Reinforcement and Axes Orientations . . . . .	61
46. Box Beam Bending Positions . . . . .	63
47. Box Beam Load vs. Deflection, Position "A" . . . . .	65
48. Box Beam Load vs. Deflection, Position "B" . . . . .	66
49. Box Beam Strain Gage Locations . . . . .	71

LIST OF FIGURES, continued

Figure	Page
50. Box Beam, Position "A" Load vs. Strain, Gages #1, #3 . . . . .	73
51. Box Beam, Position "A" Load vs. Strain, Gage #4 . . . . .	74
52. Box Beam, Position "A" Load vs. Strain, Gages #5, #6, #8 . . . . .	75
53. Box Beam, Position "B" Load vs. Strain, Gage #1, #3 . . . . .	76
54. Box Beam, Position "B" Load vs. Strain, Gage #4 . . . . .	77
55. Box Beam, Position "B" Load vs. Strain, Gage #5, #6, #8 . . . . .	78
56. Box Beam Strain vs. Gage Location, Position "A" . . . . .	80
57. Box Beam Strain vs. Gage Location, Position "B" . . . . .	81
58. Shear Lag . . . . .	82
59. Side 1 Brittle Coating . . . . .	83
60. Side 2 Brittle Coating . . . . .	84

## Chapter I

### INTRODUCTION

A composite material is one which, by most definitions, consists of two (or possibly more) distinct phases or materials on a macroscopic scale. Although other types and varieties exist, the most commonly used composites consist of a high modulus constituent for strength enhancement and a low modulus binding material known as the matrix. The high modulus material may be in the form of long directionally oriented fibers, short randomly oriented fibers, whiskers, flakes, particles, spheres, foams, etc. For those composites which use long fibers for reinforcement, multiple layers of the fibrous material are generally required to obtain the necessary laminate thickness.

The matrix is usually some type of resin, although many of the conventional engineering materials can also be used. Its primary functions are to provide binding strength, support the high modulus material, act as a filler, transfer the stresses, protect the high modulus material from abrasion and environmental agents, and provide fracture toughness.

Although much of the attention and development work today centers on those composite materials known as "advanced composites" or "high performance composites" because of the very high specific strengths available from these generally unidirectional (UD) fibrous composites, over 80% of the composite materials produced today still utilize fiberglass as the reinforcing material. FRP (fiberglass reinforced plastic) offers many advantages over steel and most of the other metals. These include a specific gravity roughly 1/5 that of steel, a strong resistance to chemical attack and corrosion, low electrical and thermal conductivity rates, and an ability to obtain physical properties which are directionally sensitive. Moreover, fiberglass is relatively inexpensive and readily available in many forms. One noteworthy characteristic of FRP is that it, like most composites, is nonisotropic. This property can mean significant weight savings in many applications, since fiber-reinforced composites can be utilized which have their maximum strength oriented in the same direction as the principal stress. However, this characteristic of being nonisotropic necessitates a more thorough understanding of the stress-strain relations and how the

composite's properties vary depending upon the type and orientation of the reinforcement. Thus composite materials can offer significant advantages in many applications, particularly the aerospace industry, but also require a careful analysis of their unique physical characteristics.

Because box beams are important structural elements and FRP is used in many industries, combining these two into the object of this research was done to provide some insight into the problems associated with using FRP for structural applications. This objective was accomplished by investigating and comparing the results of and problems associated with finding the elastic constants of a particular FRP composite, fabricating a thin-wall box beam using this FRP composite (with the primary axes of the fiberglass reinforcement rotated relative to the beam longitudinal axis), and then comparing experimentally measured strains with the theoretically calculated strains on the upper and lower surfaces of the box beam subjected to a simple load.

## Chapter II

### METHODS AND PROCEDURES

#### DESCRIPTION OF FRP COMPOSITE

The fiberglass reinforcement used in this study consisted of a plain weave fiberglass material which originally contained 16 yarns per inch in the X (warp) direction and 14 yarns per inch in the Y (fill) direction (see Figures 1 and 2). The material was modified by removing every third yarn in the Y direction, leaving  $9 \frac{1}{3}$  yarns per inch in this direction. The purpose of this modification was to increase the differential strength between the two principal directions.

Each individual yarn consisted of approximately 200 individual, twisted together, glass filaments (or fibers), each one being approximately 0.0005 inches in diameter. The overall outside diameter of the entire yarn was approximately 0.020 inches.

The matrix was a thermoset type polyester resin which is manufactured for the automotive company Balkamp, Inc. It utilizes a MEK (methyl ethyl ketone) peroxide catalyst to initiate the curing process.

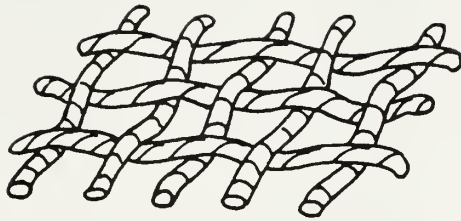


Figure 1 Detail of Plain Weave

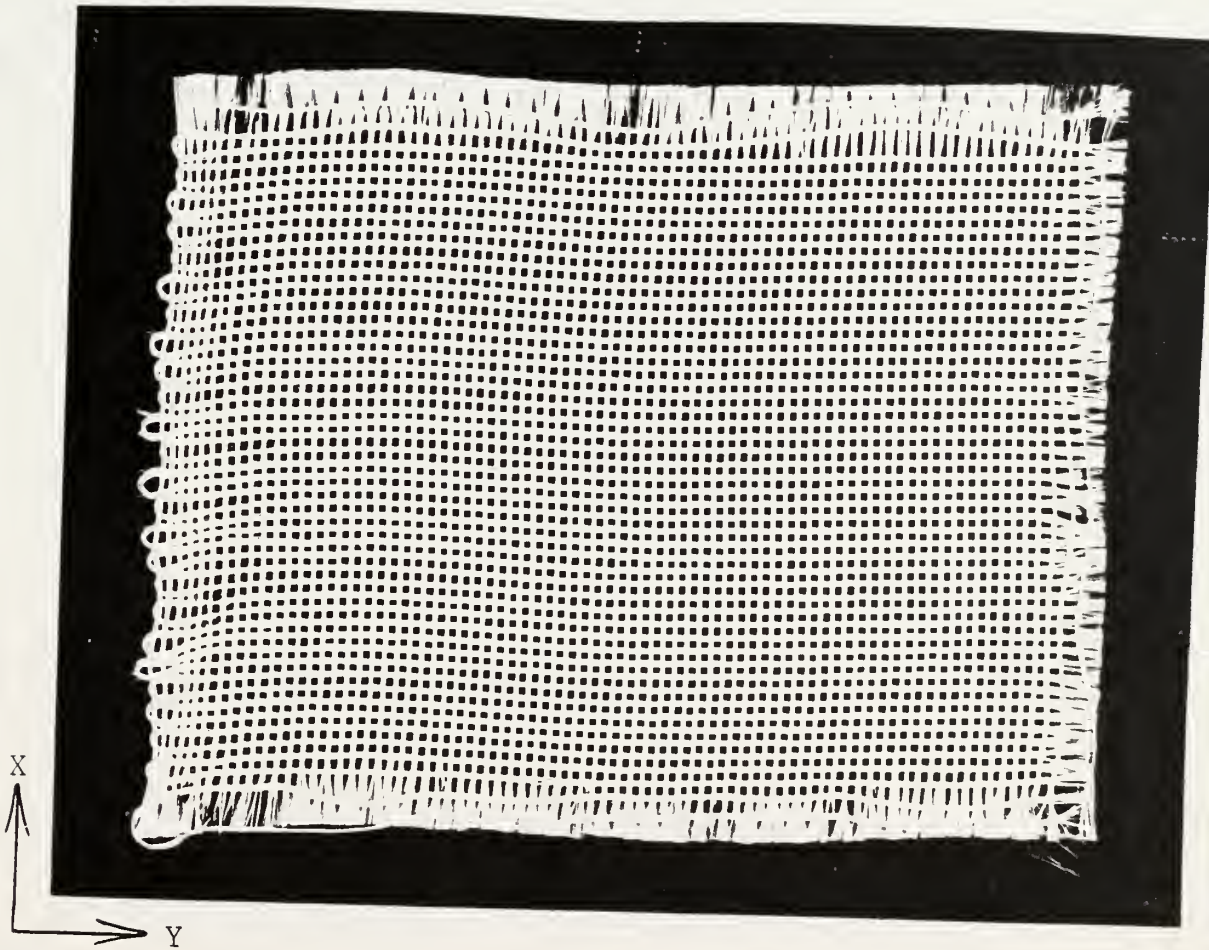


Figure 2 Original Fiberglass Reinforcing Cloth

The hand layup process consisted of manually working the catalyzed resin into the fiberglass material, one piece at a time. After each piece of fiberglass cloth was completely impregnated with resin, it was laid into the desired position. After all of the required number of pieces were properly stacked or wrapped over each other, the entire fabrication was covered with a nylon peel ply, a perforated nylon release film, an absorbent bleeder material, and an outer nylon bagging film used to provide an airtight enclosure so that a vacuum could be applied to the entire fabrication. The vacuum bagging process is intended to compress the resin-impregnated fiberglass cloth layers together, eliminating voids and air spaces; draw out the excess resin; and provide a relatively smooth surface finish.

The flat FRP composite plate from which all of the test specimens were cut was made with each layer of the fiberglass material aligned the same, ie. each layers' X and Y axes were collinear. This was done so that the physical properties of the composite could be determined in each of the two principal inplane directions. Obtaining the properties in each of the principal axis directions is essential in evaluating composite material properties since a characteristic

of directionally oriented fibrous composites is that a uniaxial normal stress may produce a shear strain and a pure shear stress may produce a normal strain [1]. These correlations are called coefficients of mutual influence by Lekhnitski [2].

The thin-wall box beam was fabricated by wrapping two pre-cut pieces of resin-impregnated fiberglass cloth around a wood core. Each piece of fiberglass cloth was of a predetermined size necessary to make four complete layers around the core, with the first piece having its X axis offset from the beam's longitudinal axis by  $+10^{\circ}$ . The second piece was of the proper dimensions to make four layers over the first four, except that the X axis of these layers was offset from the longitudinal beam axis by  $-10^{\circ}$ . See Figure 3 for details.

This procedure produced a box beam wall which would be classified as a balanced, antisymmetric angle ply laminate. Being antisymmetric will produce a coupling effect between bending and extension, which causes warping. This effect will be minimal in this analysis however, since the box beam dimensions are large compared to the beam wall thickness and the amount of bending which occurred was small.

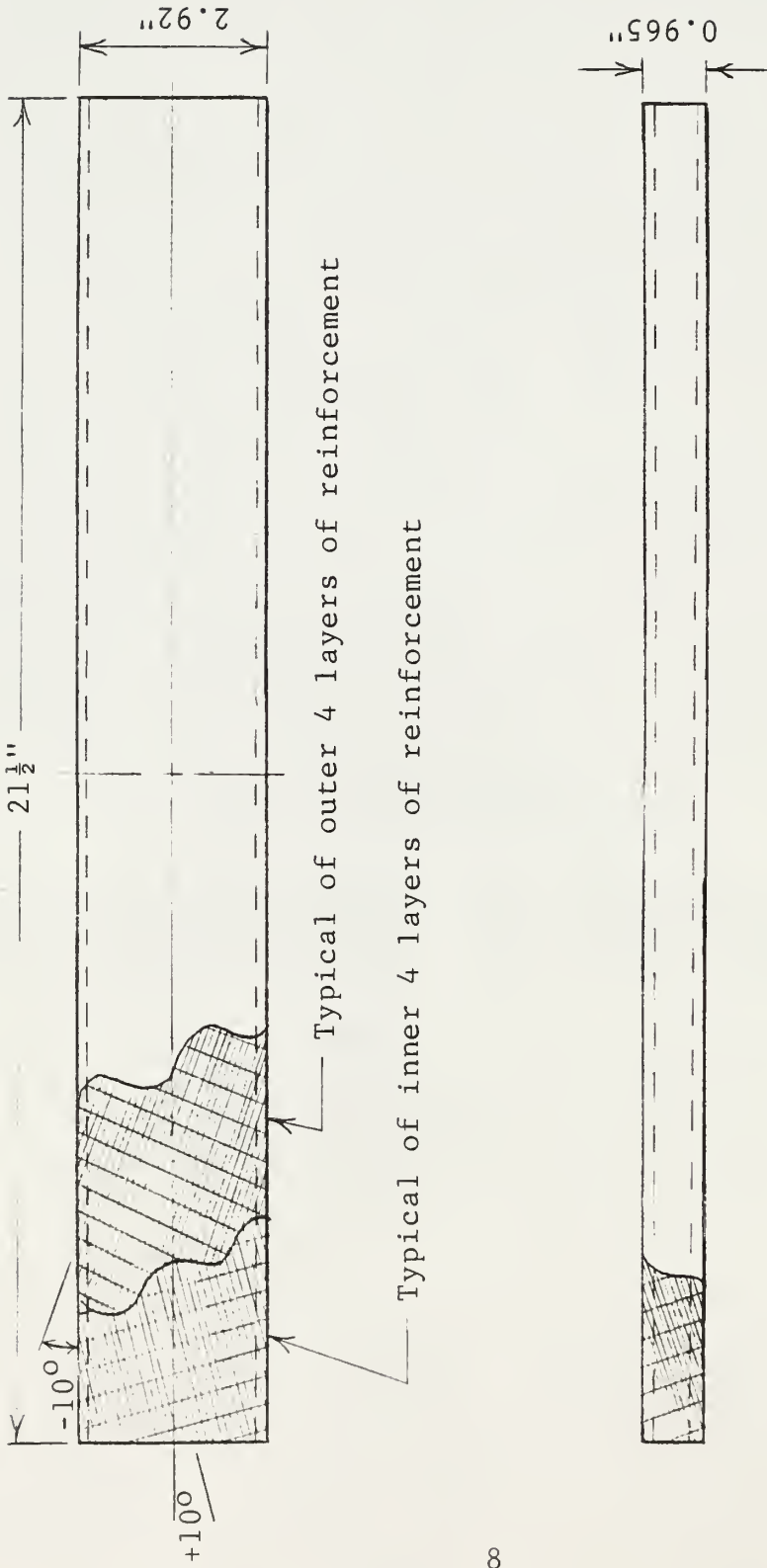


Figure 3 Box Beam Fabrication Details

One drawback of the manual layup procedure was the inability to ensure uniformity in the beam wall thickness. The side of the beam where the outer layer of bagging film was overlapped had a smaller amount of the resin squeezed out during the vacuum bagging and curing phase. This resulted in one side of the box beam having a thicker wall than the other side. Such occurrences are difficult to avoid, however, in a continuous wall structure fabricated manually.

After a vacuum was applied and the resin had cured overnight, all of the nylon covering and bleeder material was removed. The ends of the beam were cut off to the dimensions indicated in Figure 3, and the wood core, which was split and dowelled in the middle, was removed. The cut ends of the beam and all of the test specimen edges, except for the compression test specimens, were sealed with resin to eliminate the existence of free glass fibers which inevitably result from the cutting process. The teeth on the sawblade caused those fibers near the surface on the downside of the cut to become disengaged from the matrix as they were cut by the moving sawblade teeth.

The 16 layer flat plate previously described and the 8 layers of the box beam wall just described can be classified as orthogonal laminates, as long as

they are restricted to plane stress conditions. This property allows their elastic properties, as determined along the two inplane principal axes, to be transformed to yield the desired elastic properties at some angle to the principal axes. This transformation will be discussed later.

Another property of nonisotropic materials which is an important part of an experimental analysis is the fact that they have more than two independent elastic constants (for isotropic materials,  $E$ ,  $G$ , and  $\nu$  are related). For an orthotropic material subjected to plane stress, there are five independent elastic constants (any 3 of  $E_{xy}$ ,  $E_{yx}$ ,  $\nu_{xy}$ ,  $\nu_{yx}$ , and either  $G_{xy}$  or  $G_{yx}$ ).

#### EXPERIMENTAL DETERMINATION OF FRP COMPOSITE PROPERTIES

The first step necessary for both the theoretical approach and the experimental analysis was to determine the independent elastic constants of this particular FRP composite. Those which were determined experimentally included  $E_{xy}$ ,  $E_{yx}$ ,  $\nu_{xy}$ ,  $\nu_{yx}$ , and  $G_{xy}$ . The ASTM Standards were used as guides for all of the experimental analyses.

Determination of  $E_{xy}$  and  $\nu_{xy}$

Since a characteristic of most fiber-reinforced composites is that their modulus of elasticity in tension is greater than their modulus of elasticity in compression, a different set of experimental tests were performed to determine each value. The guide used for determining the modulus of elasticity in tension and poisson's ratio was ASTM Standard D3039 [3]. Figure 4 illustrates the approximate dimensions of the test specimens.

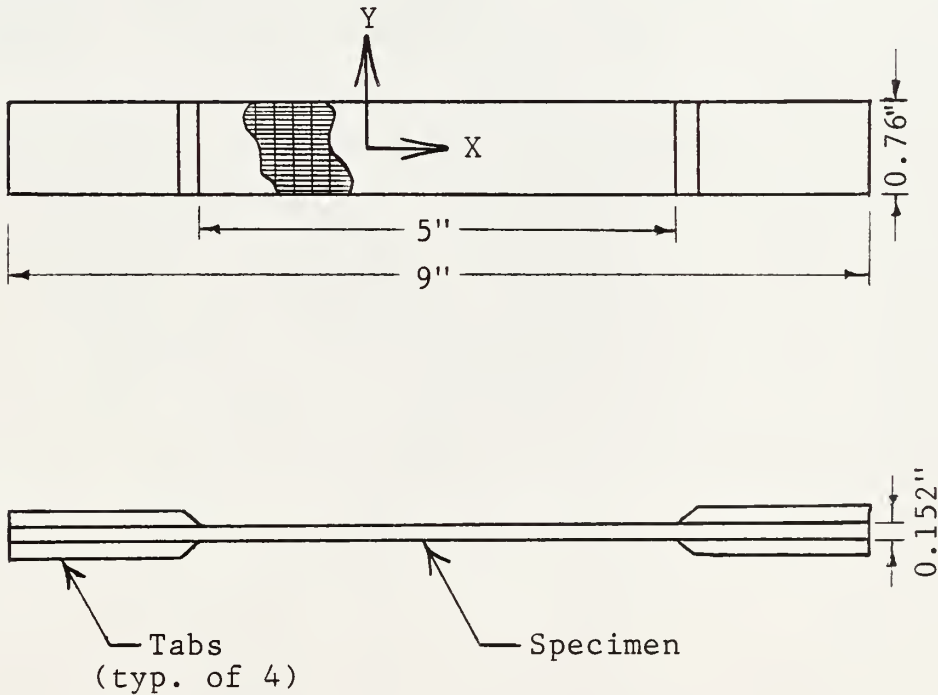


Figure 4 X Axis Tensile Test Specimen Dimensions

All tests on the test specimens and the box beam were performed utilizing a 20,000 lb. Riehle test machine. Where tabs were required on the tensile specimens, they were fabricated from the same fiber-glass material and resin as the test specimens and box beam, except that no yarns were removed from the fiber-glass cloth. They were cut from a larger piece and glued onto the test specimens using Measurements Group, Inc. M-Bond 200 adhesive. All strain gages used in this and successive applications were manufactured by Micro-Measurements Division, and were Type EA-06-120LZ-120 gages, with a gage length of 1/8". All strain readings were taken using a Measurements Group Strain Indicator, Model P-3500 (S/N 50798), and a Measurement Group Switch and Balance Unit, Model SB-1 (S/N 033433).

The graphs of the load versus strain are shown in Figures 5-10. For each specimen, the modulus of elasticity in tension was found by use of the formula

$$E_t = \frac{P/A}{\epsilon} \quad (1)$$

where  $E_t$  = modulus of elasticity in tension (psi)

$P$  = applied tensile load (lbs)

$A$  = test specimen cross-sectional area (in<sup>2</sup>)

$\epsilon$  = measured strain (in/in)

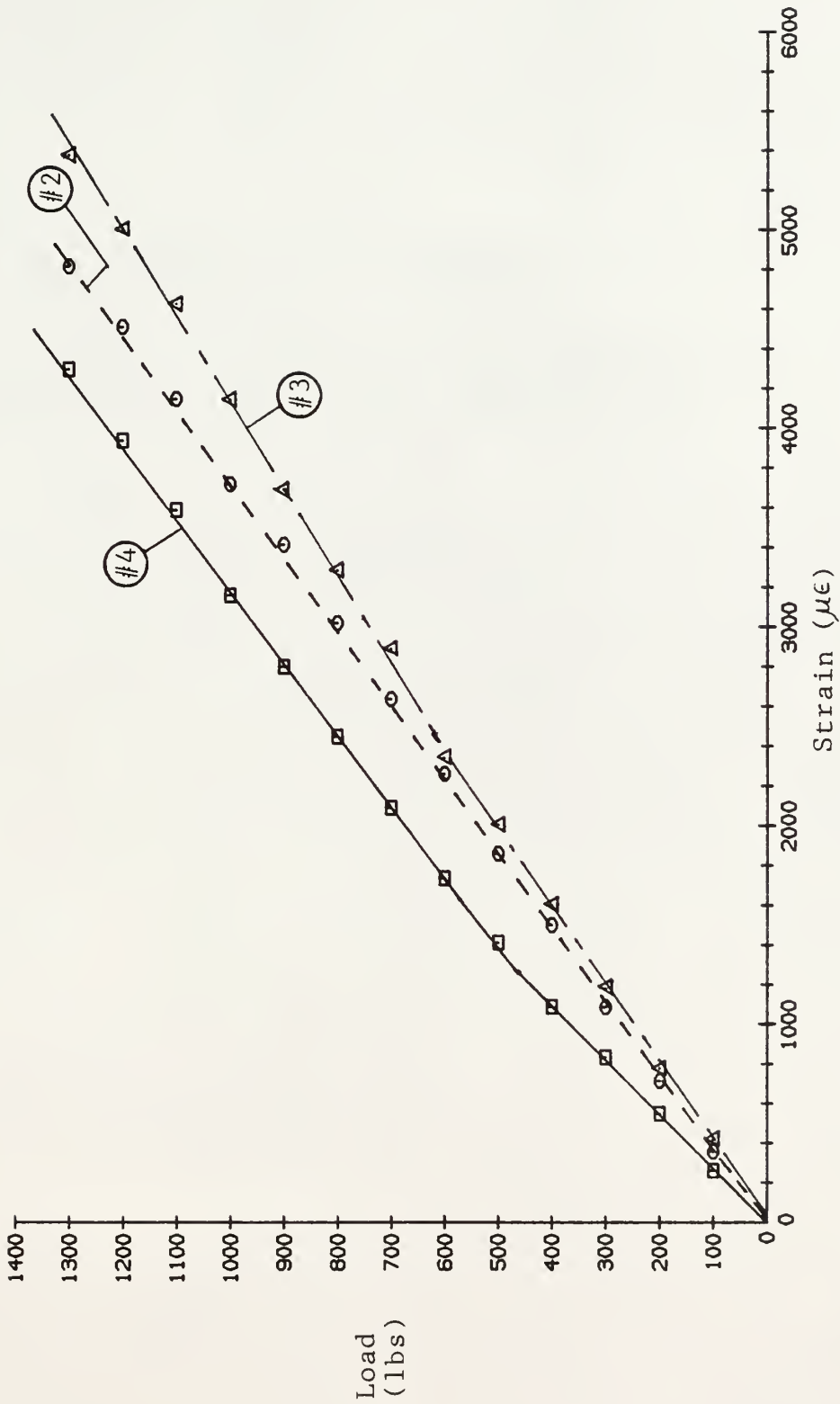


Figure 5 Tensile Test Specimen No. 1, Load vs. Longitudinal Strain

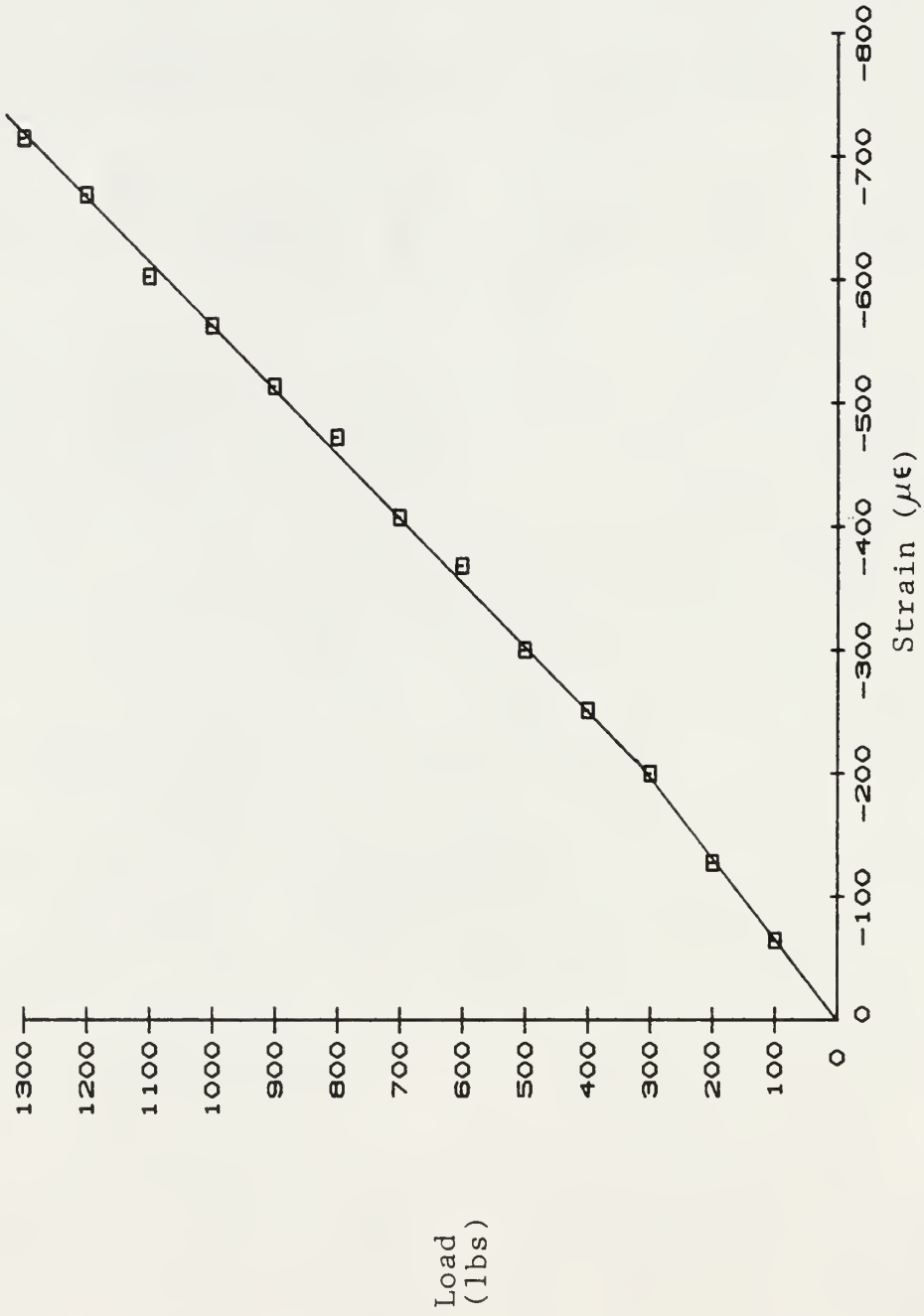


Figure 6 Tensile Test Specimen No. 1, Load vs. Transverse Strain

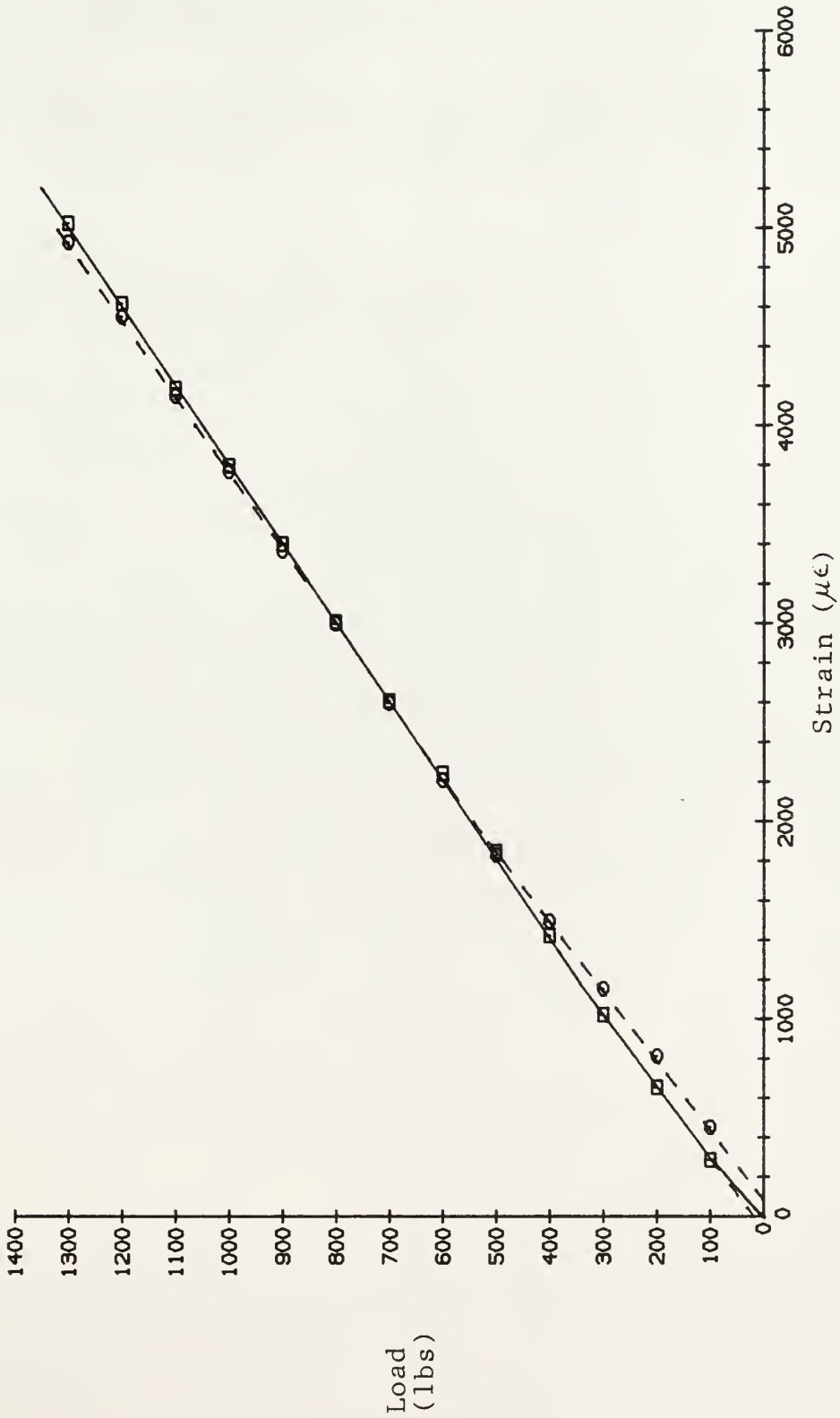


Figure 7 Tensile Test Specimen No. 2, Load vs. Longitudinal Strain

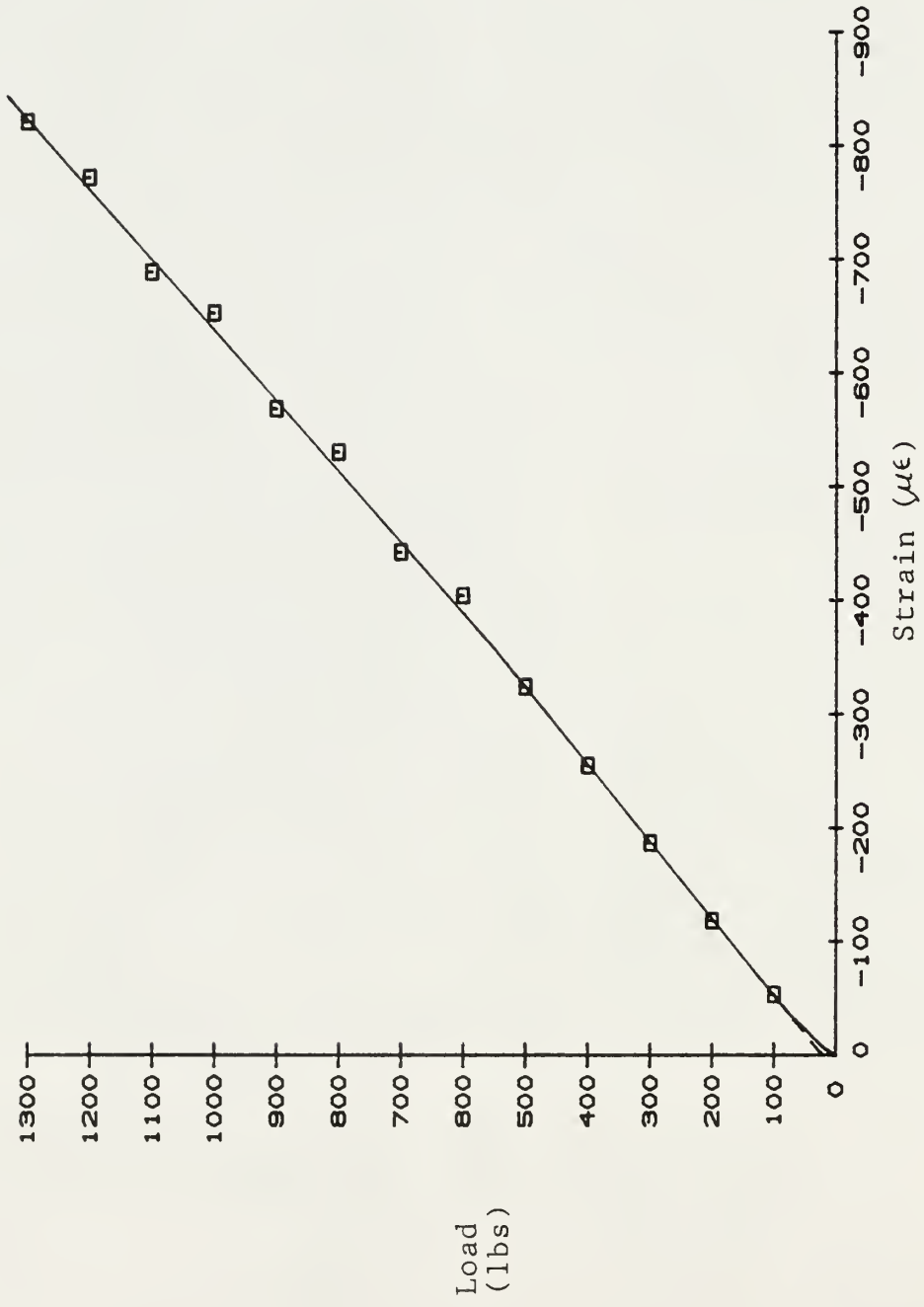


Figure 8 Tensile Test Specimen No. 2, Load vs. Transverse Strain

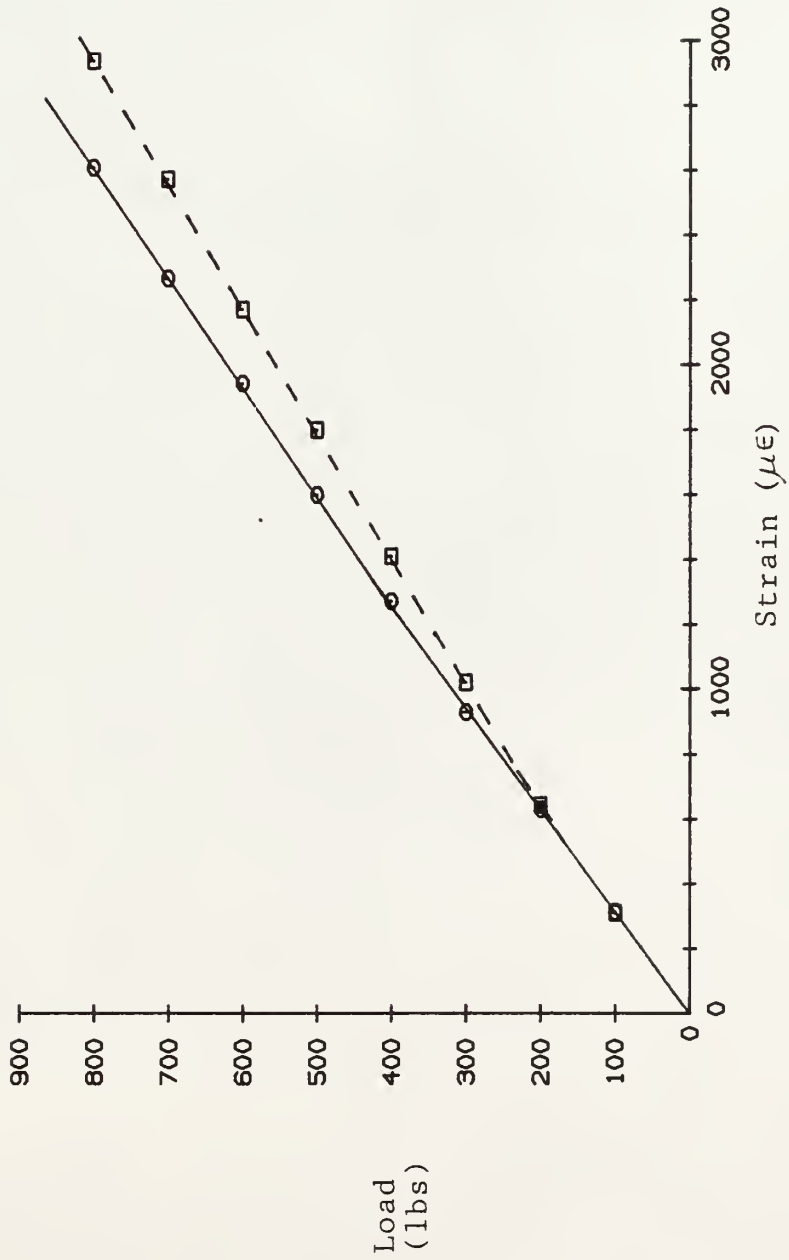


Figure 9 Tensile Test Specimen No. 3, Load vs. Longitudinal Strain

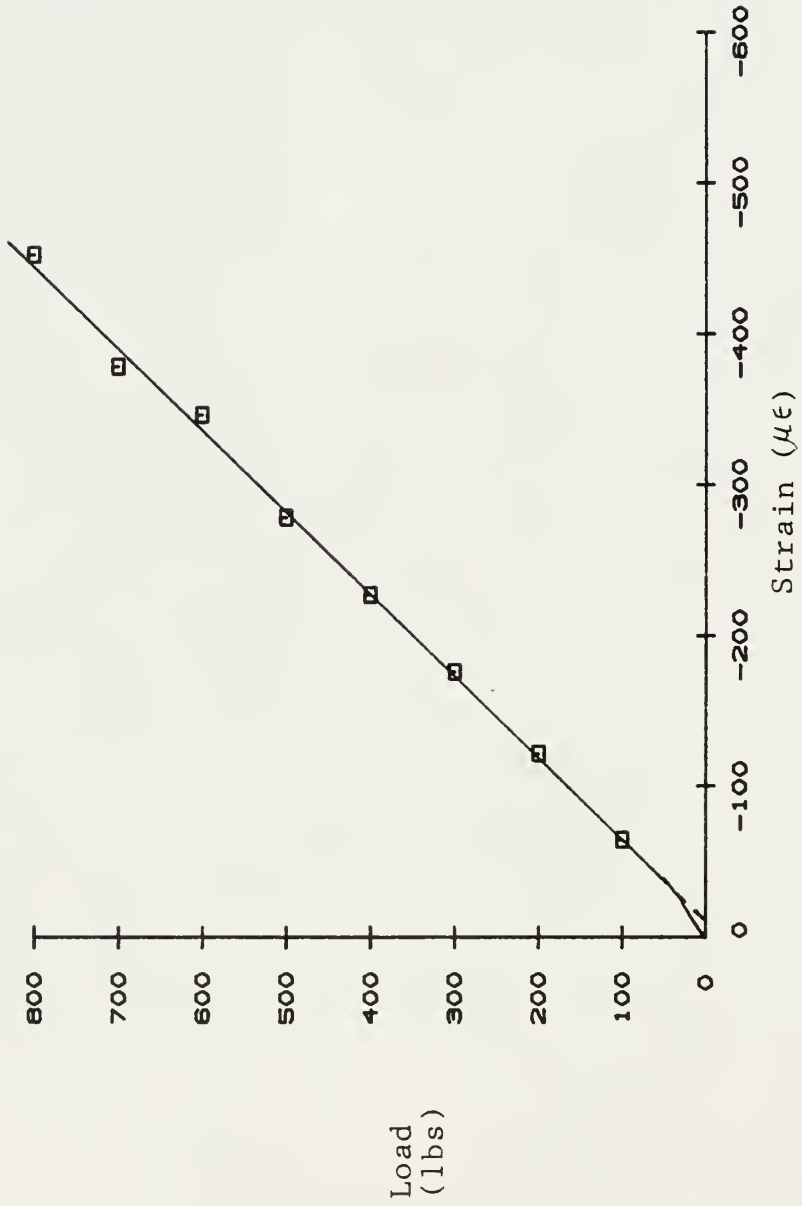


Figure 10 Tensile Test Specimen No. 3, Load vs. Transverse Strain

Specimen No. 1, on Figure 5, utilized three longitudinal strain gages rather than one or two, as did the other specimens. The purpose of the additional strain gage was to see if any bending of the specimen was occurring during the test due to misalignment of either the specimen or the test fixture. Since no bending problem was observed, one less longitudinal gage was used on subsequent tensile specimens.

It will also be noted from the referenced figure and later figures that some of the load/strain curves contain a knee joint where the line abruptly changes slope. In some cases the slope decreases, and in others the slope increases. The first case is most likely caused by the breaking of some of the individual glass fibers (filaments), leaving fewer to carry the load. The second case is probably caused by the takeup of slack by some of the load carrying yarns. With the lack of a feasible method to ensure that each layer of the reinforcing fiberglass cloth, in addition to the individual yarns, remains straight and free of any inplane curvature, it was very likely that some of the individual glass yarns incurred some curvature during layup. With such a loose weave material as that used for this project, a problem like this is difficult to completely avoid. The result was a load/strain curve

which had a sudden increase in slope after this initial slackness was taken up.

After determining a tensile modulus of elasticity for each specimen and then averaging these values, the result was  $E_{x,t} = 2.513 \times 10^6$  psi. From the strain gage mounted transverse to the specimen's longitudinal axis, the contraction in the Y direction was also measured as a function of the applied load. The poisson's ratio for each specimen was found by application of the formula

$$\nu_{xy} = - \frac{\epsilon_y}{\epsilon_x} \quad (2)$$

The resulting average value for all of the specimens was  $\nu_{xy} = 0.165$

#### Determination of $E_y$ and $\nu_{yx}$

These two properties were found in the same manner as  $E_x$  and  $\nu_{xy}$ , again using ASTM Standard D3039. The test specimen was different dimensionally, however. Figure 11 has approximate dimensions for these test specimens.

The graphs of the load versus strain for these test specimens are shown in Figures 12-17. The average value for the Y axis modulus of elasticity in tension was  $E_{y,t} = 1.586 \times 10^6$  psi. The average value for the transverse poisson's ratio was found to be  $\nu_{yx} = 0.134$ .

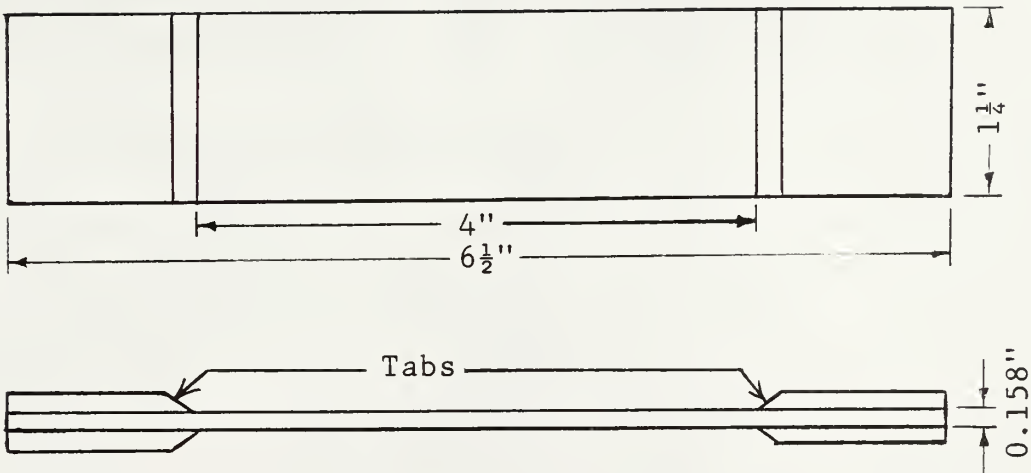


Figure 11 Y Axis Tensile Test Specimen Dimensions

There is another method which can be used for determining the modulus of elasticity of reinforced composites. Since this method generally produces slightly different values, it was also employed to see what difference in values would be observed and if these would be greater or less than those found by using the tension test. This second method utilizes a flexure test. ASTM Standard D790-86 [4] was used as a guide in performing this test. Figure 18 gives the test specimen dimensions.

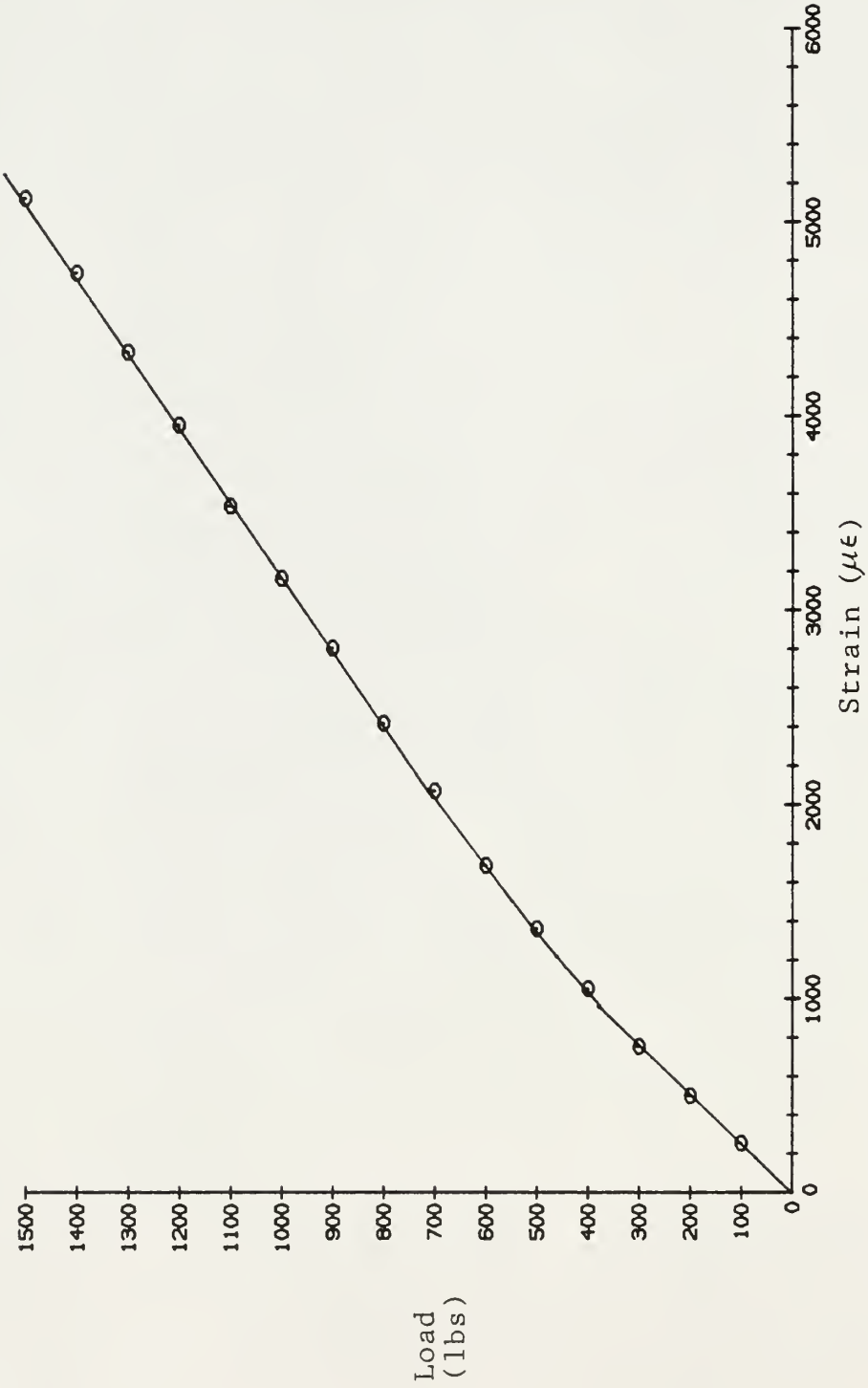


Figure 12 Tensile Test Specimen No. 4, Load vs. Longitudinal Strain

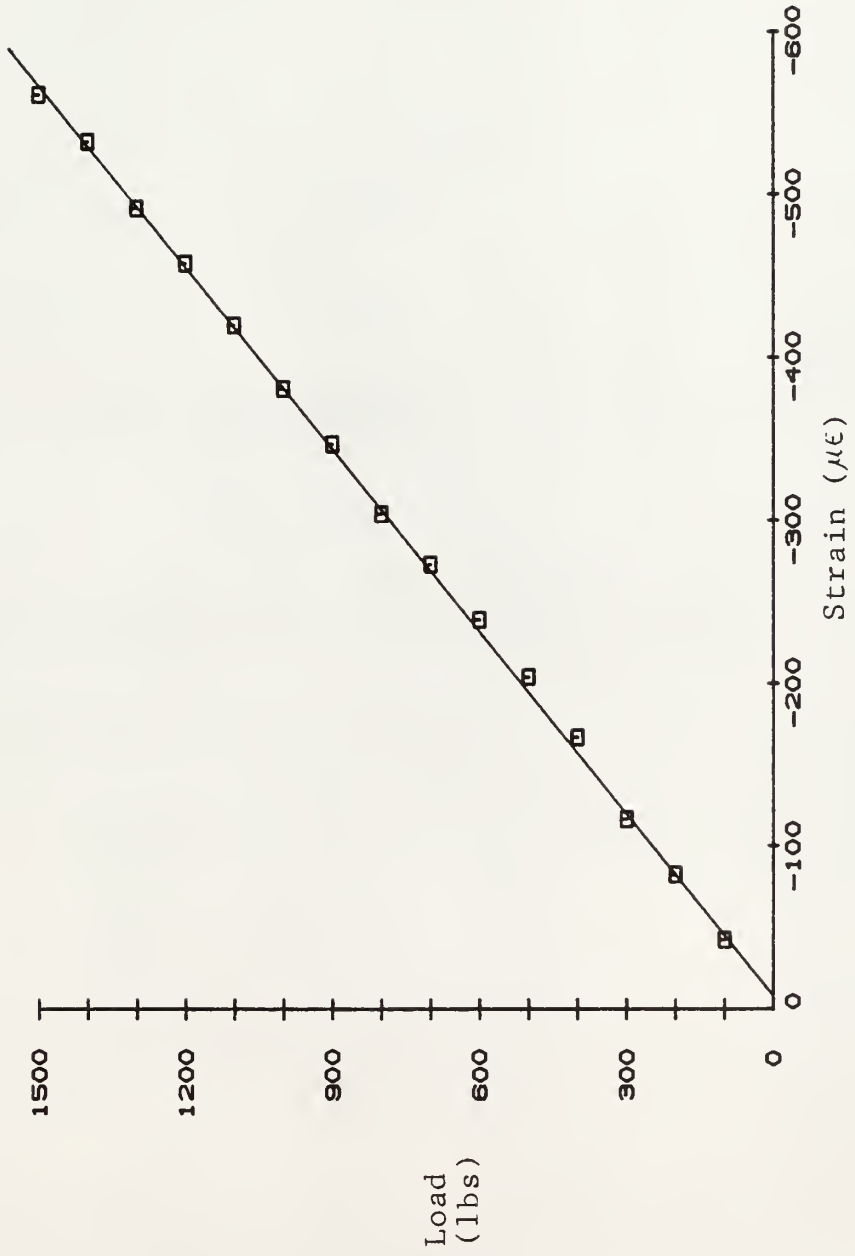


Figure 13 Tensile Test Specimen No. 4, Load vs. Transverse Strain

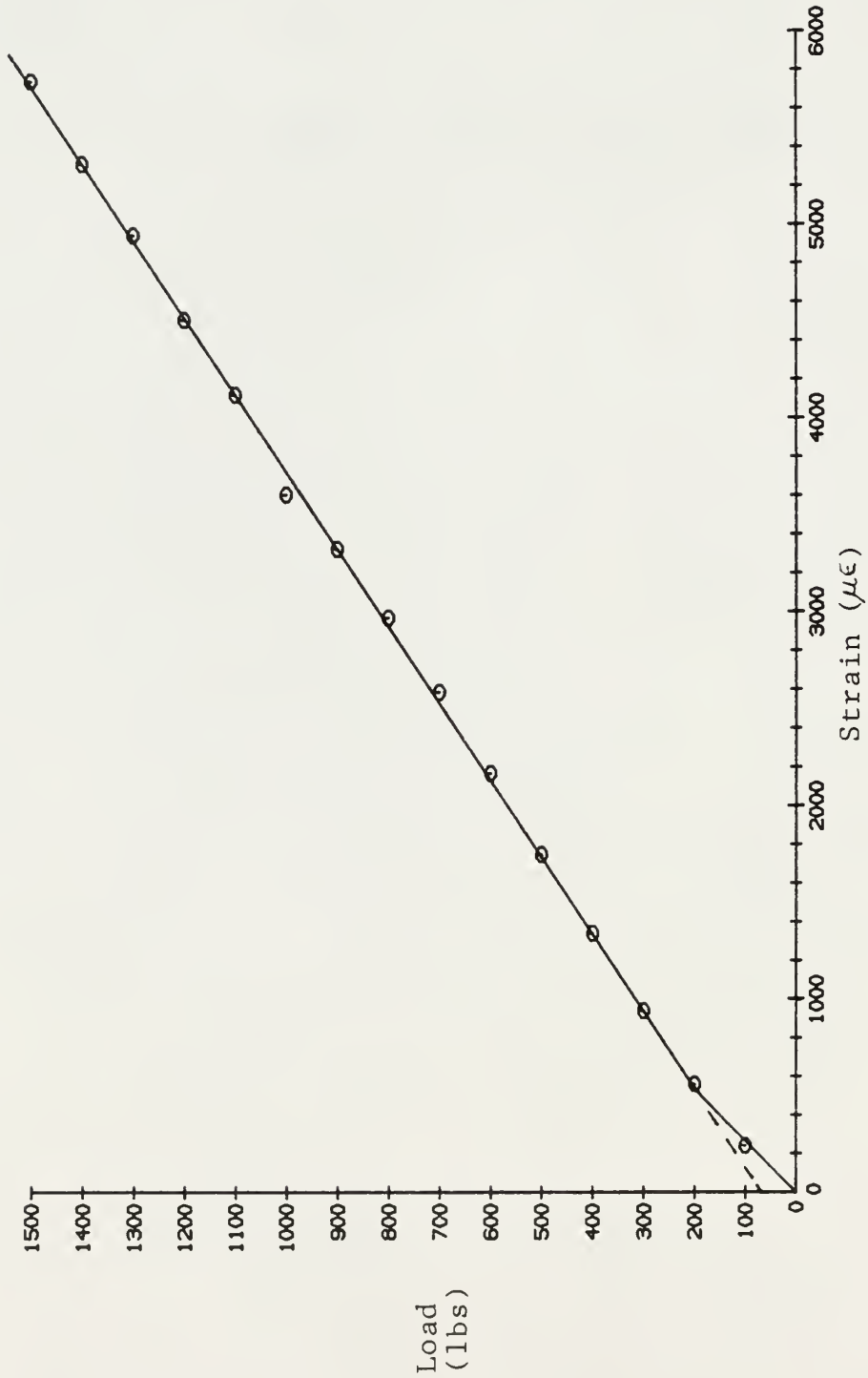


Figure 14 Tensile Test Specimen No. 5, Load vs. Longitudinal Strain

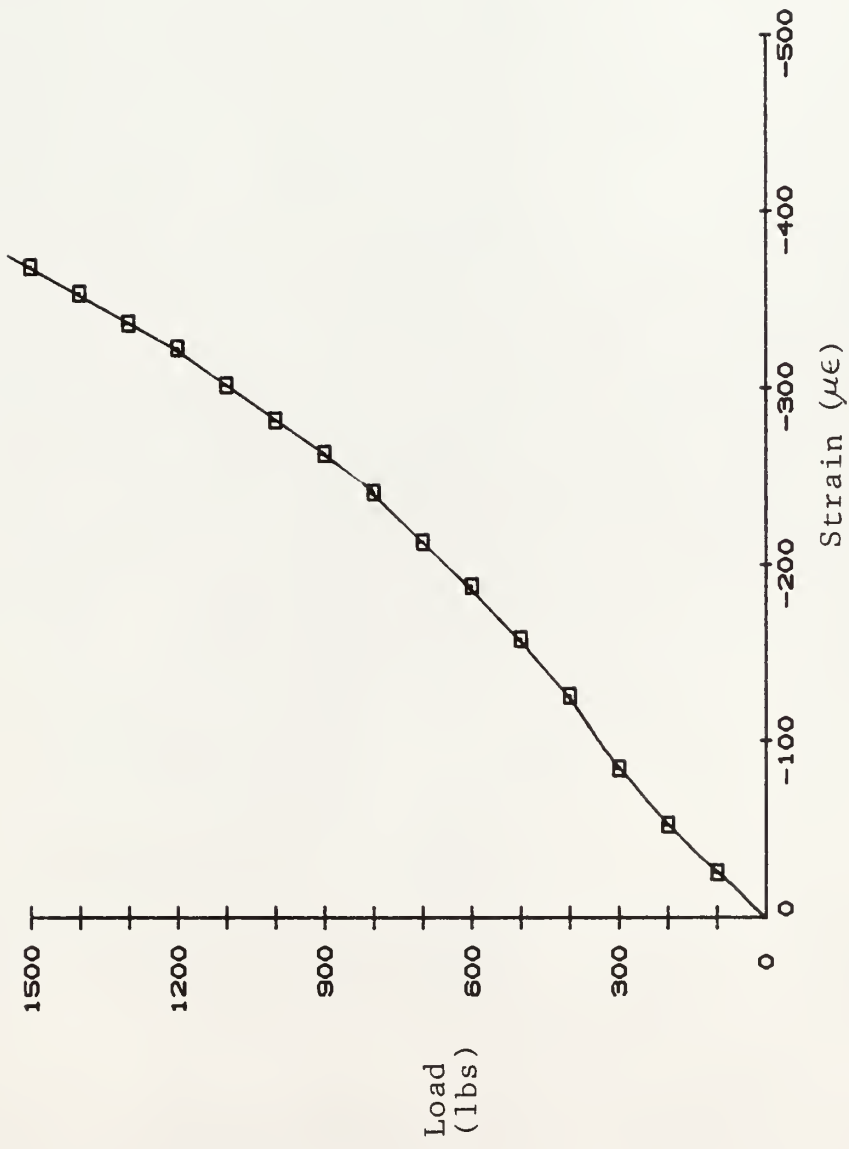


Figure 15 Tensile Test Specimen No. 5, Load vs. Transverse Strain

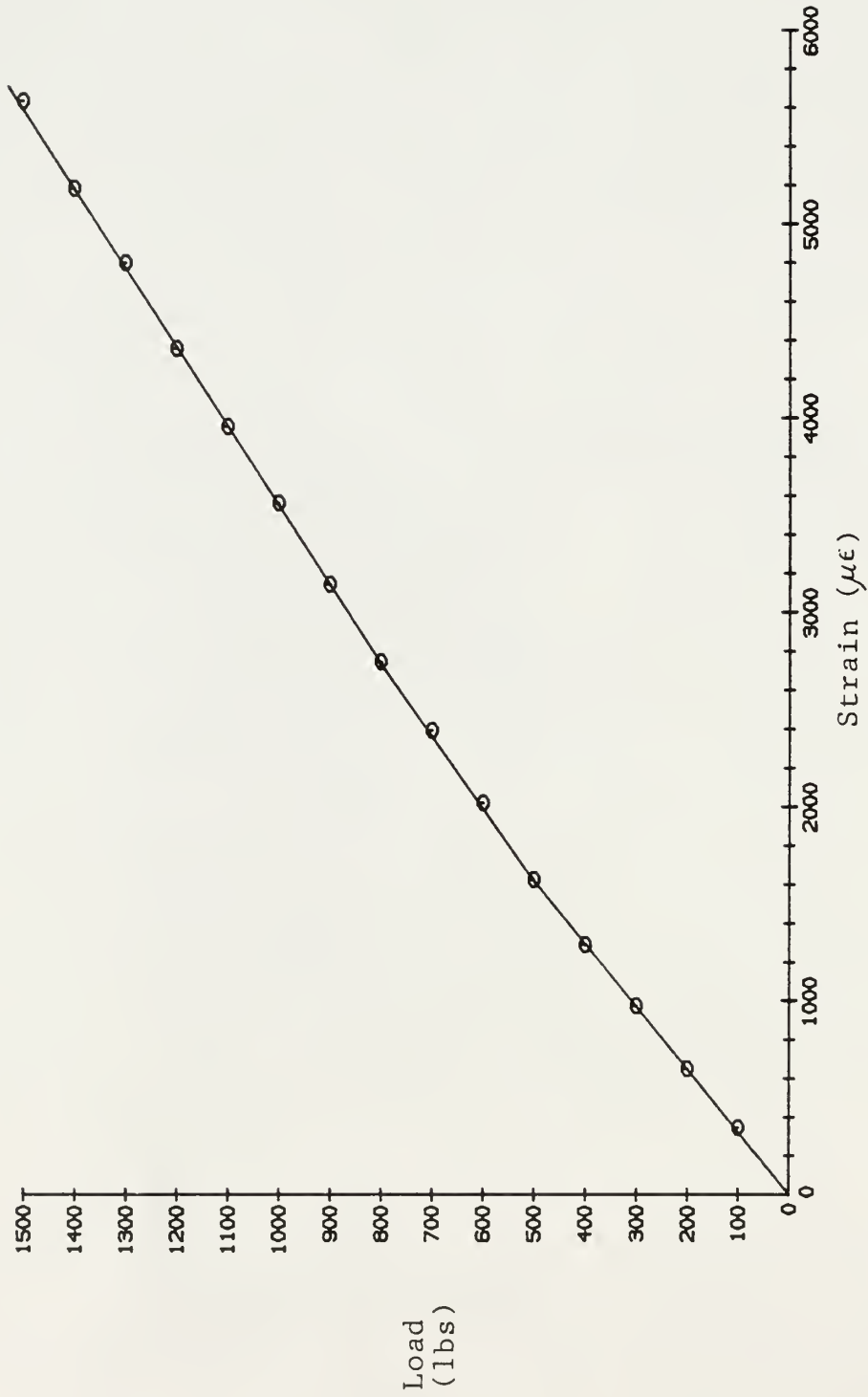


Figure 16 Tensile Test Specimen No. 6, Load vs. Longitudinal Strain

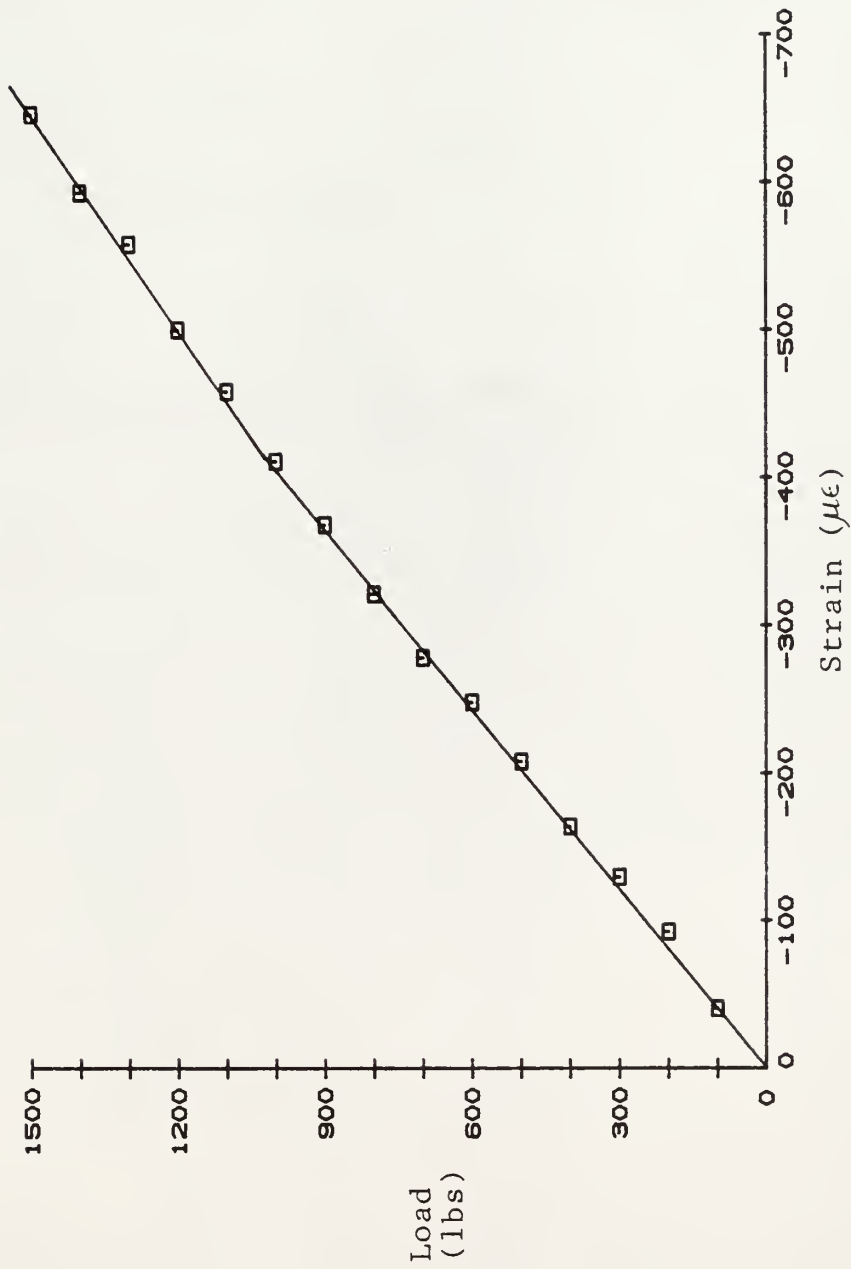


Figure 17 Tensile Test Specimen No. 6, Load vs. Transverse Strain

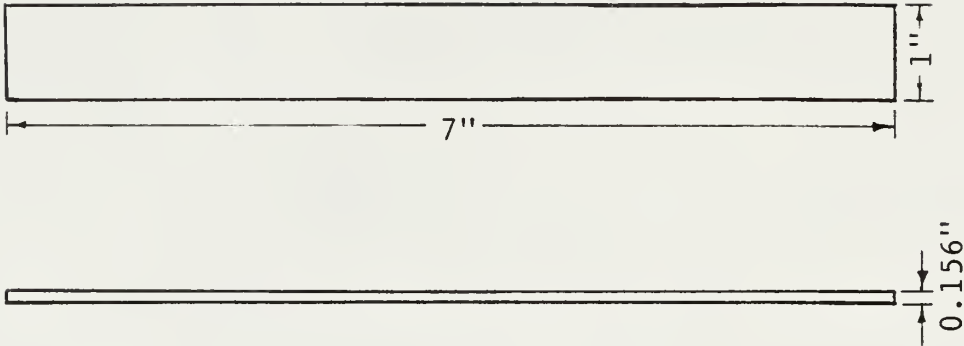


Figure 18 Flexure Test Specimen Dimensions

A four point bend test was performed on each of these specimens (ASTM Method II), with the center deflection being measured with an Enco model #340 dial indicator. Figure 19 gives the details of the loading and support arrangement.

For the curves which reflect the load versus deflection for the  $E_{x,b}$  test specimens, see Figures 20-24. The equation used to calculate the modulus of elasticity in bending was

$$E_b = \frac{.17L^3 m}{bd^3} \quad (3)$$

where  $E_b$  = modulus of elasticity in bending mode (psi)

$L$  = support span distance (in)

$m$  = slope of the tangent to the initial straight-line portion of the load-deflection curve

$b$  = width of specimen (in)

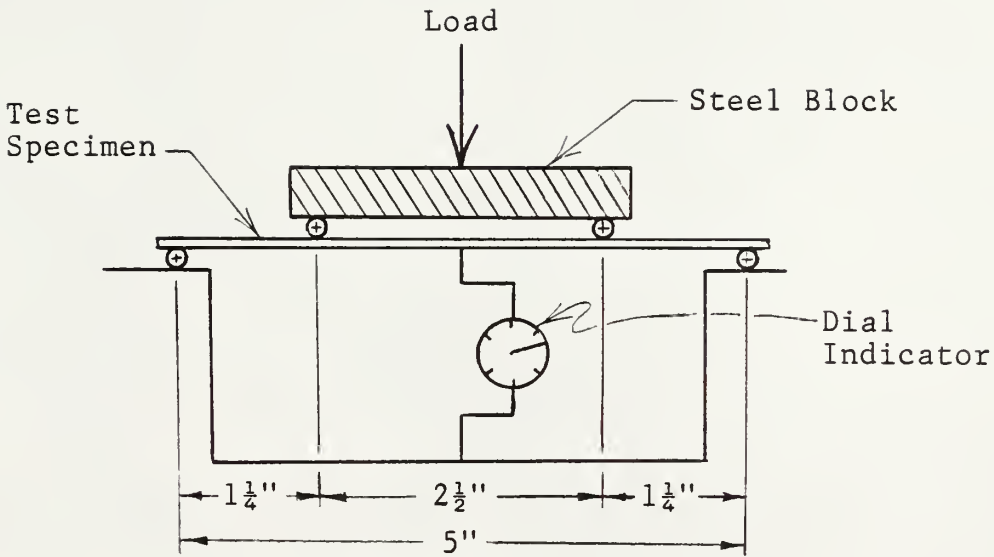


Figure 19 Flexure Test Fixture Details

The values found for  $E_b$  on the X axis test specimens were averaged, yielding a bending modulus of elasticity of  $E_{x,b} = 2.368 \times 10^6$  psi. This value is 94.2% of the value found for the modulus of elasticity in tension ( $E_{x,t} = 2.513 \times 10^6$  psi).

The same test was performed on three test specimens to find a value for the modulus in the Y direction. These specimens were generally of the same dimensions as those for testing E in the X direction.

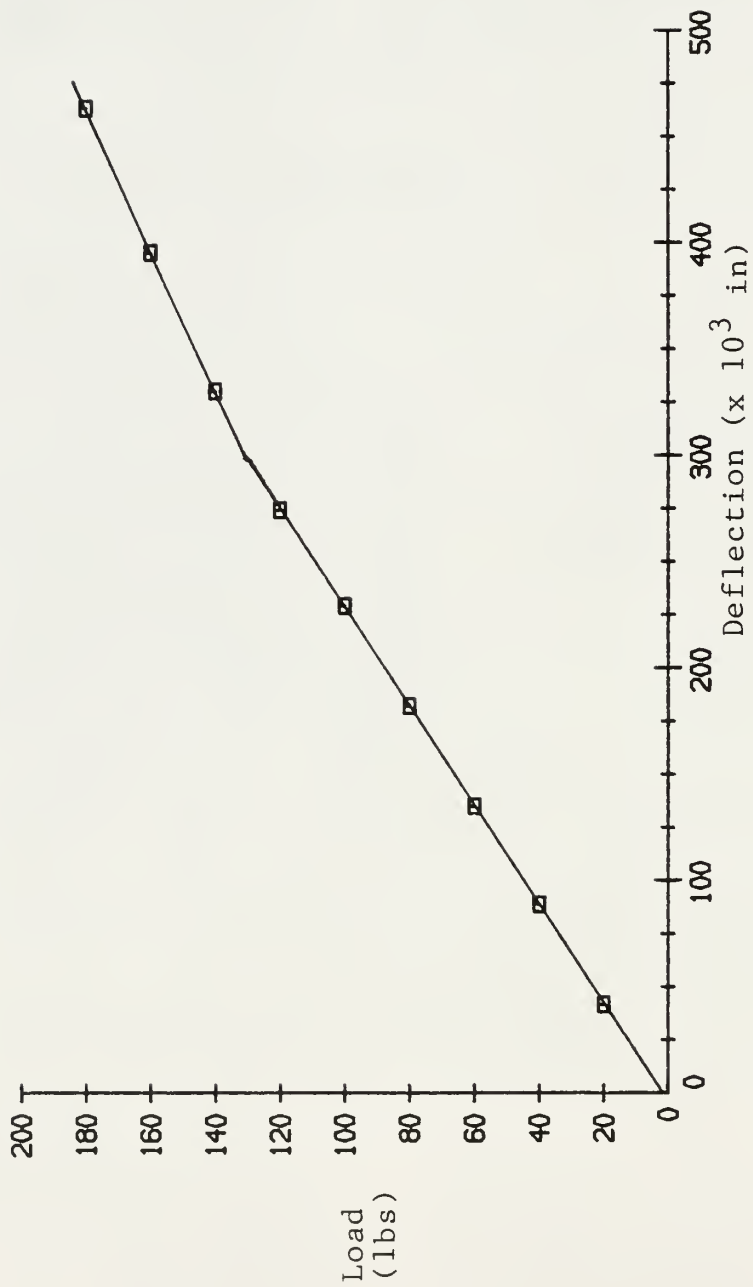


Figure 20 Flexure Test Specimen No. 7, Load vs. Deflection

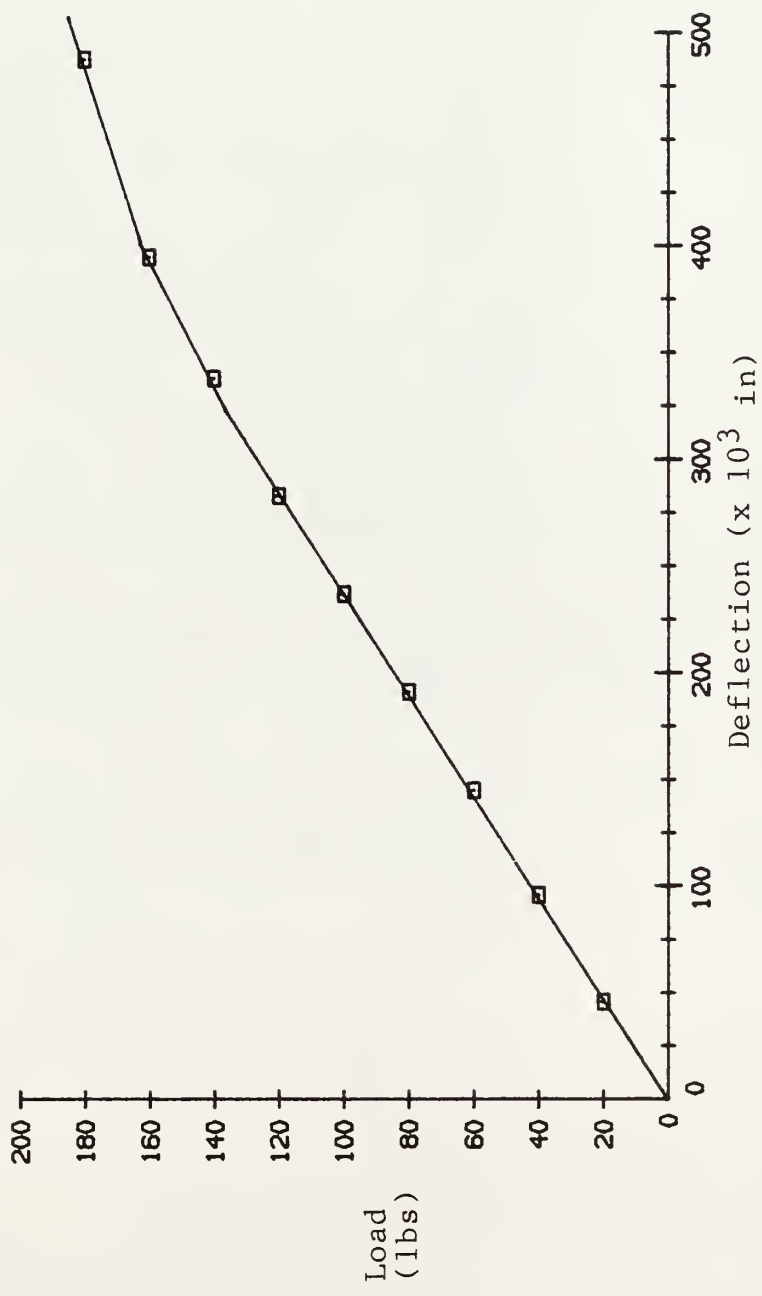


Figure 21 Flexure Test Specimen No. 8, Load vs. Deflection

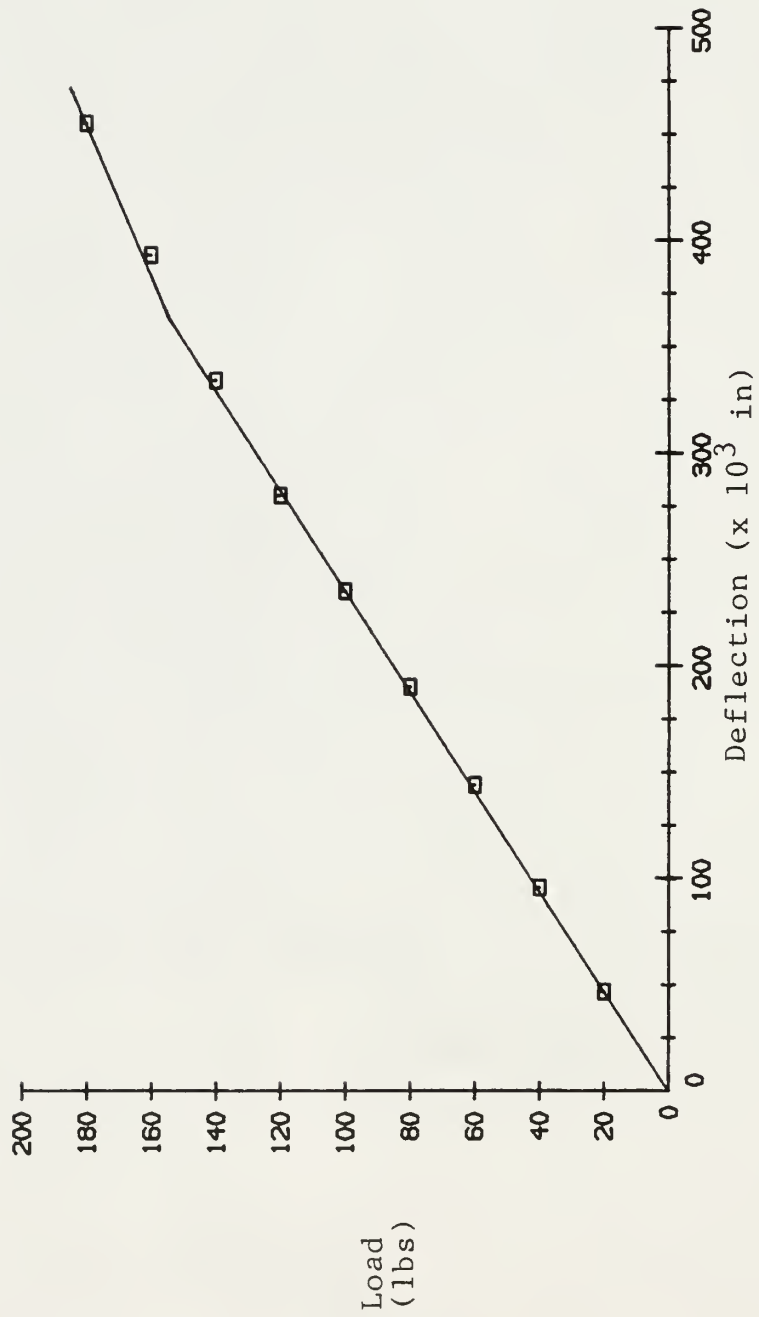


Figure 22 Flexure Test Specimen No. 9, Load vs. Deflection

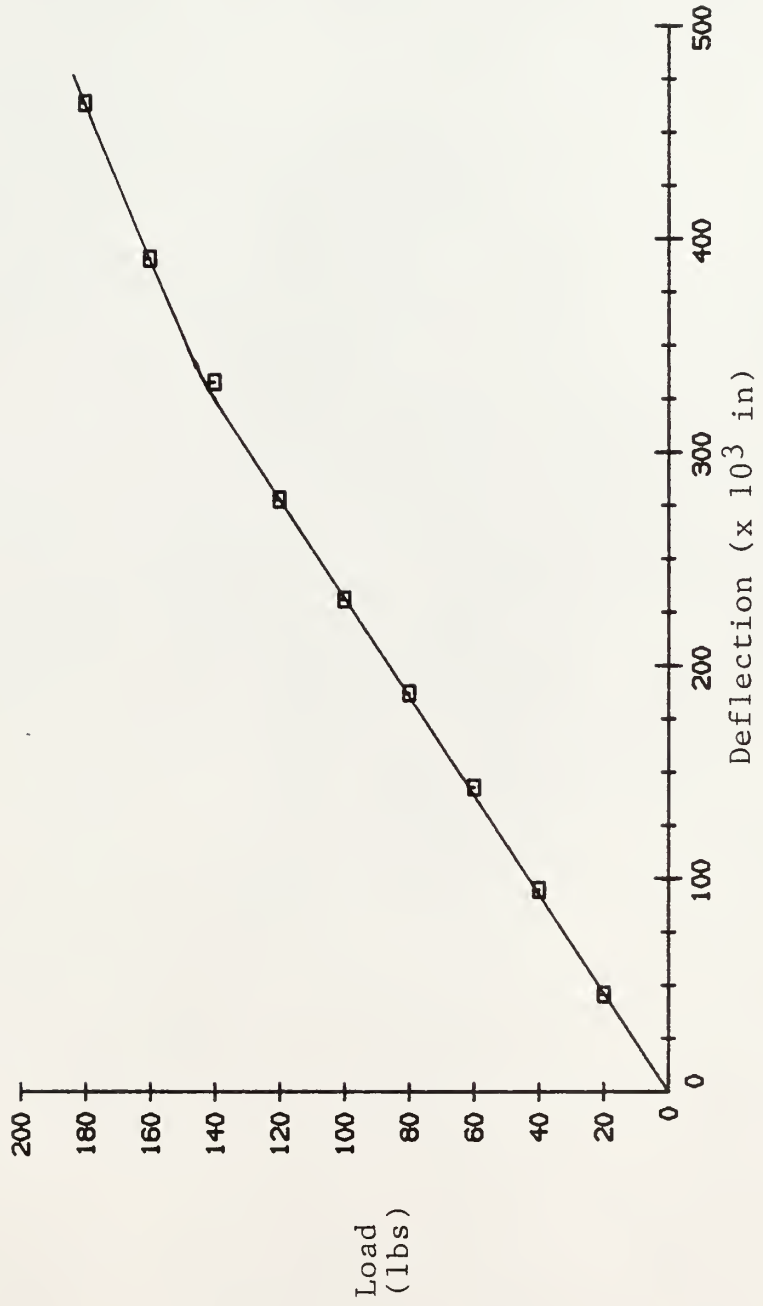


Figure 23 Flexure Test Specimen No. 10, Load vs. Deflection

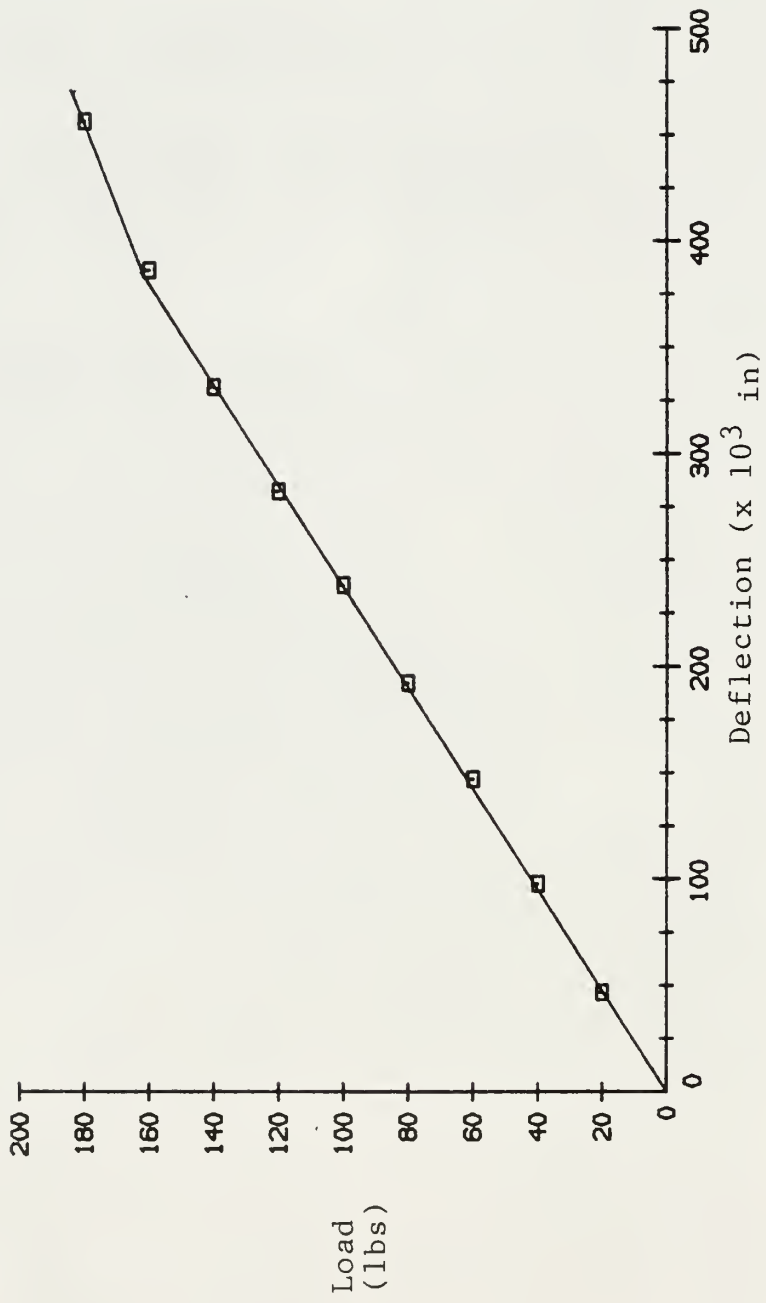


Figure 24 Flexure Test Specimen No. 11, Load vs. Deflection

The plots of the load versus deflection for these specimens are indicated in Figures 25-27. Again using Equation (3) to find the modulus of elasticity of each specimen and then finding the average, the resulting value was calculated to be  $E_{y,b} = 1.496 \times 10^6$  psi. This value is 94.3% of the value found by the tension test method ( $E_{y,t} = 1.586 \times 10^6$  psi).

Since the values found by using the flexure test method were very close to being the same percentage of the values found by the tension test method, it was deduced that the slightly higher value found by the tension test must be reasonably accurate for stress which doesn't involve significant bending.

An interesting sidenote is that Whitney, et al, [5] indicated that the modulus of elasticity in bending is generally greater in composites. However, it would seem that a lower value in bending could be explained on the basis that bending produces both tension and compression in the test specimen. If the modulus of elasticity of the composite material in compression is less than the modulus of elasticity in tension, then it would seem reasonable to assume that a flexure test which creates both tension and compression in a specimen beam will result in a modulus of elasticity which is less than the modulus of elasticity in tension and

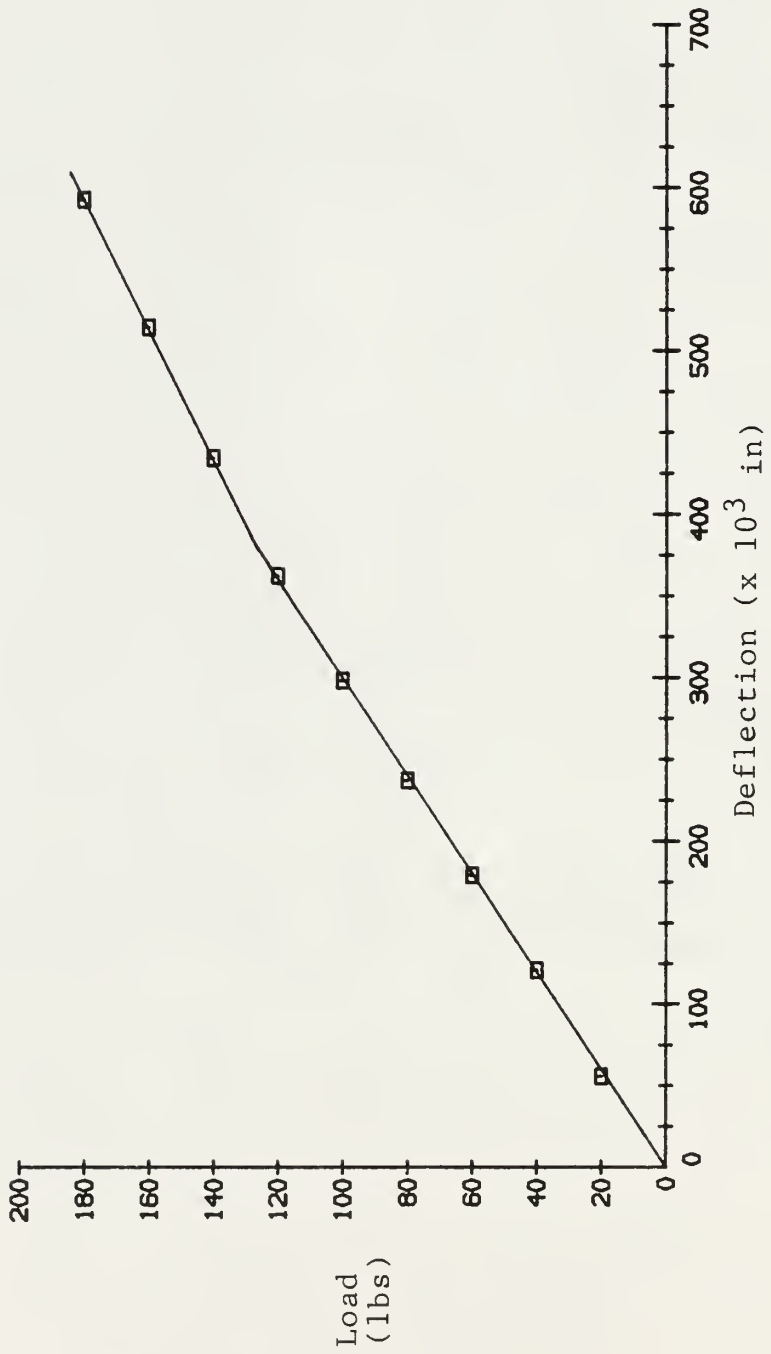


Figure 25 Flexure Test Specimen No. 12, Load vs. Deflection

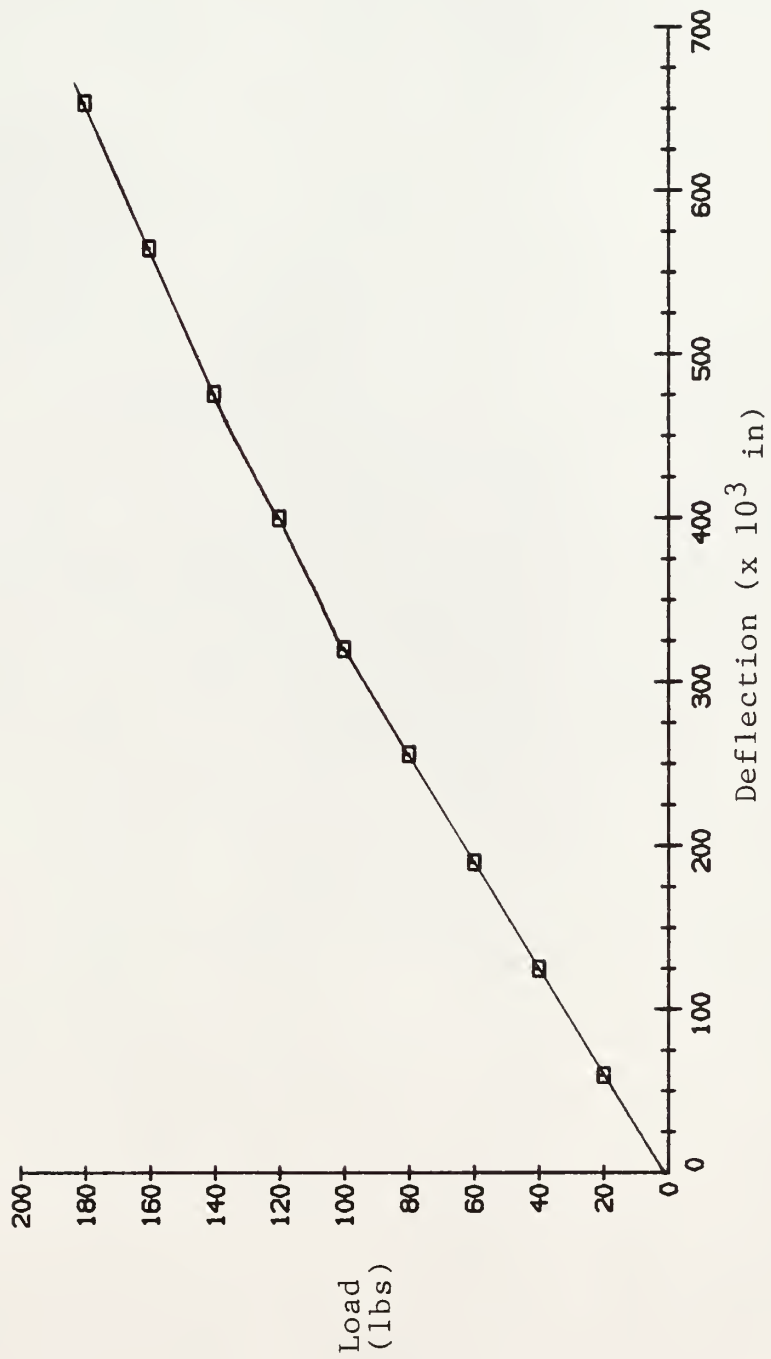


Figure 26 Flexure Test Specimen No. 13, Load vs. Deflection

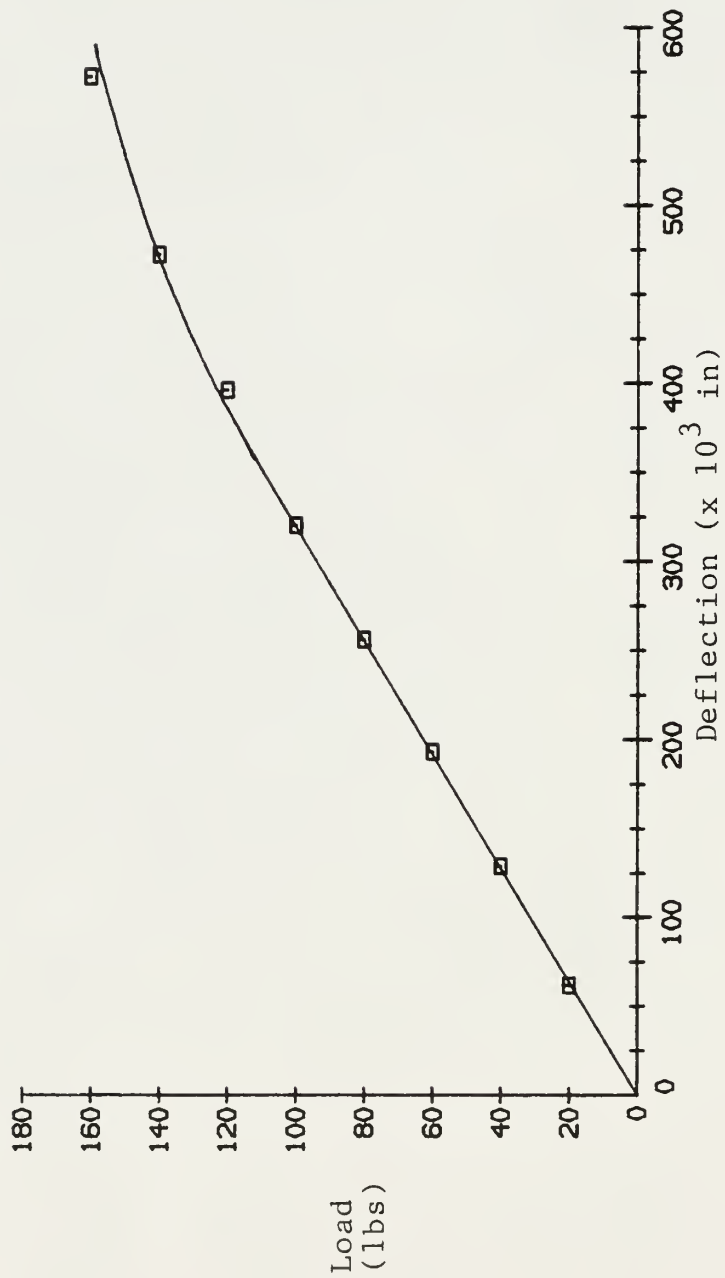


Figure 27 Flexure Test Specimen No. 14, Load vs. Deflection

more than the modulus of elasticity in compression. Moreover, bending induced interlaminar shear stresses will tend to reduce the strength and modulus of elasticity of a laminate-type composite.

In summarizing, the higher modulus of elasticity as determined by the uniaxial tension test method was deemed to be an accurate representation of the true modulus of elasticity of this FRP, particularly since the amount of bending in the box beam was small.

#### Determination of $E_x$ , $E_y$ in Compression

The guide used for determining the modulus of elasticity in compression in both the X and Y directions was ASTM Standard D695-85 [6]. All of the test specimens were approximately the same dimensionally. Figure 28 gives the dimensions of these test specimens.

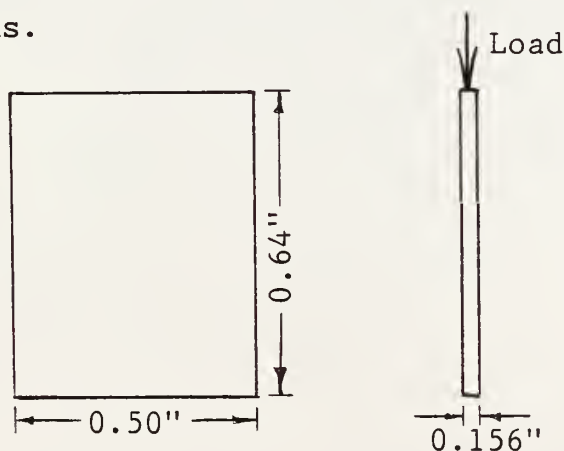


Figure 28 Compression Test Specimen Dimensions

Since the specimen length was so small, the loading crosshead movement was measured to determine the change in specimen length, instead of the actual specimen. The modulus of elasticity in compression was calculated for each specimen by use of the equation

$$E_c = \frac{P/A}{\Delta L/L} \quad (4)$$

where  $E_c$  = modulus of elasticity in compression (psi)

$P$  = load (lbs)

$A$  = specimen cross-sectional area (in<sup>2</sup>)

$\Delta L/L$  = change in specimen length divided by  
original length (in/in)

The resulting load versus strain plots for each of the ten specimens used in this test are shown in Figures 29-38. The average modulus of elasticity in compression values for each of the two principal axis directions were found to be

$E_{x,c} = 3.68 \times 10^5$  psi, and  $E_{y,c} = 4.55 \times 10^5$  psi.

These values appeared to be abnormally low, and were later determined to be substantially below the empirically determined values.

One obvious reason for these values to be suspiciously below their actual values is the damage which occurred to the edges of the test specimens by the sawblade teeth during the process of cutting the

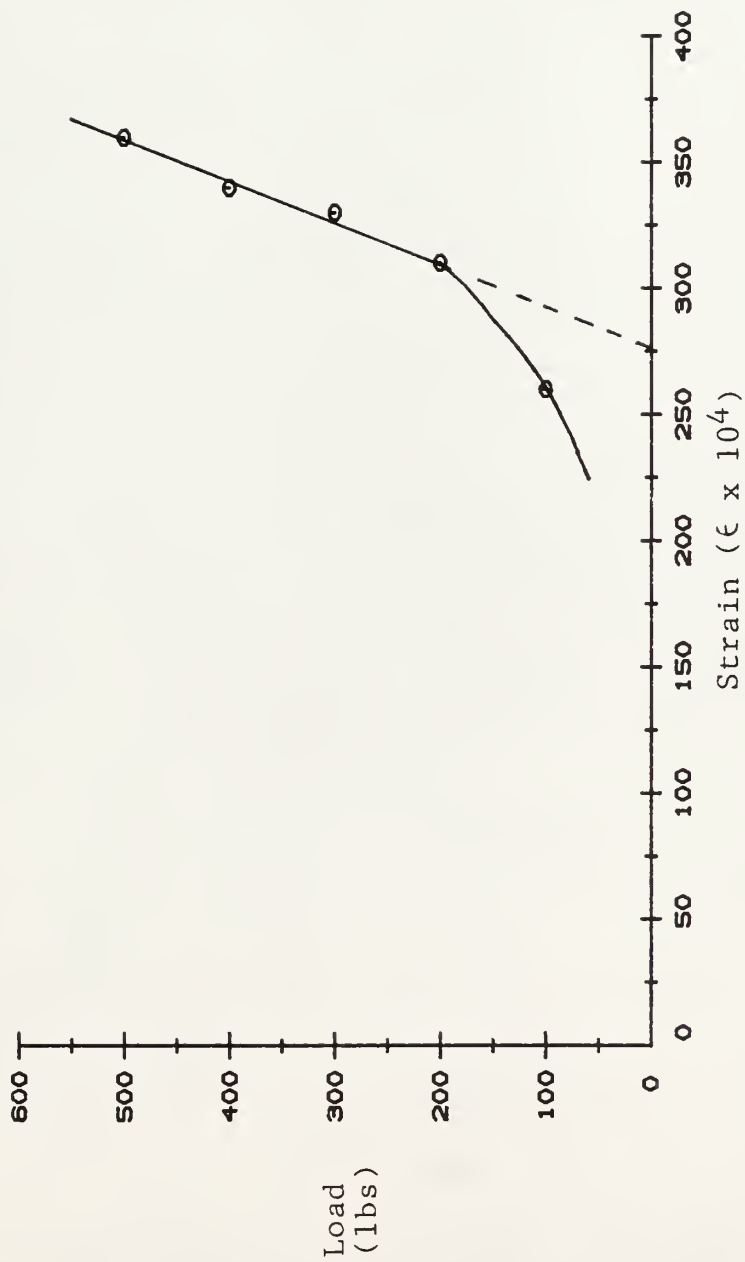


Figure 29 Compression Test Specimen No. 15, Load vs. Strain

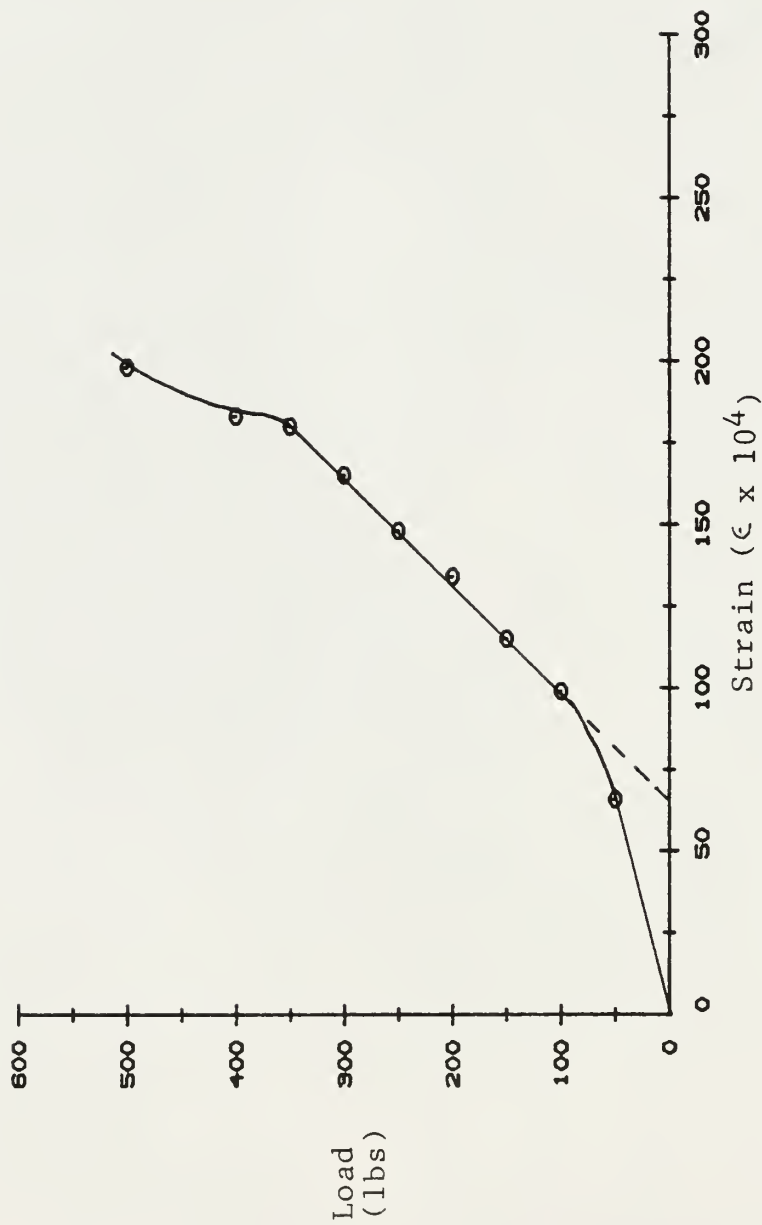


Figure 30 Compression Test Specimen No. 16, Load vs. Strain

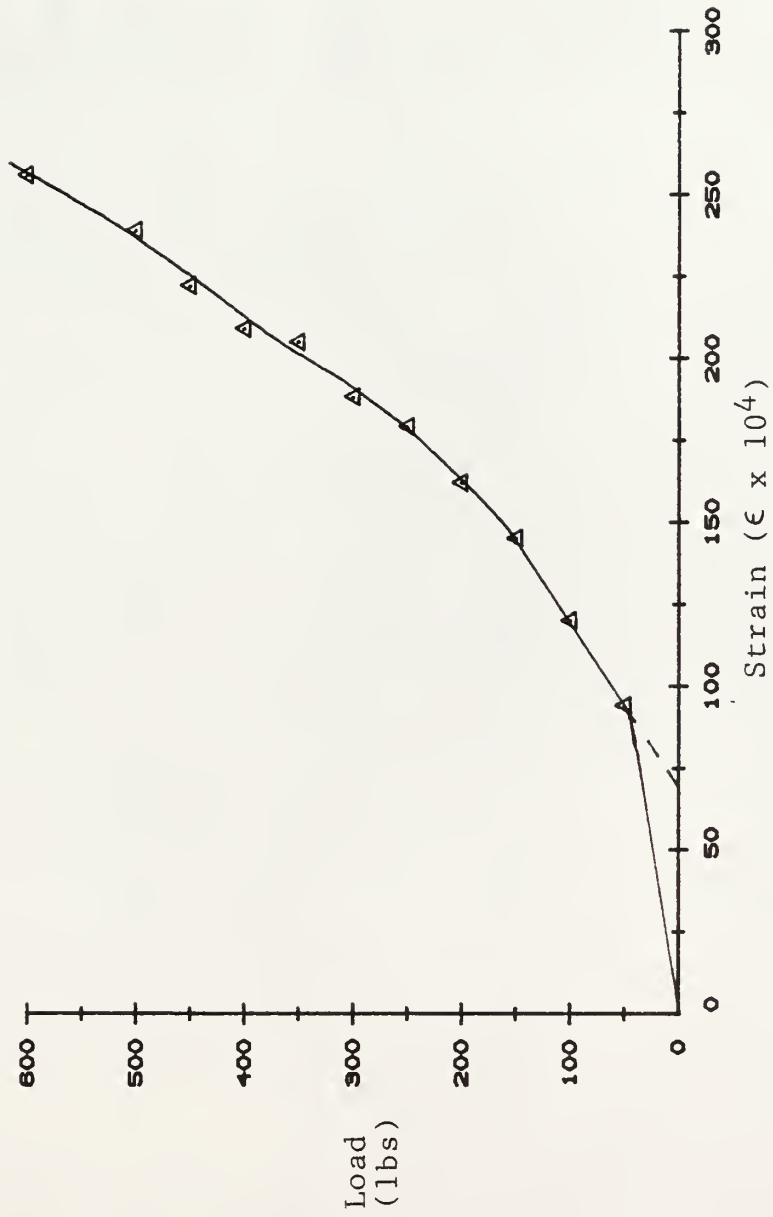


Figure 31 Compression Test Specimen No. 17, Load vs. Strain

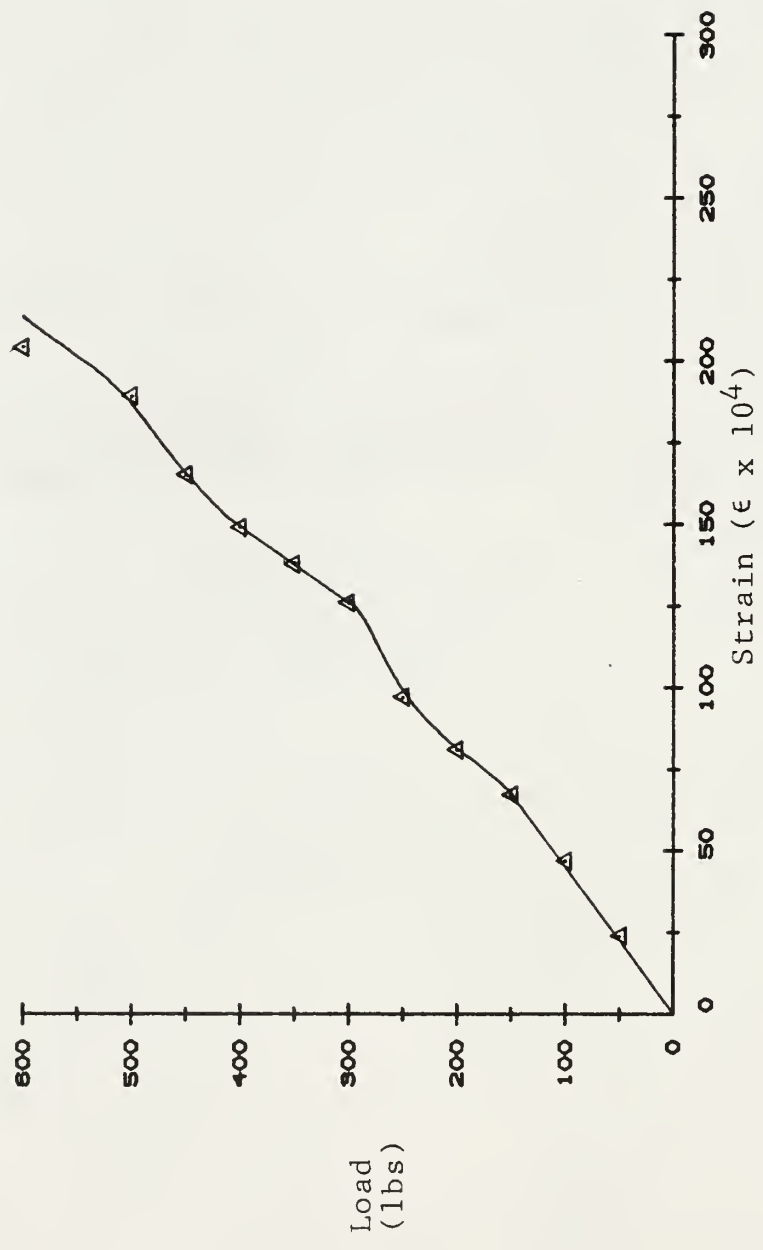


Figure 32 Compression Test Specimen No. 18, Load vs. Strain

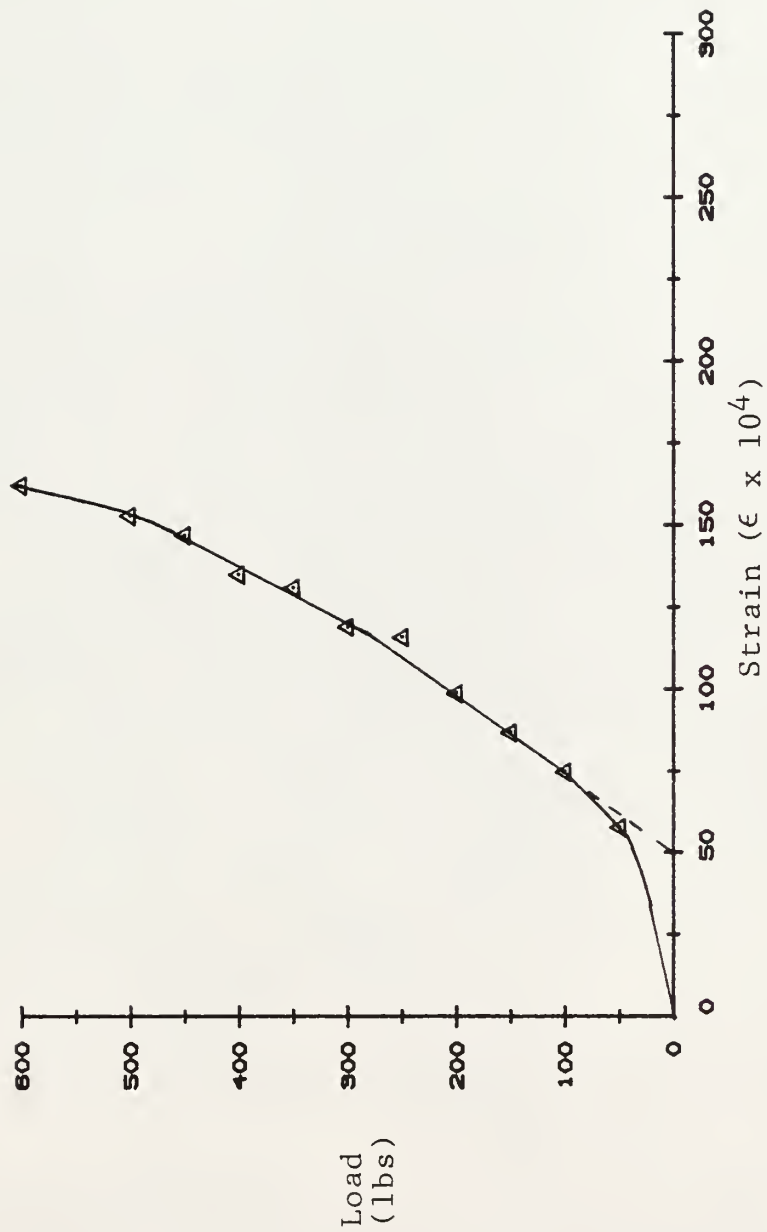


Figure 33 Compression Test Specimen No. 19, Load vs. Strain

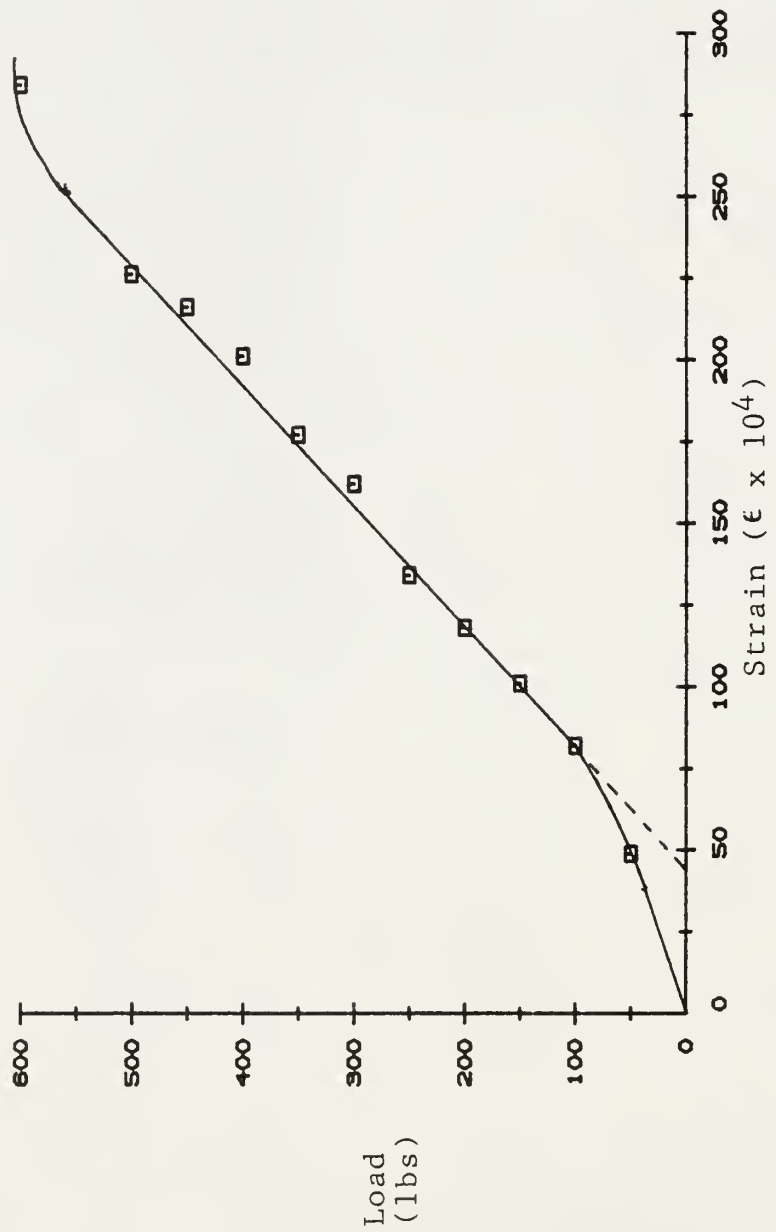


Figure 34 Compression Test Specimen No. 20, Load vs. Strain

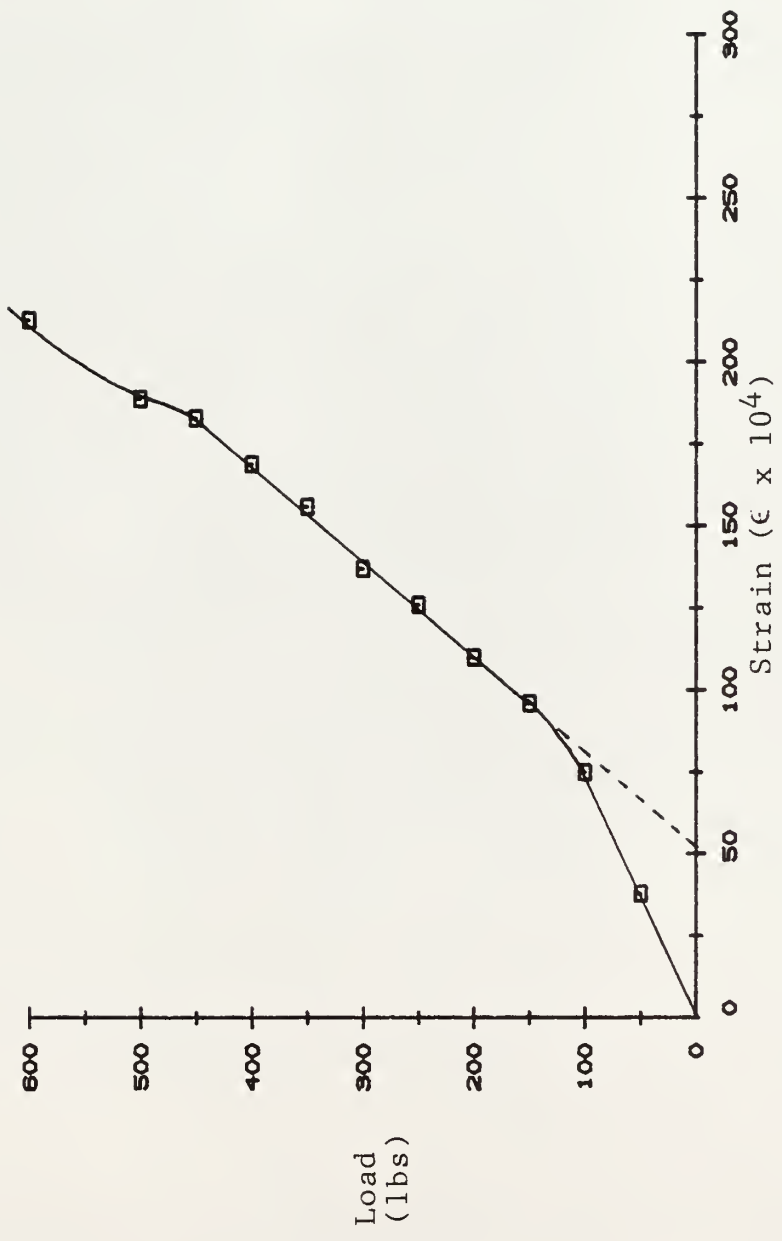


Figure 35 Compression Test Specimen No. 21, Load vs. Strain

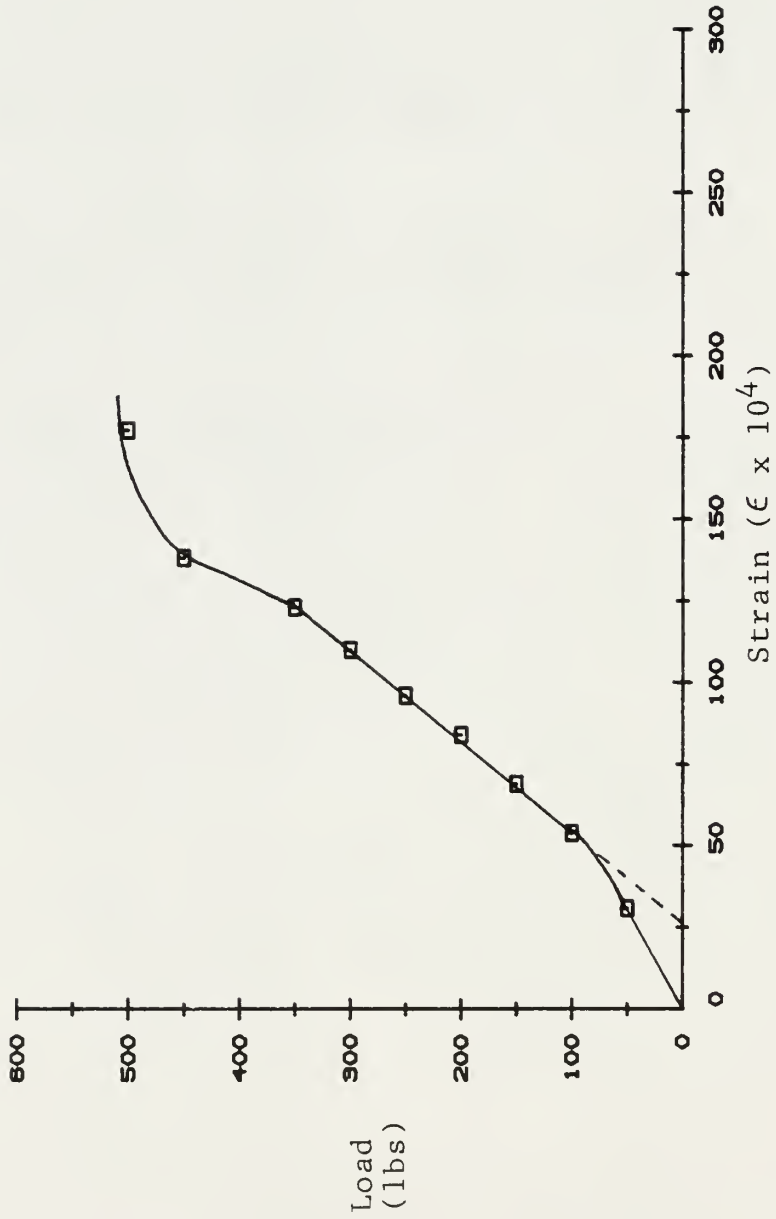


Figure 36 Compression Test Specimen No. 22, Load vs. Strain

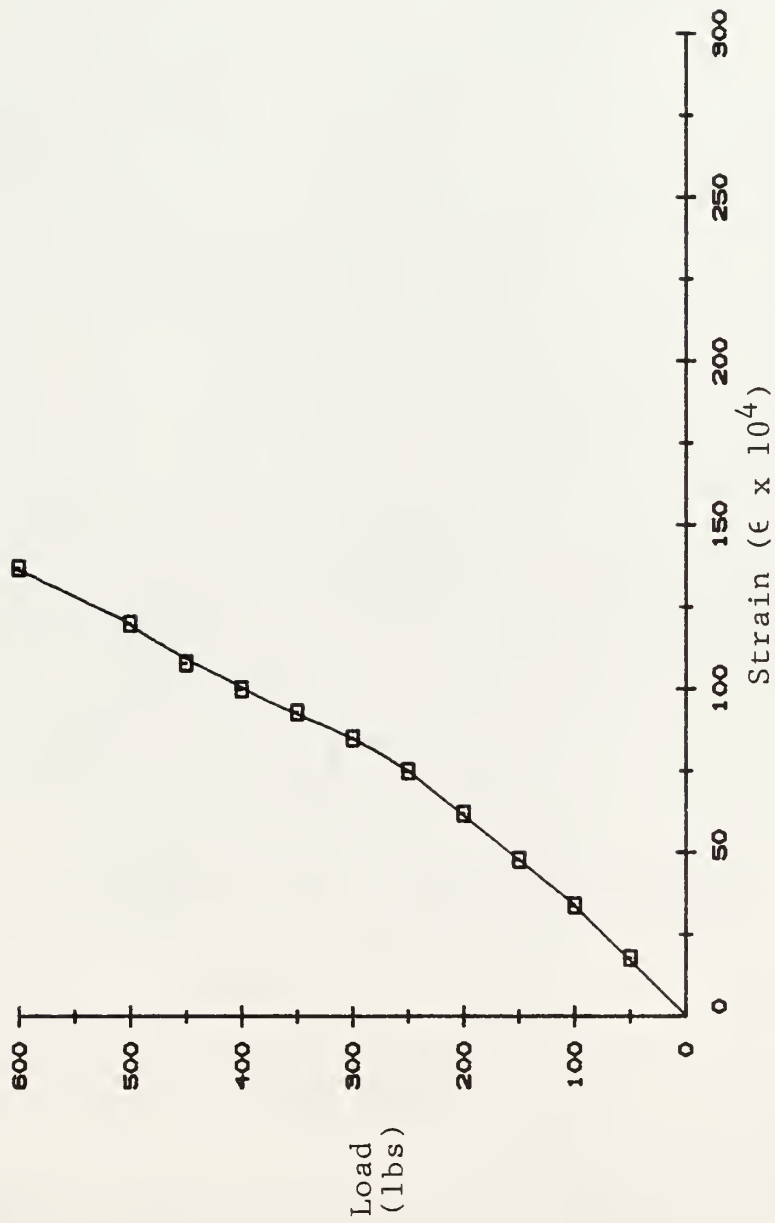


Figure 37 Compression Test Specimen No. 23, Load vs. Strain

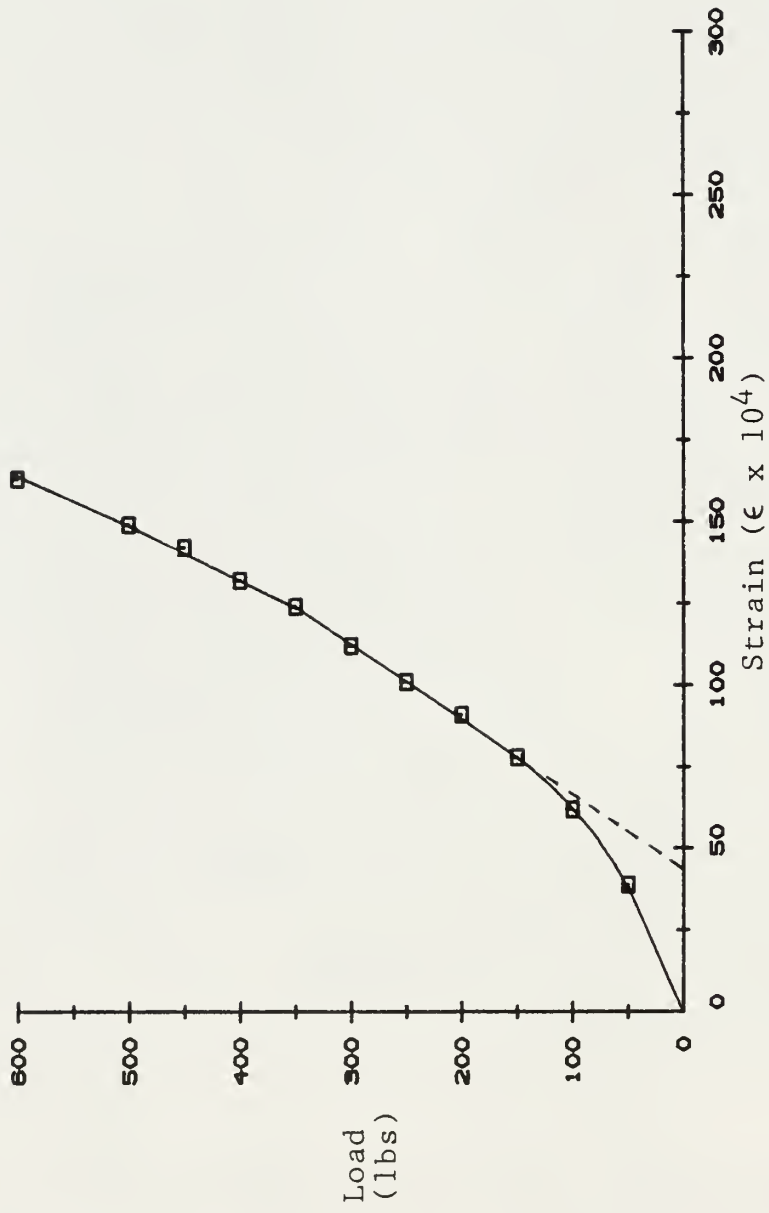


Figure 38 Compression Test Specimen No. 24, Load vs. Strain

test specimens to the proper size. This separation of the glass filaments from the matrix, as mentioned earlier, and the concurrent loss of some of the matrix near the edges, resulted in a reduction of the actual test specimen thickness near the specimen edges. This thickness reduction would not be significant for most tests; however, it would have a substantial effect in a case where the compressive forces on each end of a test specimen are acting against a relatively small area which had been further reduced by this cutting damage. As a result, this test data was considered inconsequential.

#### Determination of $G_{xy}$ and $G_{yx}$

The guide used in determining the inplane shear modulus was ASTM Standard D 4255-83 [7]. Of the two methods available in this standard, Method A was chosen. It utilizes two pairs of rails, with the test specimen bolted between them. The rails are subjected to a tensile force. See Figure 39 for details of the test specimen dimensions and Figure 40 for a view of the test fixture apparatus.

It should be noted that the referenced ASTM Standard contains a statement regarding the fact that it is to be considered a standard guide, not a standard method. The reason for this is that inplane shear test

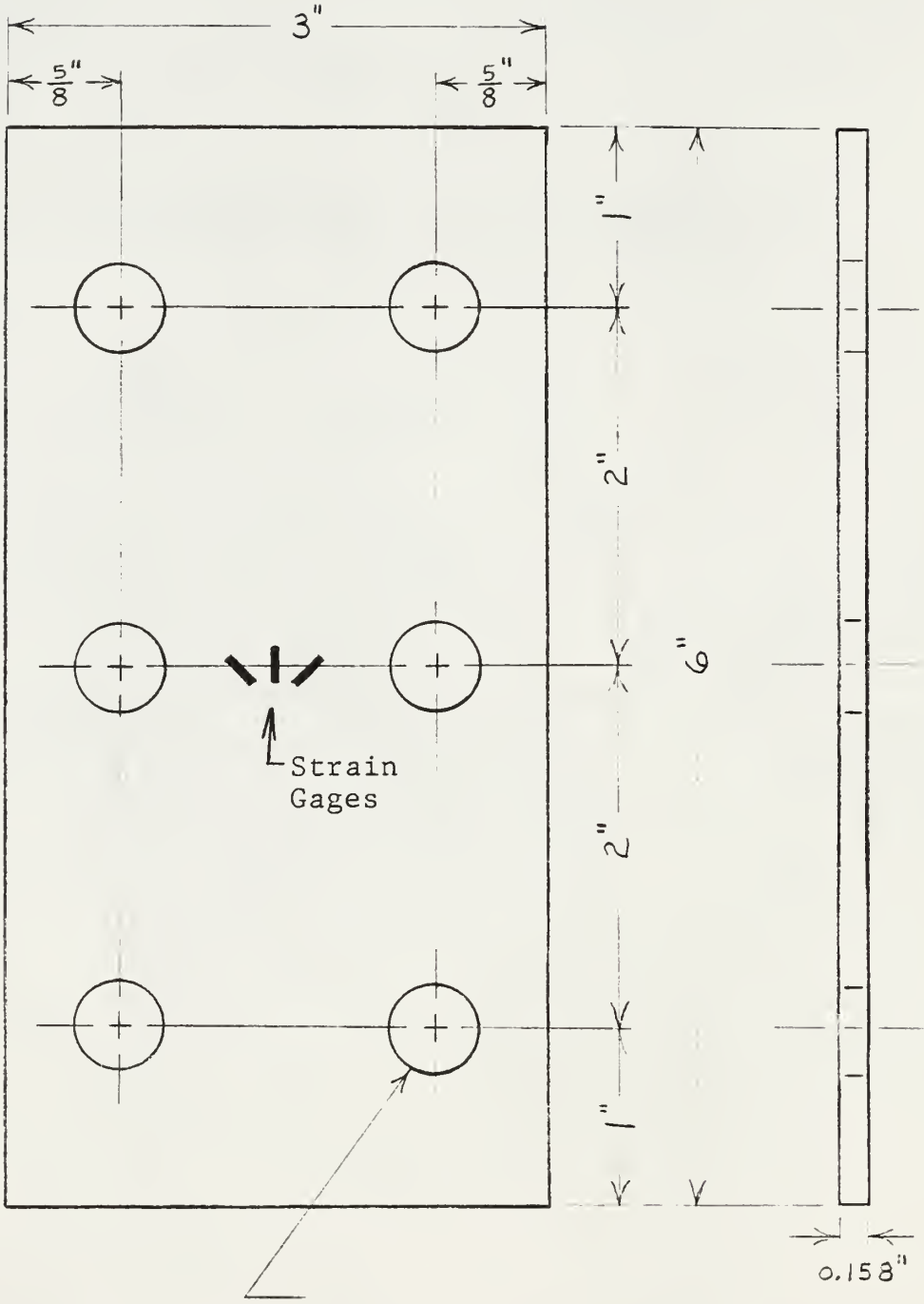


Figure 39 Shear Test Specimen Dimensions

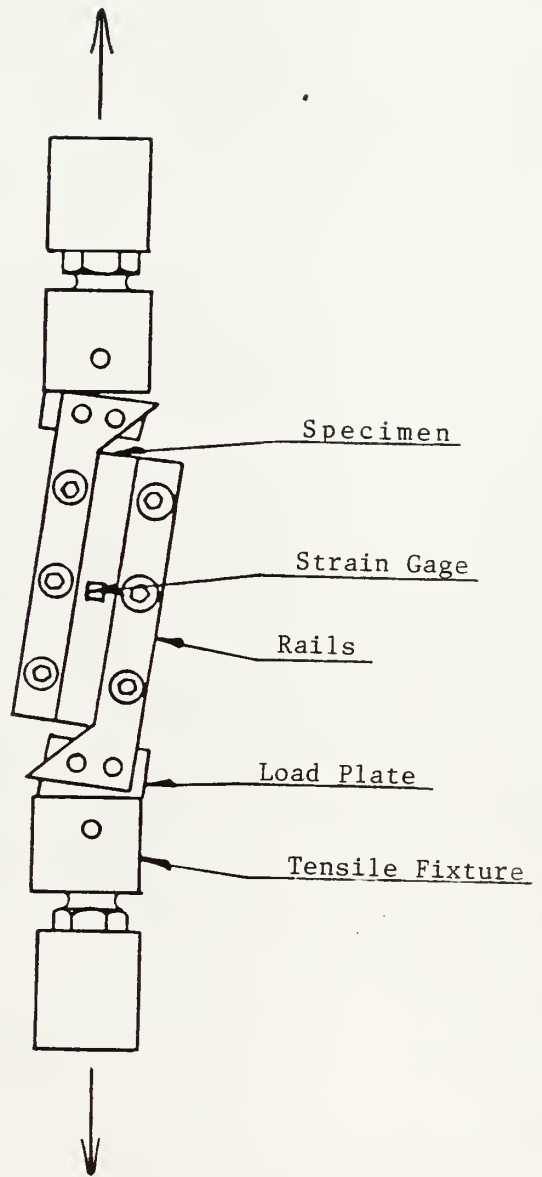


Figure 40 Shear Test Fixture

specimens normally fail by buckling out of plane. The specimen size and constraints placed on it by the clamping mechanism can affect the test results. Moreover, no single shear test seems to have gained universal acceptance for determining the shear modulus of laminated composites. A number of other shear test methods are available, but this one was selected because of the simplicity of the test apparatus and so that only the ASTM Standards were used.

On each specimen, a three element rectangular rosette strain gage was used to measure the strain, as indicated on Figure 39. See Figures 41 and 42 for plots of the load versus strain for the on-axis ( $G_{xy}$ ) test and Figures 43 and 44 for the results of the off-axis ( $G_{yx}$ ) shear test.

Since both tests produced results which indicate that the principal shear stress axis was not coincident with the longitudinal axis of the test specimen, separate calculations were necessary to find the maximum shear strain. This maximum shear strain was found from the equation

$$\gamma_{\max} = \sqrt{(\epsilon_1 - \epsilon_3)^2 + 2(\epsilon_2 - \epsilon_1 - \epsilon_3)^2} \quad (5)$$

which is the diameter of Mohr's circle [8]. After application of this equation for calculating each of

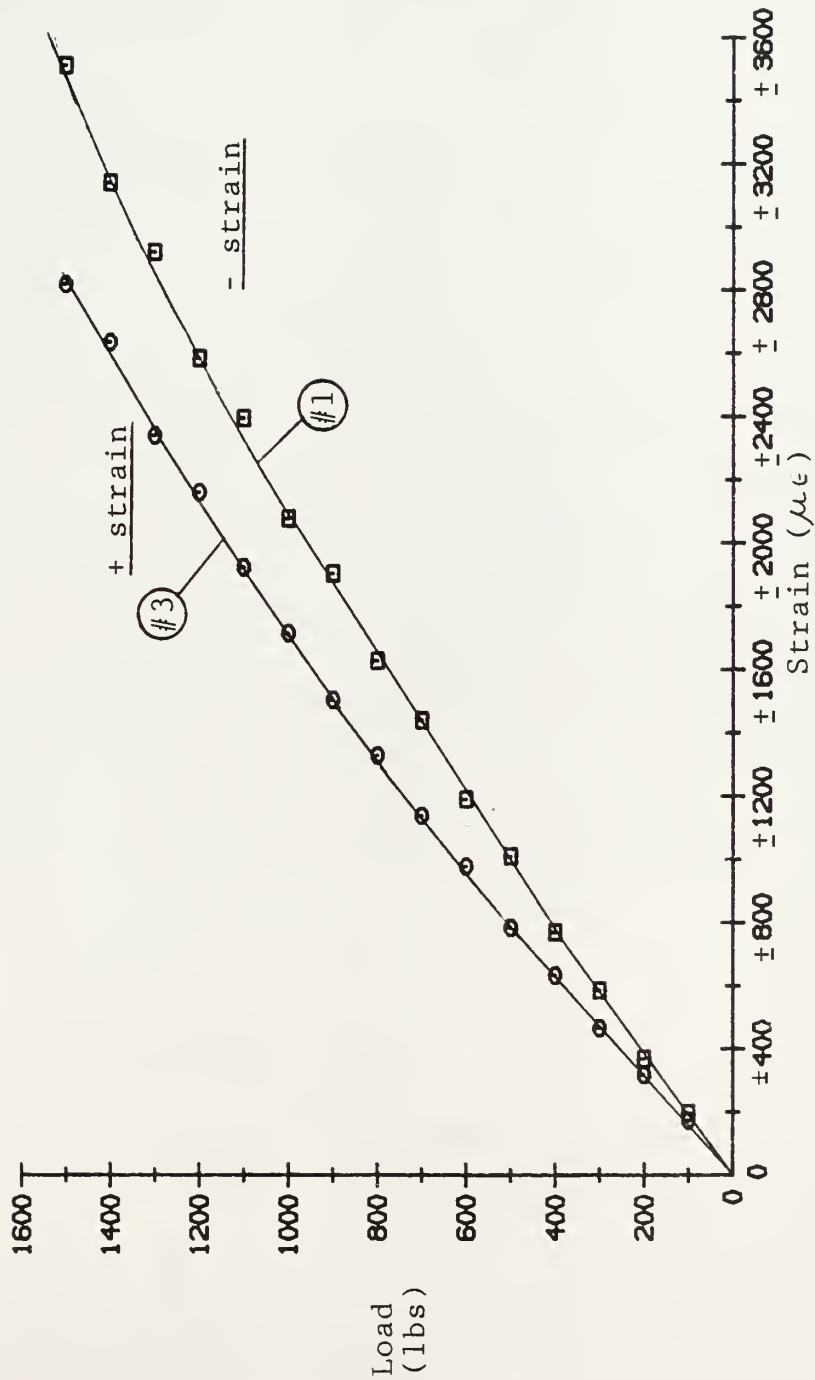


Figure 41 On-Axis Shear Test, Load vs. Strain, Gages #1, #3

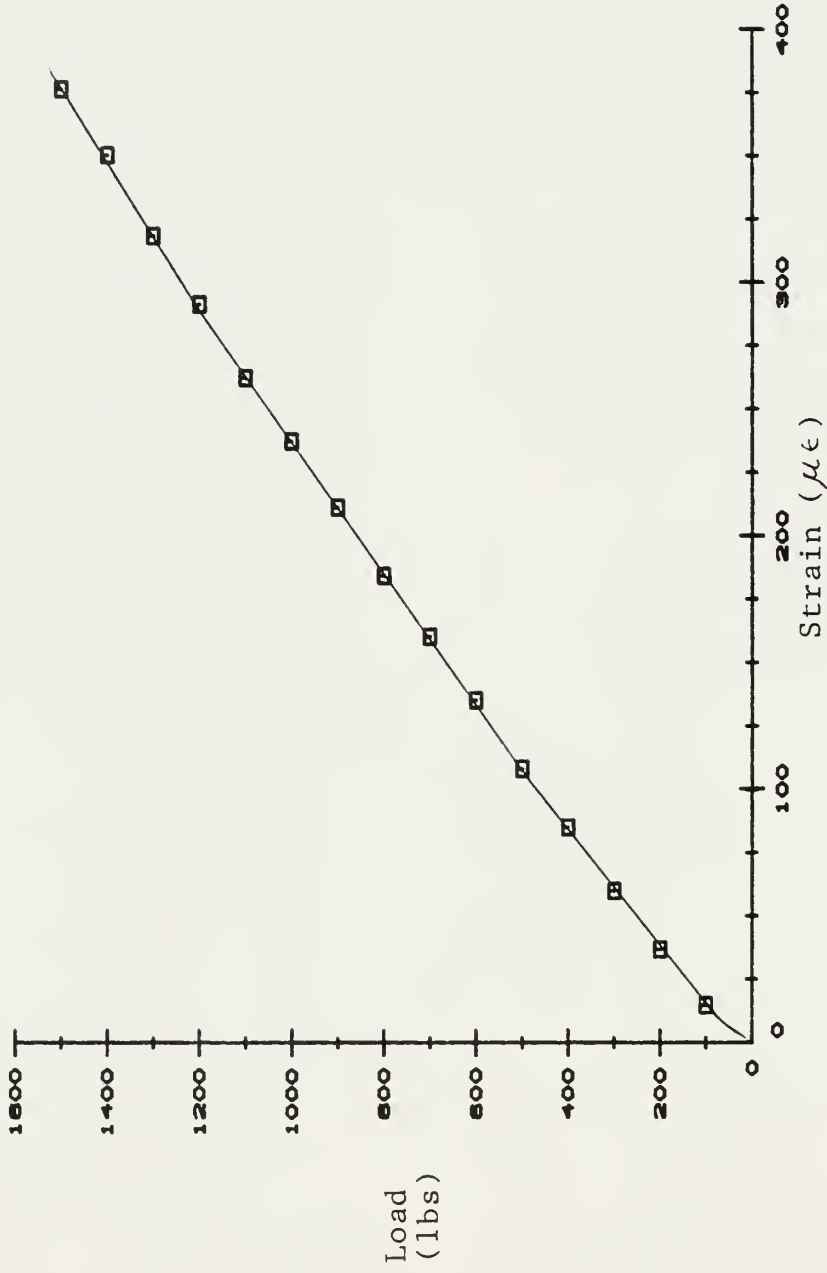


Figure 42 On-Axis Shear Test, Load vs. Strain, Axial Gage

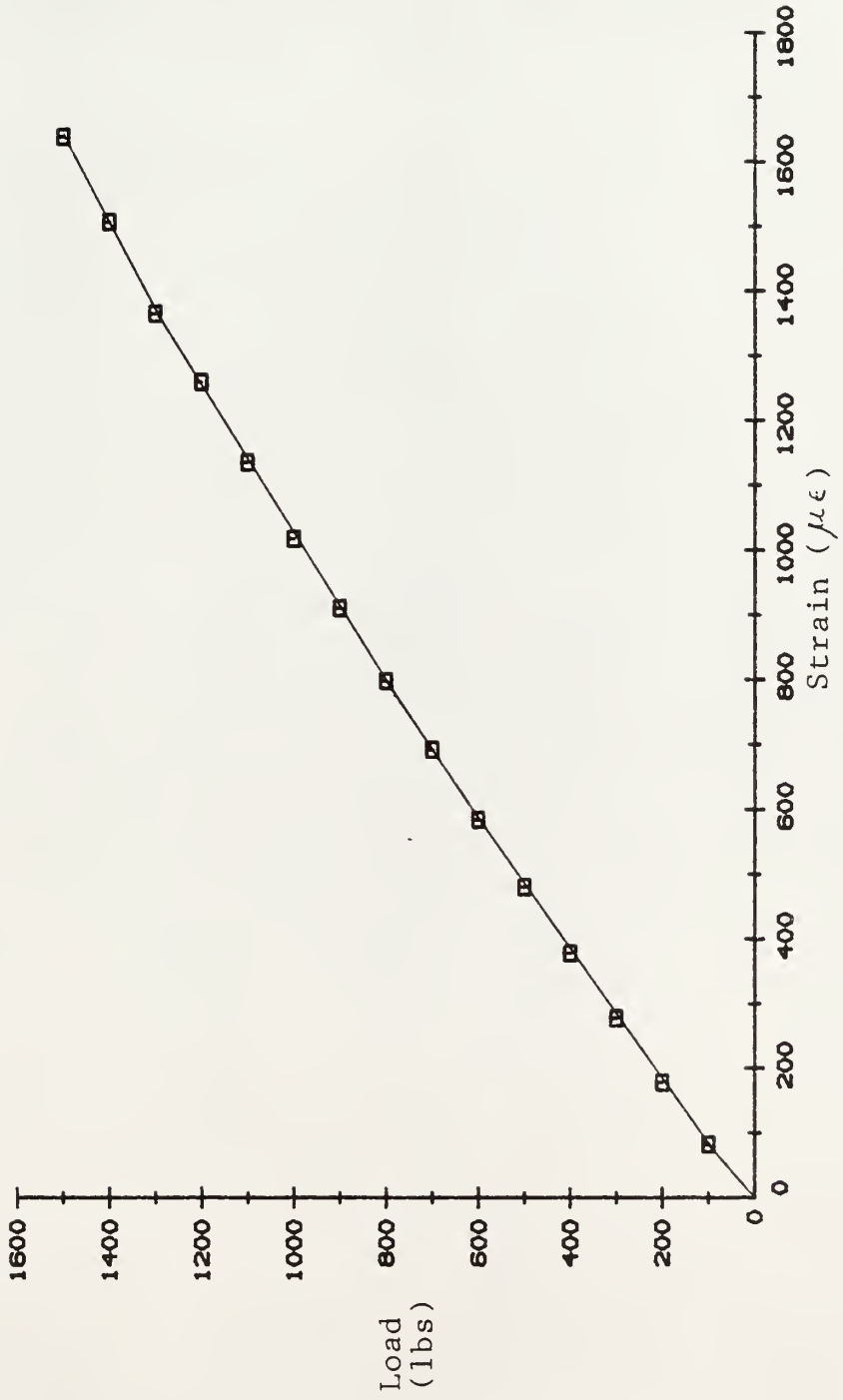


Figure 43 Off-Axis Shear Test, Load vs. Strain, Gage #1

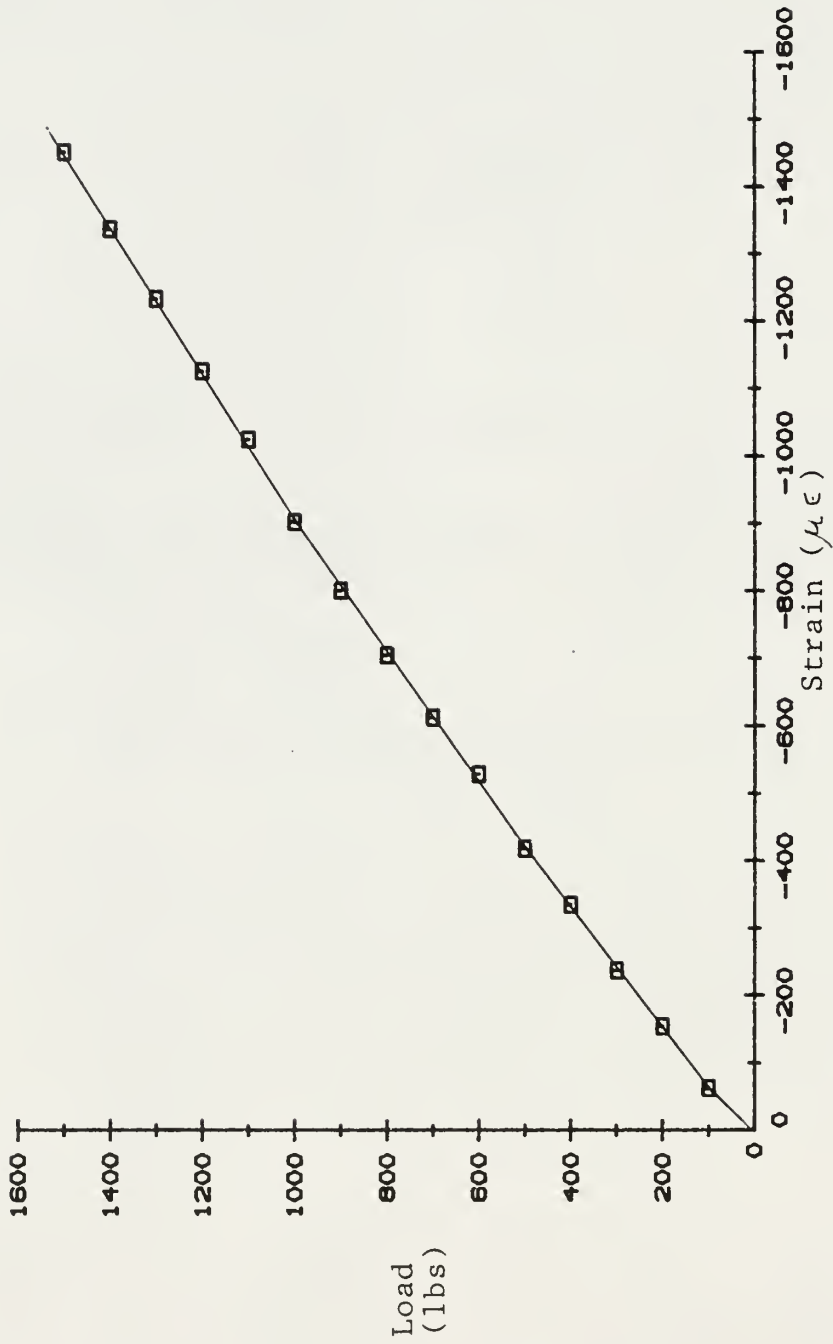


Figure 44 Off-Axis Shear Test, Load vs. Strain, Gage #3

the principal strains, the following results were obtained:

On-axis specimen:  $\gamma_{\max} = 3615\mu\epsilon$  w/1000 lb load

Off-axis specimen:  $\gamma_{\max} = 1654\mu\epsilon$  w/900 lb load

The shear modulus was then calculated from the equations

$$G = \frac{\tau}{\gamma_{\max}}, \text{ and } \tau = \frac{P}{tL} \quad (6), (7)$$

where  $\tau$  = shear stress (psi)

P = load (lbs)

t = specimen thickness (in.)

L = length of specimen (in.)

After substituting in the proper values, the following results were obtained:

$$G_{xy} = 2.96 \times 10^5 \text{ psi}$$

$$G_{yx} = 5.81 \times 10^5 \text{ psi}$$

The larger value for  $G_{yx}$  could be expected since a greater force is required to cause a transverse shearing of the glass fibers in the X-X direction than would be required to produce shear between the matrix and the fibers in this direction.

#### TRANSFORMATION OF PROPERTIES

Now that all of the on-axis elastic properties have been found for each of the two principal fiber

directions, the off-axis elastic properties must be found for the angle at which the fiber reinforcement was rotated in the box beam ( $\pm 10^\circ$ ). To do this, the method of compliance transformation developed by Tsai and Hahn [9] was used. This method uses the power functions of  $\sin\theta$  and  $\cos\theta$ ,  $\theta$  being the angle of rotation from the principal (X) axis direction. The process is represented in matrix form as

$$\begin{Bmatrix} S_{11} \\ S_{22} \\ S_{12} \\ S_{66} \\ S_{16} \\ S_{26} \end{Bmatrix} = \begin{bmatrix} m^4 & n^4 & 2m^2n^2 & m^2n^2 \\ n^4 & m^4 & 2m^2n^2 & m^2n^2 \\ m^2n^2 & m^2n^2 & m^4 + n^4 & -m^2n^2 \\ 4m^2n^2 & 4m^2n^2 & -8m^2n^2 & (m^2 - n^2)^2 \\ 2m^3n & -2mn^3 & 2(mn^3 - m^3n) & mn^3 - m^3n \\ 2mn^3 & -2m^3n & 2(m^3n - mn^3) & m^3n - mn^3 \end{bmatrix} \begin{Bmatrix} S_{xx} \\ S_{yy} \\ S_{xy} \\ S_{ss} \end{Bmatrix} \quad (8)$$

$$\text{where } S_{11} = \frac{1}{E_1}$$

$$S_{22} = \frac{1}{E_2}$$

$$S_{12} = -\frac{\nu_2}{E_2}$$

$$S_{66} = \frac{1}{G_{12}}$$

$S_{16}, S_{26}$  = normal coupling coefficients

$$m = \cos \theta \quad (\theta = \pm 10, \text{ depending on layer})$$

$$n = \sin \theta \quad (\theta = \pm 10, \text{ depending on layer})$$

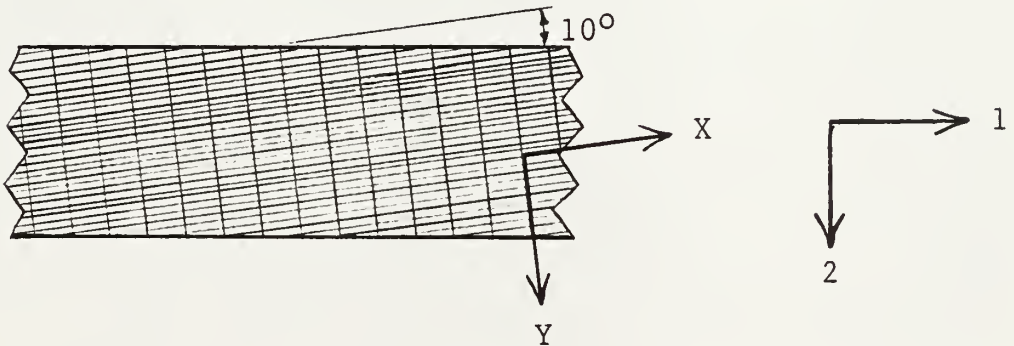
$$S_{xx} = \frac{1}{E_x} = \frac{1}{2.513 \times 10^6} = 3.979 \times 10^{-7}$$

$$S_{YY} = \frac{1}{E_y} = \frac{1}{1.586 \times 10^6} = 6.305 \times 10^{-7}$$

$$S_{xy} = -\frac{\nu_x}{E_x} = -\frac{0.165}{2.513 \times 10^6} = -6.566 \times 10^{-8}$$

$$S_{ss} = \frac{1}{G_{xy}} = \frac{1}{2.96 \times 10^5} = 3.378 \times 10^{-6}$$

Figure 45 illustrates the axes orientations of the fiberglass reinforcement and the box beam.



Box Beam, top view (not to scale)

Figure 45 Fiberglass Reinforcement and Axes Orientations

After substituting in the proper values and performing the necessary operations, the following values were found:

$$S_{11} = 4.6978 \times 10^{-7}, \text{ or } E_1 = 2.129 \times 10^6 \text{ psi}$$

$$S_{22} = 6.8835 \times 10^{-7}, \text{ or } E_2 = 1.453 \times 10^6 \text{ psi}$$

$$S_{12} = -1.3053 \times 10^{-7}$$

$$S_{66} = 3.1185 \times 10^{-6}, \text{ or } G_{12} = 3.207 \times 10^5 \text{ psi}$$

$$S_{16} = -3.963 \times 10^{-7} \text{ (+}3.963 \times 10^{-7} \text{ for } -10^\circ \text{ rotation)}$$

$$S_{26} = 3.167 \times 10^{-7} \text{ (-}3.667 \times 10^{-7} \text{ for } -10^\circ \text{ rotation)}$$

In the box beam analysis, the transverse shear modulus  $G_{21}$  was also calculated. It was determined by transposing the values of  $S_{xx}$  and  $S_{yy}$ , substituting  $G_{yx}$  for  $G_{xy}$  in  $S_{ss}$ , and leaving  $S_{xy}$  unchanged since  $S_{yx}$  must equal  $S_{xy}$  for symmetry. The fourth order transformation matrix is unchanged, with the resulting operation yielding the following value:

$$S_{ss}' = 1.655 \times 10^{-6} \text{ or } G_{21} = 6.041 \times 10^5 \text{ psi}$$

This transverse shear modulus is the one which would determine the beam deflection due to shear in the vertical web or sides of the beam, as the resistance of the horizontal top and bottom would be negligible.

#### EXPERIMENTAL DETERMINATION OF BEAM DEFLECTIONS

The next step in the analysis was to find the deflection of the composite box beam due to a known load, and to plot this deflection versus load to determine whether the beam behaved in a linear elastic manner. If found to be true, then the principle of superposition could have been utilized in the analysis. The beam was loaded with the Riehle test machine as indicated in Figure 46. The beam's center deflection

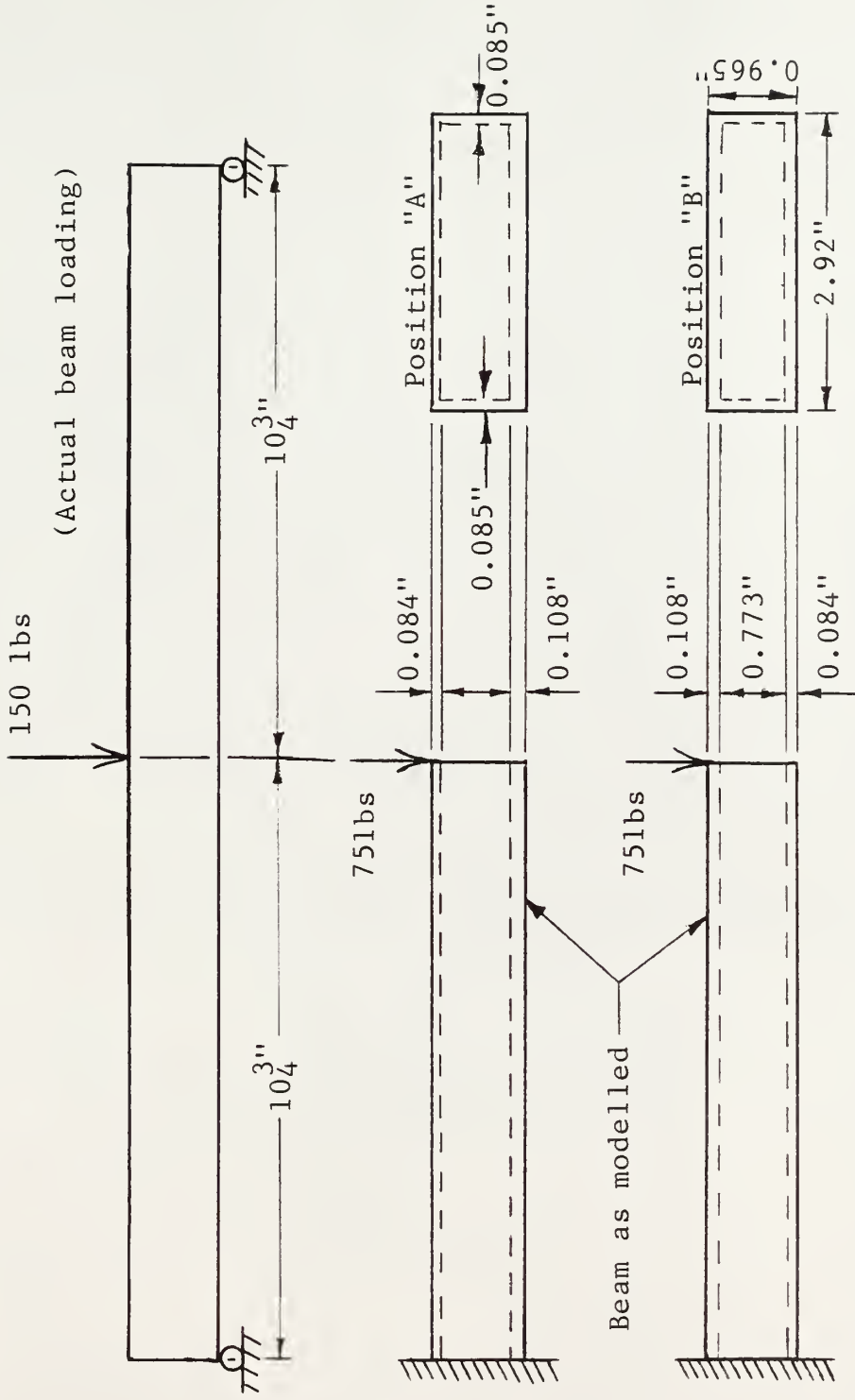


Figure 46 Box Beam Bending Positions

was measured to the nearest .001" with the Enco dial indicator mentioned previously. A plot of the load versus deflection is given in Figure 47 for the beam in Position "A". As this plot indicates, the beam did behave in a linear elastic manner within the applied load region. However, several minutes were required for the beam to recover the imposed deflection after the load was removed.

Since the beam was unsymmetric, it was loaded in both directions as indicated by positions "A" and "B" in Figure 46. The load versus deflection plot for loading in Position "B" is shown in Figure 48.

To simplify the solutions to this problem, this simply supported center loaded beam was modelled as an end loaded cantilever beam, as shown in Figure 46. In all computations, the center deflection for a 150 lb load is used, although for the cantilever model the equivalent end load would be 75 lbs to produce the same deflection. Although always behaving in Hookean fashion (linear elastic), the deflections varied too much from one test to another to be of any use. In six bending tests in each position, the measured deflections ranged from 0.163" to 0.176".

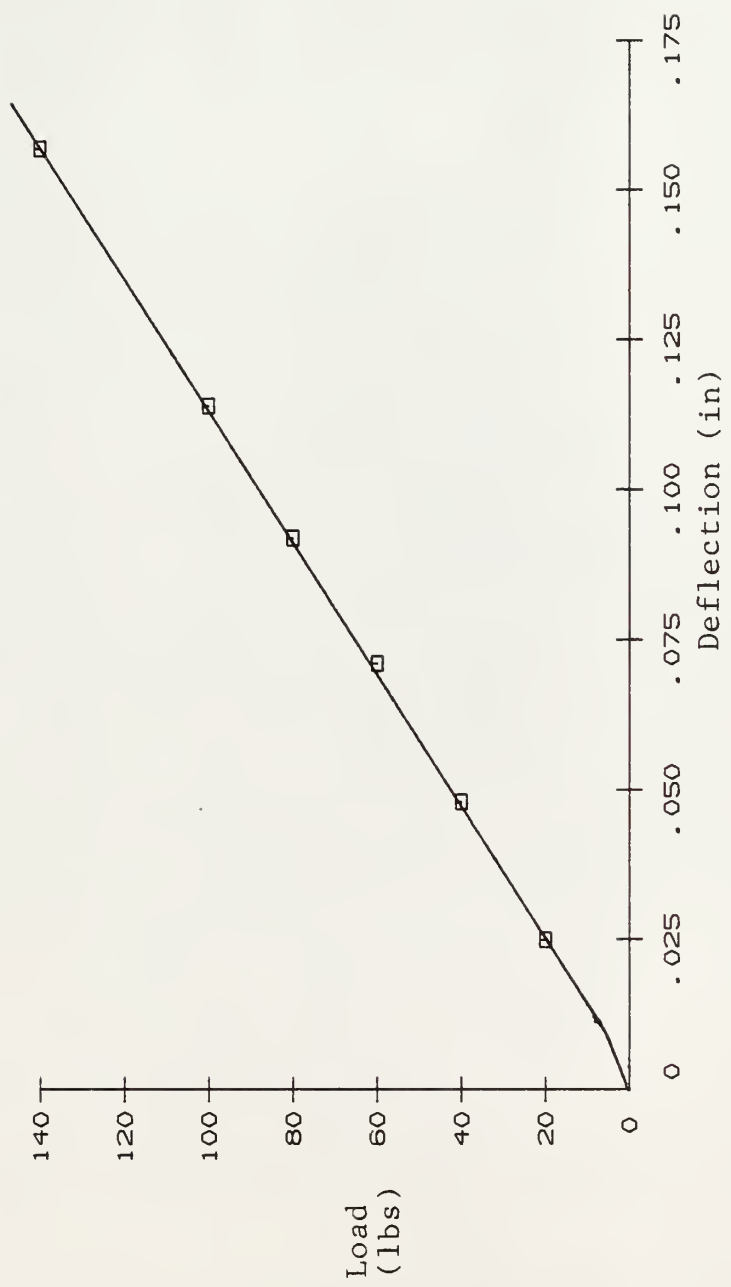


Figure 47 Box Beam Load vs. Deflection, Position "A"

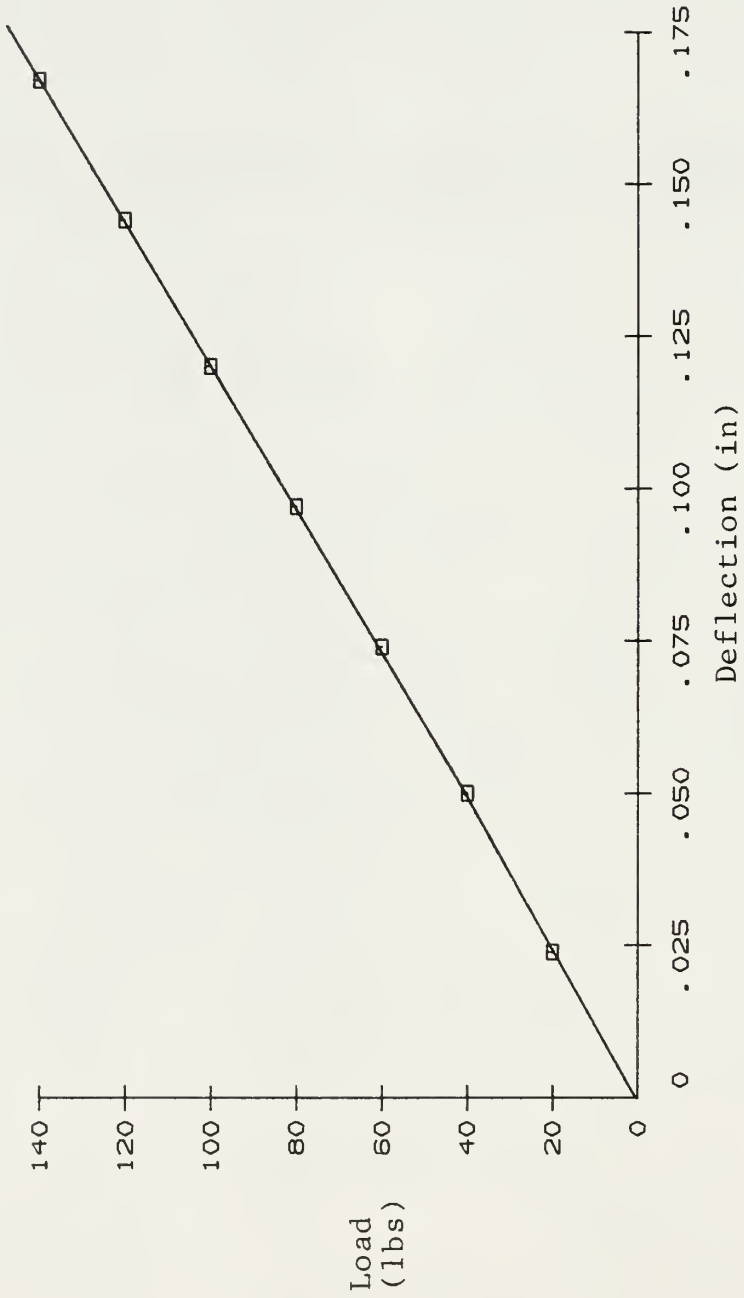


Figure 48 Box Beam Load vs. Deflection, Position "B"

THEORETICAL DETERMINATION OF COMPRESSIVE  
MODULUS OF ELASTICITY

The original plan involved the use of beam deflections and strain energy equations to find the compressive modulus of elasticity. However, since the measured deflections varied excessively from one test to another, a different approach had to be employed. The method which was used employs the principle that the sum of the first moments multiplied by their respective moduli of elasticity for the tension and compression portions of the beam must equal zero [10]. This can be written as

$$E_t \int_t y \, dA + E_c \int_c y \, dA = 0 \quad (9)$$

By using the appropriate known values, this equation becomes

$$2.129 \times 10^6 [.085(.965 - h)^2 + 2.750(.965 - h - t_1/2)] + E_c [.085 h^2 + 2.750 t_2(h - t_2/2)] = 0 \quad (10)$$

The unknown  $h$  is the distance from the bottom surface, in compression, to the neutral axis;  $t_1$  is the upper wall thickness while  $t_2$  is the lower wall thickness. By rearranging this equation, the value of  $E_c$  was obtained in terms of  $h$ . The value of  $h$ , and the location of the neutral axis, will be different for each of the two bending modes. However, the value of

$E_c$  should be the same in each case. Its value can then be found by using an iterative process for each bending mode and varying the value of  $h$ . When the two values of  $E_c$  are very close to being equal, then the correct value can be assumed to have been found. The values of  $E_c$  and  $h$  which were found in this manner were:

Position "A":  $h = 0.526"$

$$E_c = 2.057 \times 10^6 \text{ psi}$$

Position "B":  $h = 0.452"$

$$E_c = 2.060 \times 10^6 \text{ psi}$$

Each of these two positions represents one of the bending configurations of the box beam. Figure 46 illustrated the two positions. The difference in  $E_c$  between these two values is only 0.15%. In addition, this value is 96.7% of the experimentally determined value for the tensile modulus of elasticity, which is a reasonable proportion for a fiber-reinforced composite. This value also indicates that the previous assumption was correct regarding the abnormally low value of the modulus of elasticity in compression found by experimental methods.

## THEORETICAL BEAM STRESSES AND STRAINS

From the previously determined values of  $E_t$ ,  $E_c$ , and  $h$ , the theoretical strains can be readily calculated by using the appropriate formulas. The strains to be determined will be those maximum compressive and tensile strains on the lower and upper surfaces at the support of the cantilever beam, where their values will be maximized.

Prior to performing any strain calculations, the stresses must first be calculated. These are determined by the following two formulas for composite beams:

$$\sigma_t = \frac{M y E_t}{E_t I_t + E_c I_c}, \quad \sigma_c = \frac{M y E_c}{E_t I_t + E_c I_c} \quad (11), (12)$$

where  $M$  = moment (lb-in)

$y$  = distance from neutral axis (in)

$I$  = moment of inertia ( $\text{in}^4$ )

By using the values of  $h$ ,  $E_c$ , and  $E_t$  previously determined, the stresses can be calculated at the upper and lower surfaces of the beam. The results are listed in Table 1.

Table 1. Theoretical Beam Stresses

	Compression	Tension
Position "A"	3743 psi	3233 psi
Position "B"	3209 psi	3764 psi

From these stresses, the strains could be easily calculated since uniaxial stress were assumed. The strains are found by using the equation  $\epsilon = \frac{\sigma}{E}$ . By using this equation and the stresses just calculated, the strains were found and are listed in Table 2.

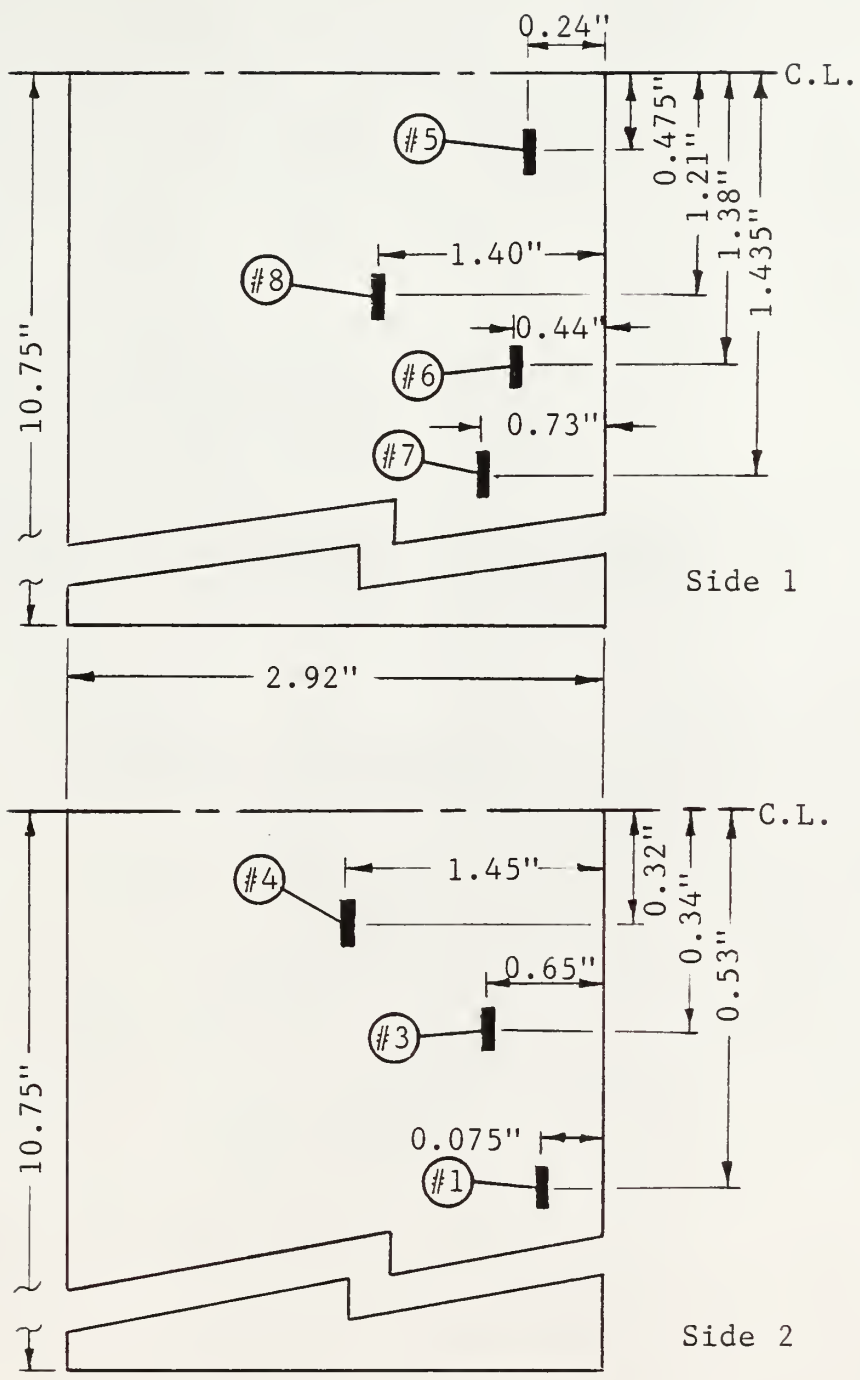
Table 2. Theoretical Beam Strains

	Compression ( $\mu\epsilon$ )	Tension ( $\mu\epsilon$ )
Position "A"	1819	1519
Position "B"	1558	1768

#### EXPERIMENTAL BEAM STRAIN

The next step involved evaluating the actual strain on the beam's surfaces by the use of strain gages. The gages are of the same type, length, etc. as those used previously on the test specimens. Since the beam was loaded in both positions, none of the gages could be located in the center of the actual beam, where the stresses and strains would be maximized. Their actual locations are depicted in Figure 49, although they weren't necessarily all on the same side of the beam's centerline, as shown in this figure.

Since the strain at the center of the beam is desired, the measured strain values must be multiplied



(Not to scale)

Figure 49 Box Beam Strain Gage Locations

by an appropriate correction factor to get the extrapolated strain value on the beam centerline. Since the stress and strain vary linearly from zero at the outer end to a maximum value in the center, the factors were determined solely on the distances shown in Figure 49. The factors were determined according to the equation

$$R = \frac{10.75}{10.75 - a} \quad (13)$$

where R = multiplying factor (dimensionless)

a = gage distance from centerline (in)

Each of the factors which were determined from this formula are listed in Table 3 below.

Table 3. Strain Gage Multiplying Factors

Gage No.	a	R
1	0.53"	1.052
3	0.34"	1.033
4	0.32"	1.031
5	0.475"	1.046
6	1.38"	1.147
7	1.435"	1.154
8	1.21"	1.127

Strain Gage No. 2 produced erroneous readings, so they were discarded. Plots of the load versus strain for each strain gage and for each bending mode are given in Figures 50-55. The actual strain values and the centerline converted strain values for each strain gage are given in Table 4 for bending in Position "A" and in Table 5 for bending in Position "B".

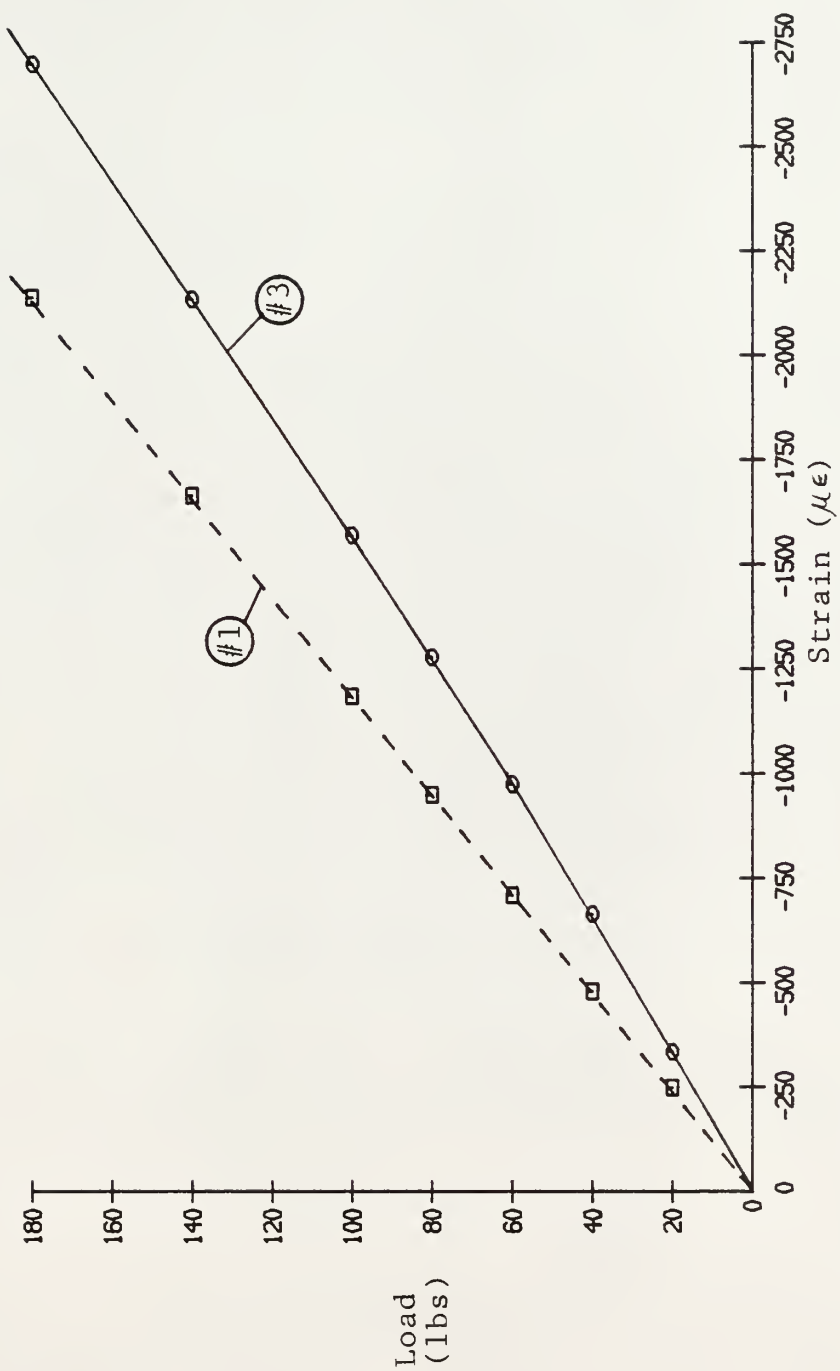


Figure 50 Box Beam, Position "A" Load vs. Strain, Gages #1, #3

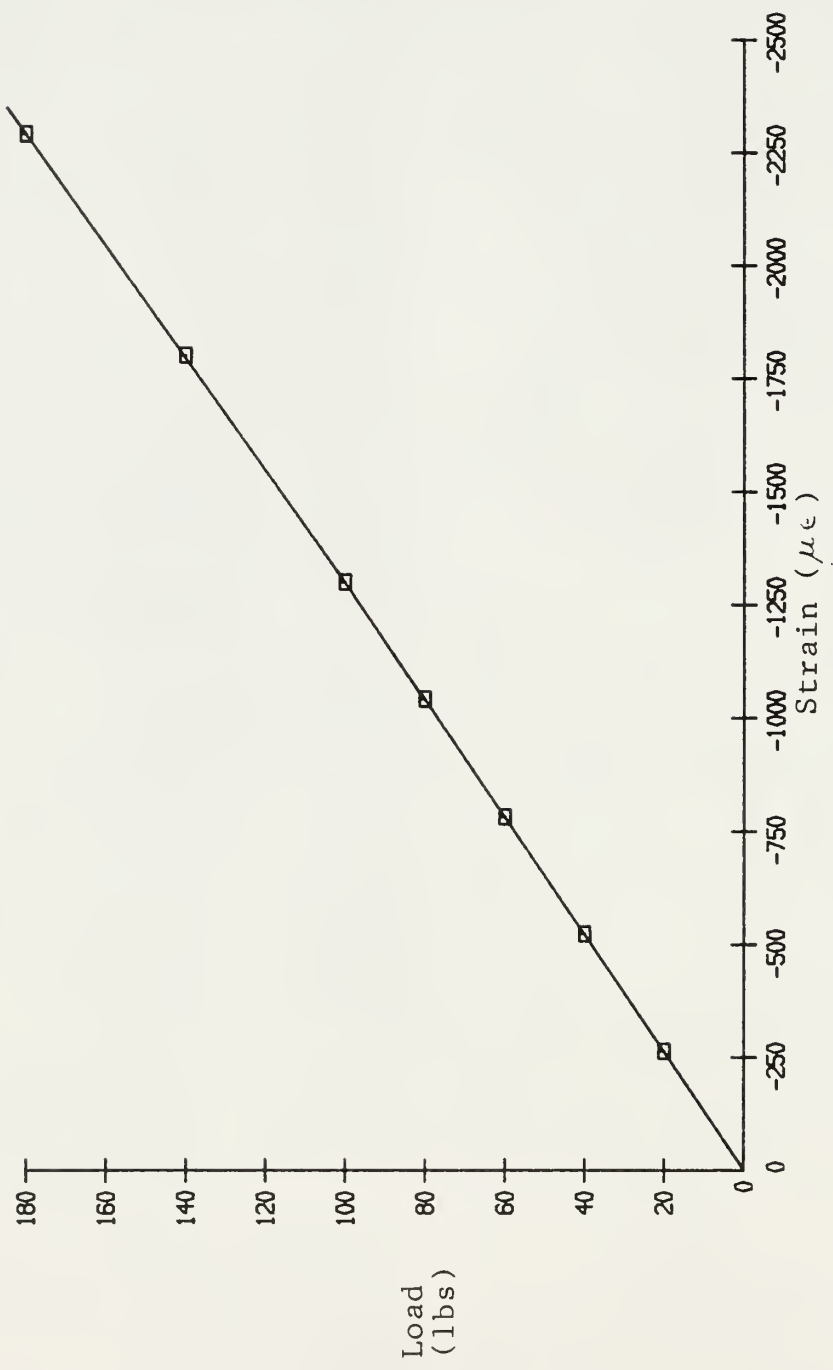


Figure 51 Box Beam, Position "A" Load vs. Strain, Gage #4

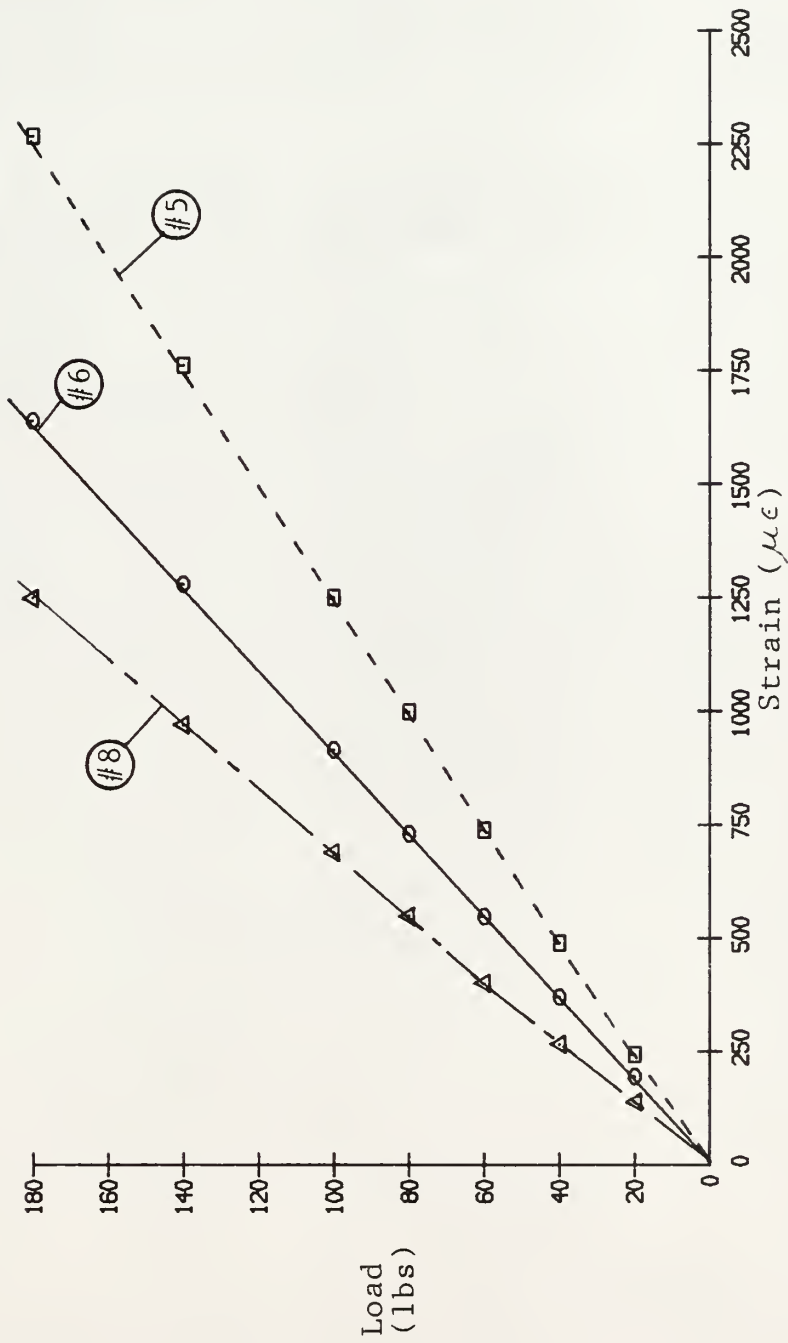


Figure 52 Box Beam, Position "A" Load vs. Strain, Gages #5, #6, #8

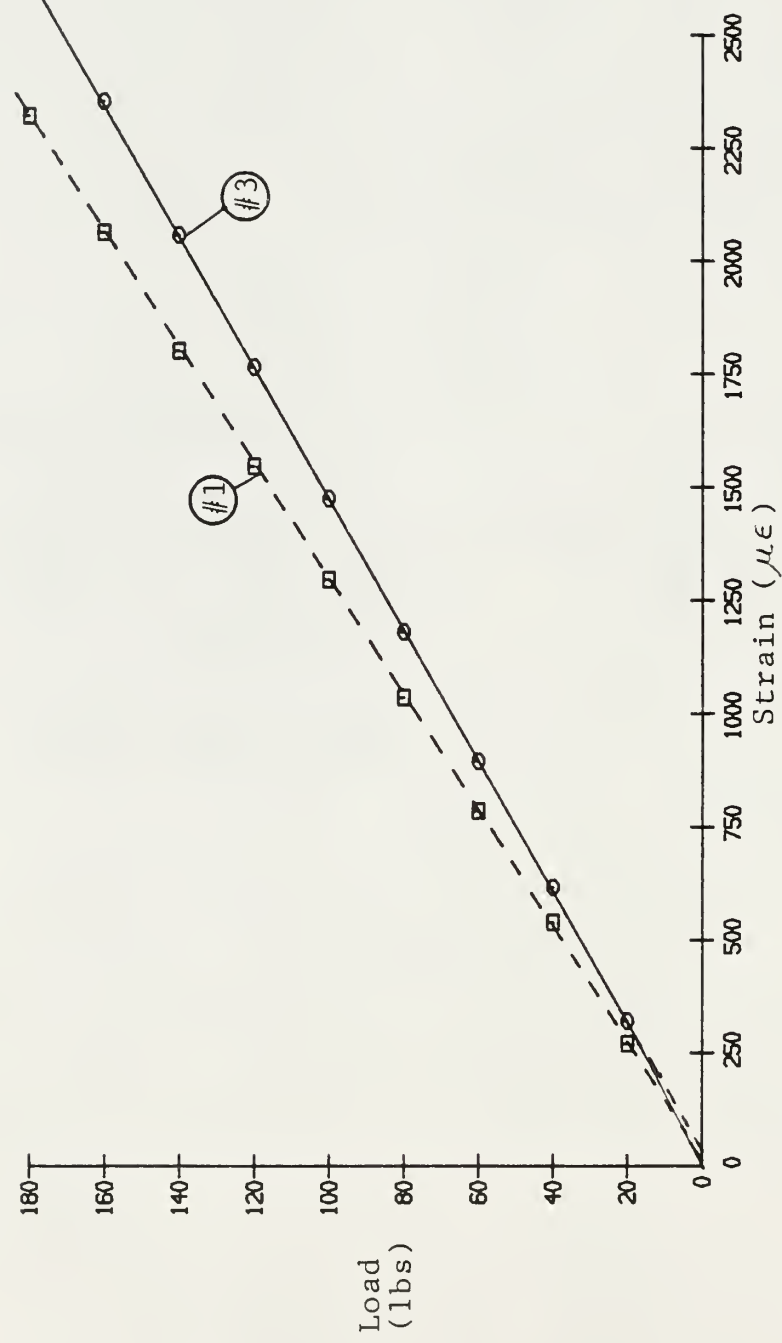


Figure 53 Box Beam, Position "B" Load vs. Strain, Gages #1, #3

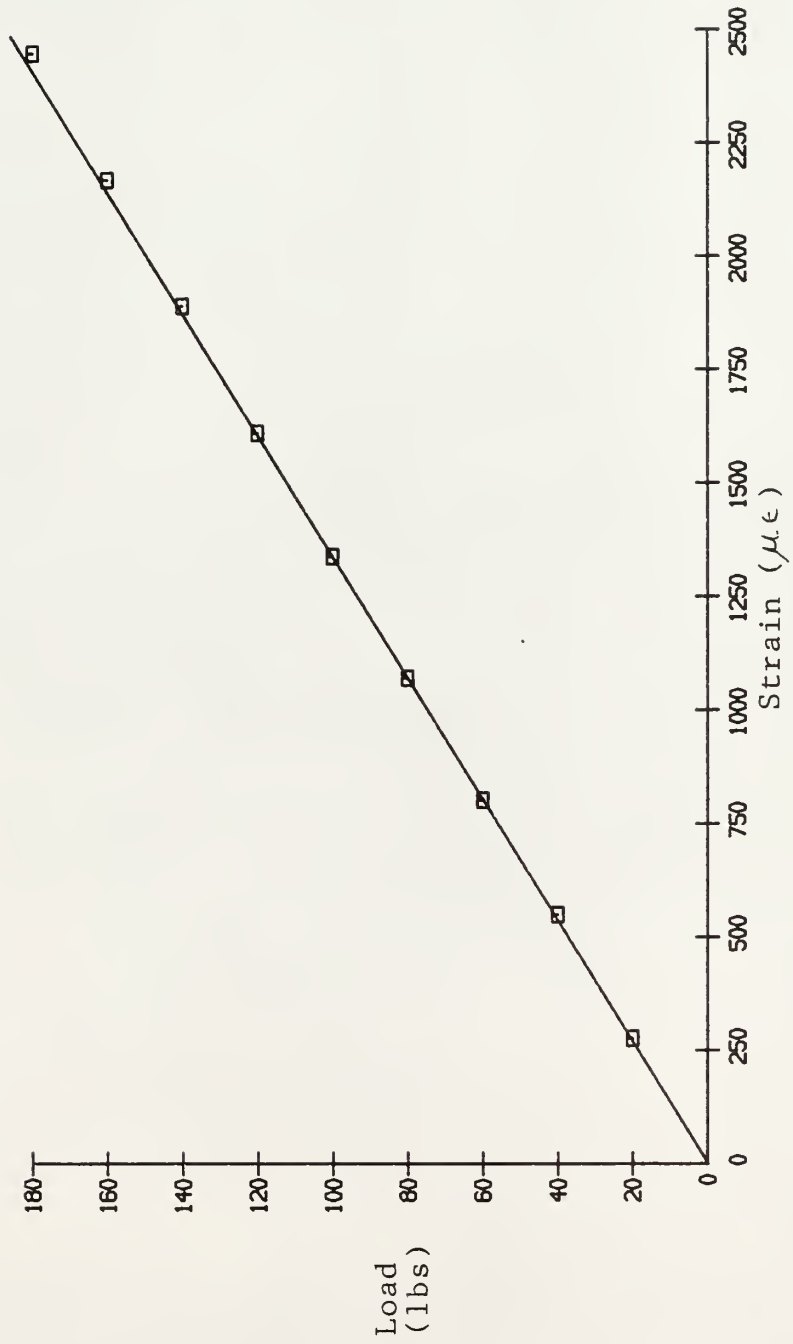


Figure 54 Box Beam, Position "B" Load vs. Strain, Gage #4

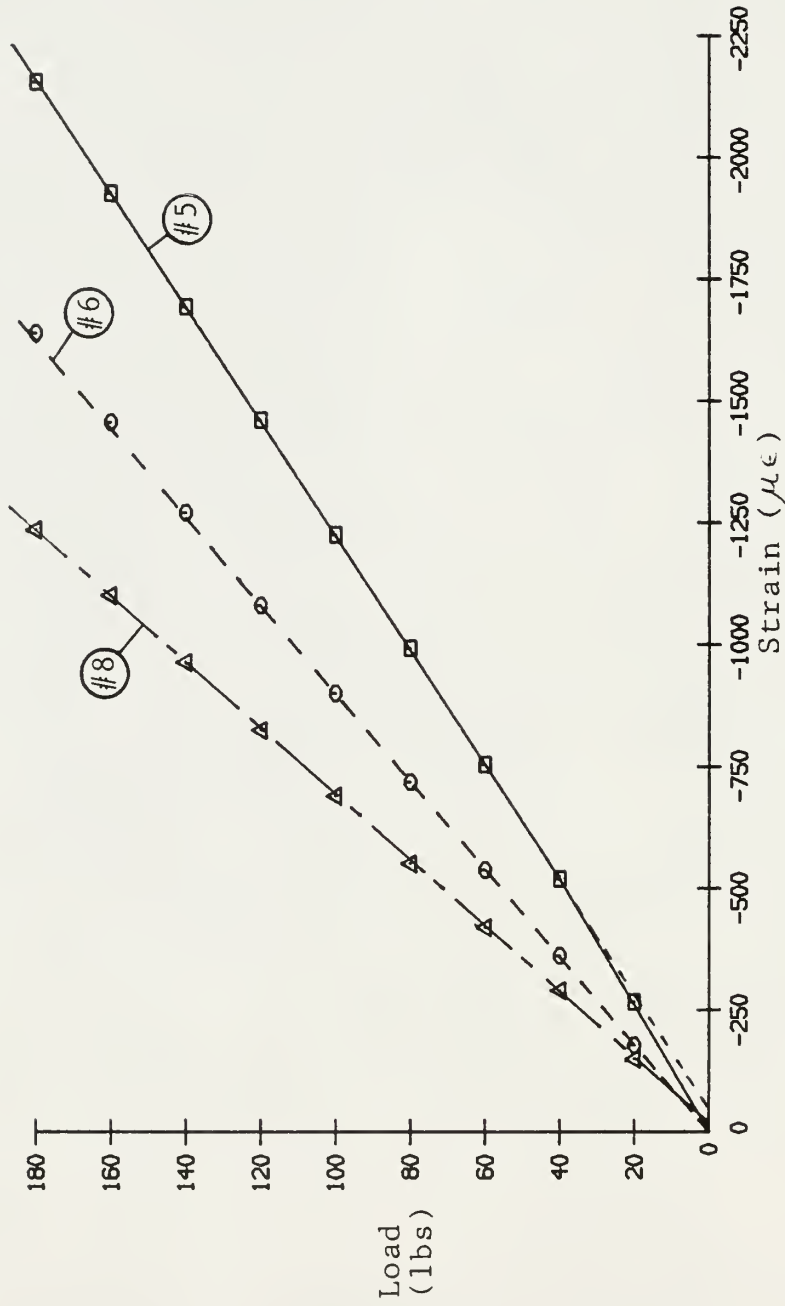


Figure 55 Box Beam, Position "B" Load vs. Strain, Gages #5, #6, #8

Table 4. Strains for Position "A"

Gage No.	Actual Strain ( $\mu\epsilon$ )	R	Centerline Strain ( $\mu\epsilon$ )
1	-1781	1.052	-1874
3	-2375	1.033	-2453
4	-1913	1.031	-1972
5	-1875	1.046	1961
6	1355	1.147	1554
7	1333	1.154	1538
8	1026	1.127	1156

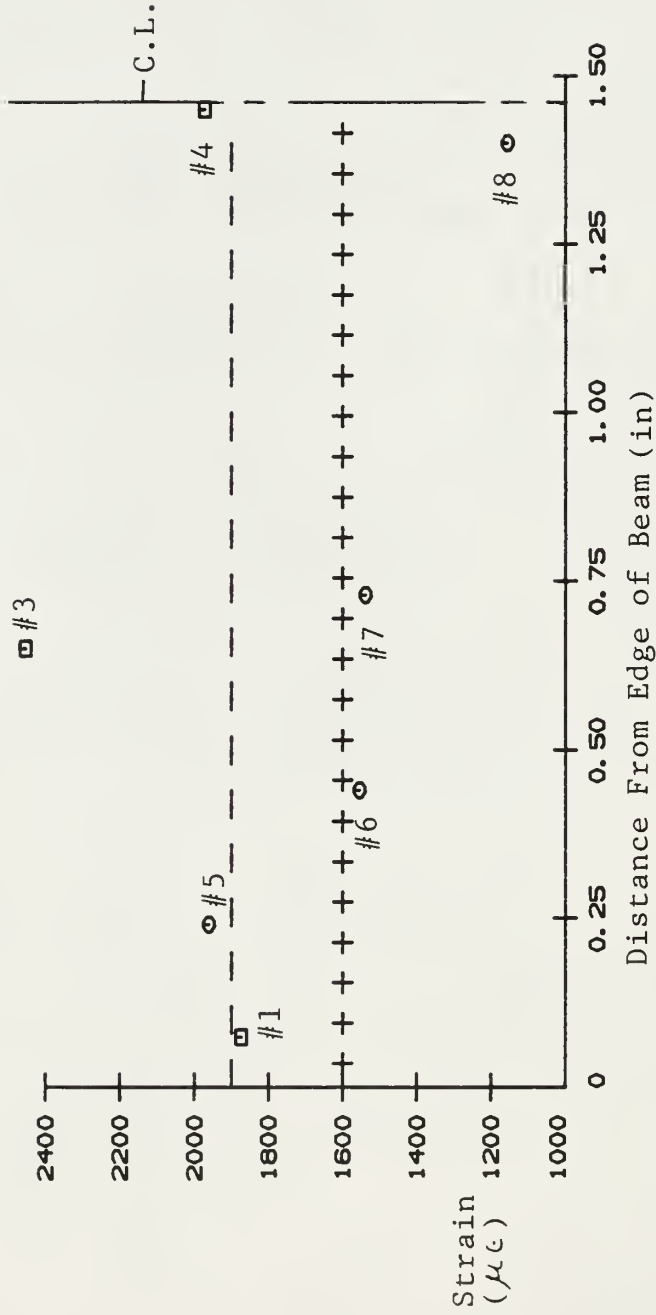
Table 5. Strains for Position "B"

Gage No.	Actual Strain ( $\mu\epsilon$ )	R	Centerline Strain ( $\mu\epsilon$ )
1	1903	1.052	2002
3	2160	1.033	2231
4	2019	1.031	2082
5	-1760	1.046	-1841
6	-1364	1.147	-1565
7	-1368	1.154	-1578
8	-1011	1.127	-1139

These strains are plotted in Figures 56 and 57. Due to symmetry, only one side of the beam's longitudinal axis needs to be shown.

#### SHEAR LAG EFFECT ON BEAM STRAIN MEASUREMENTS

In the ideal case, and the one which is presumed by the elementary beam theory, the normal stresses and strains across the width of a rectangular beam subjected to a load such as the one in this analysis would not vary across the width of the



Legend: o = Tension Strain  
 □ = Compression Strain

Figure 56 Box Beam Strain vs. Gage Location, Position "A"

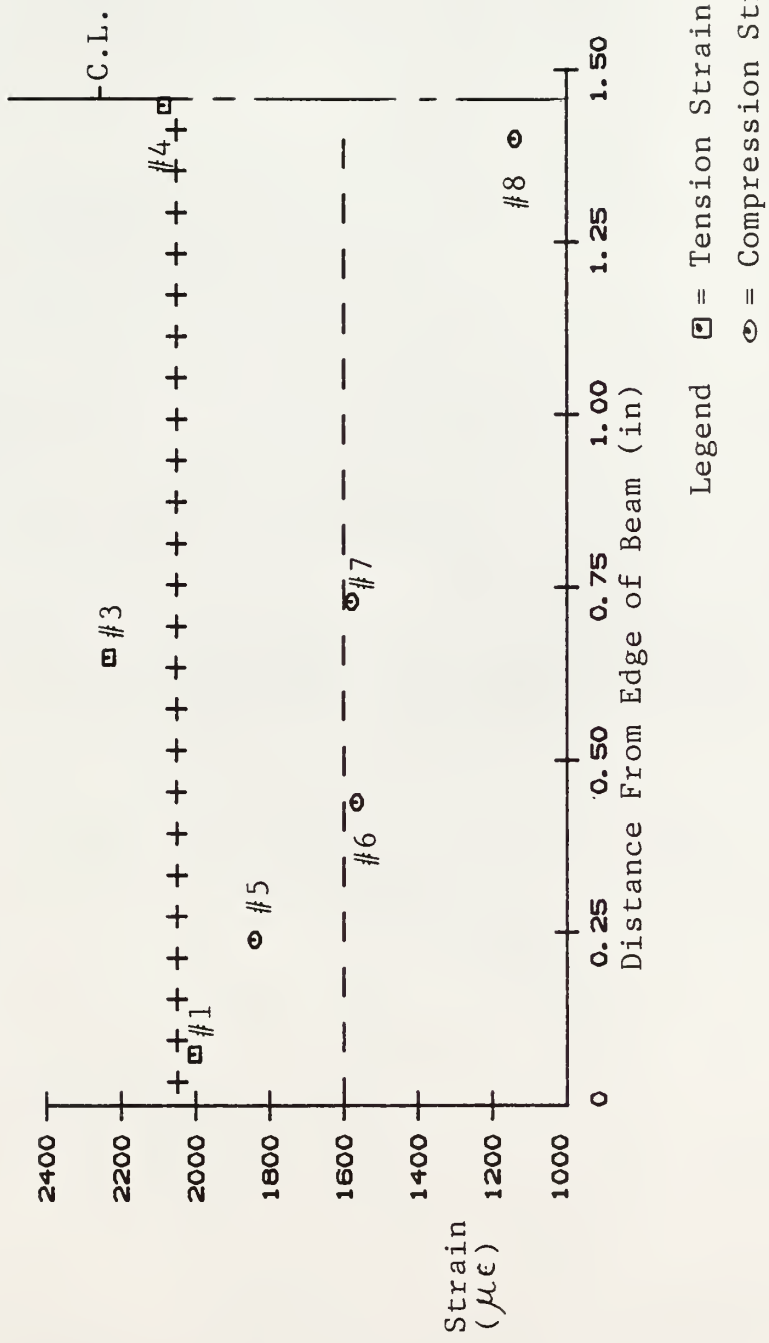


Figure 57 Box Beam Strain vs. Gage Location, Position "B"

beam. In reality, however, the stresses (and strains) will vary from a maximum on each side to a minimum in the middle of the beam, as shown in Figure 58. This phenomenon is known as shear lag. Shear lag is caused by the fact that the normal stresses in both the upper and lower wall sections are transmitted to them by the shear stress in the vertical side walls of the box beam.

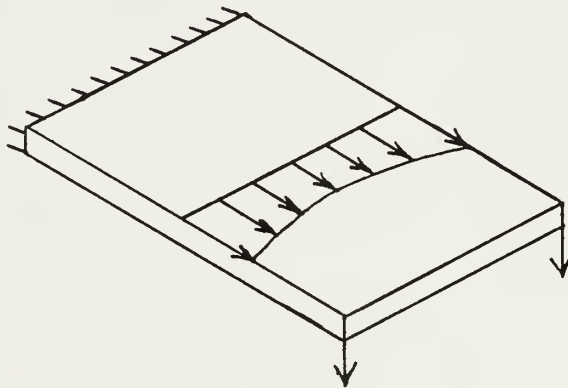


Figure 58 Shear Lag

Since the middle of a center loaded, simply supported beam and the area where a cantilevered beam is fixed cannot experience this shear deformation, the shear lag phenomenon will be non-existent in this area but will gradually increase as the distance from this area increases. This can be seen on Figures 59 and 60.

To verify the presence of shear lag and its effect on the strain gage readings, a brittle coating

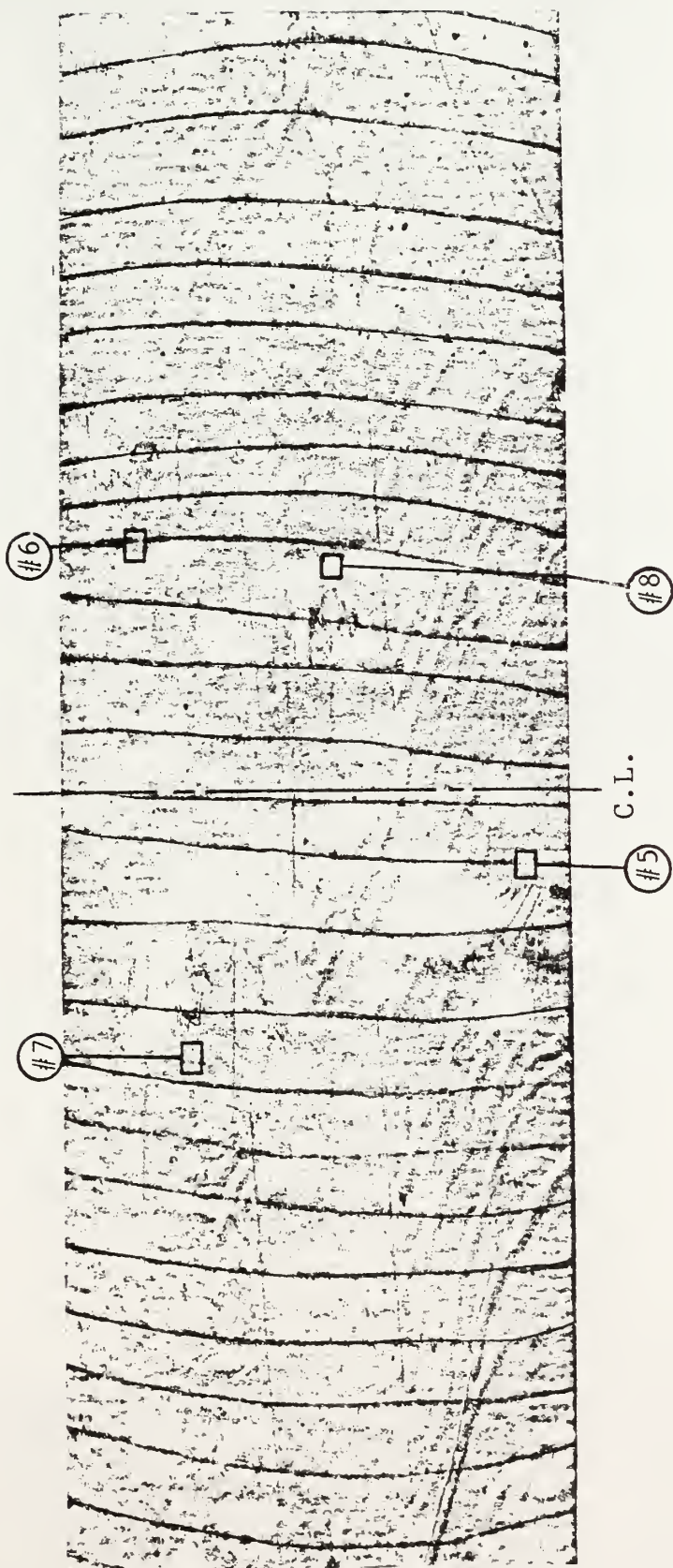


Figure 59 Side 1 Brittle Coating

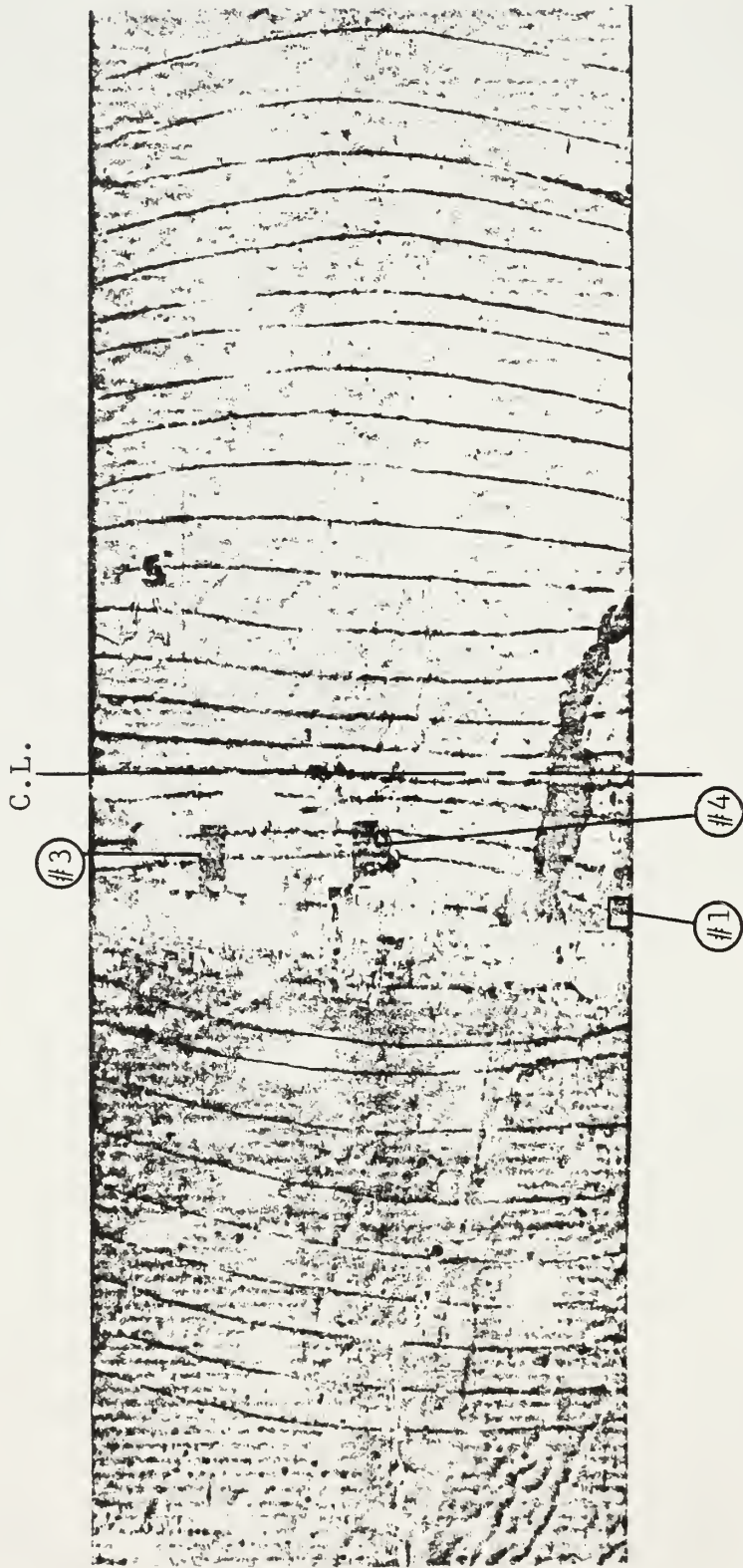


Figure 60 Side 2 Brittle Coating

analysis was employed to get a qualitative look at its effect. This was done after all of the other testing had been completed. The first step consisted of applying an aluminum undercoating, Tens-lac Type UN-10-A, and then applying the brittle coating, which was Tens-lac Type TL-500-75A lacquer, both of which are products of Measurements Group, Inc. After allowed to dry, the beam was loaded in the same manner as before, except that no quantitative data was recorded. Figure 59 shows side 1 of the beam and Figure 60 shows side 2. Since the cracks were too small to be easily visible, a felt tip pen was used to mark some of the stress crack lines. The curves shown represent isostatic lines, which are lines of constant stress. As already mentioned, these lines are generally straight in the middle of the actual beam, where shear lag would not be present. As the distance from the center of the beam increases, this phenomenon gradually increases until the isostatic lines look like arcs of a circle at some distance from the middle of the beam.

## Chapter III

### RESULTS AND CONCLUSIONS

#### RESULTS

Upon looking again at Figures 56 and 57, it can be seen that lines have been drawn which represent an approximation to the average strain gage readings which were recorded during beam loading. However, the lines were adjusted based upon whether the gage readings appeared to be somewhat low or high based on the brittle coating analysis. These lines can't be considered accurate representations of the true average strain across the width of the beam, but do provide some idea of the approximate average value. The resulting values are summarized in Table 6 below.

Table 6. Comparison of Strain Values

Loading Position	Theoretical Strain ( $\mu\epsilon$ )	Average of Strain Gage Measurements ( $\mu\epsilon$ )	Difference (% of Theoretical)
A (Tens.)	1519	1600	5.3%
A (Comp.)	1819	1900	4.5%
B (Tens.)	1768	2050	16.0%
B (Comp.)	1558	1600	2.7%

As can be seen from the data in this table, there is generally good agreement, except in Loading Position "B" on the tension side of the beam.

The dispersion of the strain gage readings can most likely be attributed to imperfections in the beam's wall due to the hand layup process. As mentioned in the Introduction, these are very difficult to avoid in a hand layup procedure where the wet resin-impregnated cloth must be handled. These problems can be avoided by using a form of fibers in which the fibers have been impregnated with resin by the manufacturer. The resin has also been partially cured (B-staged) by the manufacturer, so many of the problems associated with handling a sticky material are eliminated. These materials are known as pre-pregs.

Another problem which was encountered in this project was the difficulty in obtaining reliable experimental values for use in determining the compressive modulus of elasticity. Other methods would need to be utilized, as the ASTM Standard used in this analysis certainly did not produce satisfactory results.

#### CONCLUSIONS

Finally, the results of this research indicate the necessity of using experimental techniques when

using a composite material which has been fabricated by hand or one for which the physical properties aren't known. The problems with using a material which was manually fabricated were readily observed in this project. Since the walls of this box beam were thin and imperfections in them were present, the brittle coating analysis proved to be very helpful in locating anomalies in the walls, which adversely affected the accuracy of the strain gage readings.

This research also suggests that reasonably good comparisons can be obtained between experimental techniques and theoretical analyses of composite materials. Since the properties of FRP are dependent upon a number of factors, it is important to use whatever techniques are available to obtain the elastic properties in the directions of the stresses in a structure which contains composite materials. Any additional measures which can provide information critical to the analysis should also be utilized.

## Chapter IV

### SELECTED BIBLIOGRAPHY

1. Jones, R.M., Mechanics of Composite Materials, Scripta Book Company, Washington, D.C., 1975, pp. 53-56.
2. Lekhnitski, S.G., Theory of Elasticity of an Anisotropic Body, Holden-Day, San Francisco, California, 1963.
3. 1988 Annual Book of ASTM Standards, Volume 15.03, pp. 117-121.
4. 1988 Annual Book of ASTM Standards, Volume 8.01, pp. 280-89.
5. Whitney, J.M., Daniel, I.M., and Pipes, R.B., Experimental Mechanics of Fiber Reinforced Composite Materials, Society for Experimental Stress Analysis, Englewood Cliffs, New Jersey, 1982.
6. 1988 Annual Book of ASTM Standards, Volume 8.01, pp. 199-204.
7. 1988 Annual Book of ASTM Standards, Volume 15.03, pp. 195-204.
8. Dally, J.W., and Riley, W.F., Experimental Stress Analysis, McGraw-Hill Book Company, 1978, pp. 321-23.
9. Tsai, S.W., and Hahn, H.T., Introduction to Composite Materials, Technomic Publishing Company, Westport, Connecticut, 1980, pp. 88-91.
10. Gere, J.M., and Timoshenko, S.P., Mechanics of Materials, 2nd. edition, PWS Publishers, Boston, Massachusetts, 1984, pp. 249-50.

Chapter V

APPENDIX

Table 7. X Axis Tension Test, Specimen No. 1

Load (lbs)	Strain ( $\mu \epsilon$ )			
	Gage #1	Gage #2	Gage #3	Gage #4
100	-65	360	418	260
200	-128	716	778	548
300	-200	1087	1180	834
400	-251	1500	1600	1089
500	-300	1860	2004	1412
600	-368	2260	2340	1736
700	-407	2637	2890	2090
800	-472	3020	3285	2448
900	-513	3415	3693	2800
1000	-562	3720	4144	3160
1100	-602	4450	4630	3590
1200	-668	4514	5010	3940
1300	-714	4820	5382	4300

Table 8. X Axis Tension Test, Specimen No. 2

Load (lbs)	Strain ( $\mu \epsilon$ )		
	Gage #1	Gage #2	Gage #4
100	-54	454	285
200	-119	814	654
300	-187	1154	1023
400	-255	1495	1424
500	-324	1830	1848
600	-404	2208	2242
700	-442	2598	2608
800	-530	3000	3008
900	-568	3368	3402
1000	-652	3770	3798
1100	-688	4152	4190
1200	-771	4554	4620
1300	-820	4932	5028

Table 9. X Axis Tension Test, Specimen No. 3

Load (lbs)	Strain ( $\mu \epsilon$ )		
	Gage #1	Gage #3	Gage #4
100	316	-65	310
200	632	-122	644
300	930	-176	1022
400	1272	-227	1410
500	1600	-278	1800
600	1943	-346	2172
700	2268	-378	2574
800	2610	-452	2940

Table 10. Y Axis Tension Test, Specimen No. 4

Load (lbs)	Strain ( $\mu \epsilon$ )	
	Gage #1	Gage #2
100	257	-43
200	502	-83
300	756	-117
400	1054	-167
500	1362	-204
600	1687	-239
700	2069	-273
800	2417	-304
900	2804	-347
1000	3163	-381
1100	3534	-420
1200	3950	-458
1300	4326	-492
1400	4733	-533
1500	5117	-562

Table 11. Y Axis Tension Test, Specimen No. 5

Load (lbs)	Strain ( $\mu\epsilon$ )	
	Gage #1	Gage #2
100	244	-26
200	562	-53
300	941	-85
400	1340	-126
500	1747	-158
600	2164	-188
700	2581	-213
800	2964	-241
900	3318	-263
1000	3598	-282
1100	4112	-302
1200	4498	-323
1300	4934	-337
1400	5302	-354
1500	5728	-369

Table 12. Y Axis Tension Test, Specimen No. 6

Load (lbs)	Strain ( $\mu\epsilon$ )	
	Gage #1	Gage #2
100	348	-41
200	652	-93
300	976	-130
400	1290	-164
500	1624	-208
600	2018	-248
700	2390	-278
800	2742	-321
900	3141	-368
1000	3558	-411
1100	3950	-458
1200	4351	-500
1300	4792	-558
1400	5176	-593
1500	5626	-646

Table 13. X Axis Flexure Test, Specimen No. 7

Load (lbs)	Deflection (in)
20	0.042
40	.089
60	.135
80	.182
100	.239
120	.274
140	.330
160	.395
180	0.463

Table 14. X Axis Flexure Test, Specimen No. 8

Load (lbs)	Deflection (in)
20	0.046
40	.096
60	.145
80	.191
100	.237
120	.283
140	.338
160	.395
180	0.488

Table 15. X Axis Flexure Test, Specimen No. 9

Load (lbs)	Deflection (in)
20	0.047
40	.096
60	.144
80	.190
100	.235
120	.280
140	.334
160	.393
180	0.455

Table 16. X Axis Flexure Test, Specimen No. 10

Load (lbs)	Deflection (in)
20	0.046
40	.095
60	.143
80	.187
100	.231
120	.278
140	.333
160	.391
180	0.464

Table 17. X Axis Flexure Test, Specimen No. 11

Load (lbs)	Deflection (in)
20	0.047
40	.098
60	.147
80	.192
100	.238
120	.282
140	.331
160	.386
180	0.456

Table 18. Y Axis Flexure Test, Specimen No. 12

Load (lbs)	Deflection (in)
20	0.056
40	.121
60	.179
80	.237
100	.298
120	.363
140	.434
160	.514
180	0.592

Table 19. Y Axis Flexure Test, Specimen No. 13

Load (lbs)	Deflection (in)
20	0.060
40	.125
60	.190
80	.256
100	.320
120	.400
140	.476
160	.565
180	0.654

Table 20. Y Axis Flexure Test, Specimen No. 14

Load (lbs)	Deflection (in)
20	0.062
40	.129
60	.193
80	.256
100	.320
120	.396
140	.472
160	0.572

Table 21. X Axis Compression Test, Specimen No. 15

Load (lbs)	Deflection (in)	Strain ( $\Delta L/L$ )
100	0.016	0.026
200	.019	.031
300	.020	.033
400	.021	.034
500	0.022	0.036

Table 22. X Axis Compression Test, Specimen No. 16

Load (lbs)	Deflection (in)	Strain ( $\Delta L/L$ )
50	0.004	0.0066
100	.006	.0099
150	.007	.0115
200	.008	.0134
250	.009	.0148
300	.010	.0165
350	.011	.0180
400	.011	.0183
500	0.012	0.0198

Table 23. X Axis Compression Test, Specimen No. 17

Load (lbs)	Deflection (in)	Strain ( $\Delta L/L$ )
50	0.006	0.0094
100	.007	.0120
150	.009	.0145
200	.010	.0162
250	.011	.0179
300	.011	.0188
350	.012	.0205
400	.012	.0209
450	.013	.0222
500	.014	.0239
600	0.015	0.0256

Table 24. X Axis Compression Test, Specimen No. 18

Load (lbs)	Deflection (in)	Strain ( $\Delta L/L$ )
50	0.002	0.0024
100	.003	.0047
150	.004	.0067
200	.005	.0081
250	.006	.0097
300	.007	.0126
350	.009	.0138
400	.010	.0149
450	.011	.0165
500	.012	.0189
600	0.013	0.0204

Table 25. X Axis Compression Test, Specimen No.19

Load (lbs)	Deflection (in)	Strain ( $\Delta L/L$ )
50	0.004	0.0058
100	.005	.0075
150	.005	.0087
200	.006	.0099
250	.007	.0116
300	.007	.0119
350	.008	.0131
400	.008	.0135
450	.009	.0147
500	.009	.0153
600	0.010	0.0162

Table 26. Y Axis Compression Test, Specimen No. 20

Load (lbs)	Deflection (in)	Strain ( $\Delta L/L$ )
50	0.003	0.0049
100	.005	.0082
150	.007	.0101
200	.008	.0118
250	.009	.0134
300	.011	.0162
350	.012	.0177
400	.013	.0201
450	.014	.0216
500	.015	.0226
600	0.019	0.0284

Table 27. Y Axis Compression Test, Specimen No. 21

Load (lbs)	Deflection (in)	Strain ( $\Delta L/L$ )
50	0.003	0.0038
100	.005	.0075
150	.006	.0096
200	.007	.0110
250	.008	.0126
300	.009	.0137
350	.010	.0156
400	.011	.0169
450	.012	.0183
500	.012	.0189
600	0.014	0.0213

Table 28. Y Axis Compression Test, Specimen No. 22

Load (lbs)	Deflection (in)	Strain ( $\Delta L/L$ )
50	0.002	0.0031
100	.004	.0054
150	.005	.0069
200	.006	.0084
250	.006	.0096
300	.007	.0110
350	.008	.0123
400	.009	--
450	.010	.0138
500	0.012	0.0177

Table 29. Y Axis Compression Test, Specimen No. 23

Load (lbs)	Deflection (in)	Strain ( $\Delta L/L$ )
50	0.001	0.0018
100	.002	.0034
150	.003	.0048
200	.004	.0062
250	.005	.0075
300	.006	.0085
350	.006	.0093
400	.007	.0100
450	.007	.0108
500	.008	.0120
600	0.009	0.0137

Table 30. Y Axis Compression Test, Specimen No. 24

Load (lbs)	Deflection (in)	Strain ( $\Delta L/L$ )
50	0.003	0.0039
100	.004	.0062
150	.005	.0078
200	.006	.0091
250	.007	.0101
300	.007	.0112
350	.008	.0124
400	.009	.0132
450	.009	.0142
500	.010	.0149
600	0.011	0.0163

Table 31. On-Axis Shear Test

Load (lbs)	Strain ( $\mu\epsilon$ )		
	Gage #1	Gage #2	Gage #3
100	-198	15	172
200	-371	37	317
300	-587	60	466
400	-770	85	633
500	-1010	108	784
600	-1190	135	978
700	-1440	160	1138
800	-1628	184	1329
900	-1904	211	1505
1000	-2078	237	1715
1100	-2396	262	1924
1200	-2586	291	2162
1300	-2922	318	2341
1400	-3142	350	2636
1500	-3514	376	2820

Table 32. Off-Axis Shear Test

Load (lbs)	Strain ( $\mu\epsilon$ )		
	Gage #1	Gage #2	Gage #3
100	83	2	-63
200	179	6	-155
300	278	7	-238
400	378	8	-335
500	480	9	-418
600	584	9	-528
700	692	10	-612
800	798	11	-704
900	911	12	-800
1000	1018	13	-902
1100	1136	14	-1024
1200	1260	15	-1125
1300	1366	16	-1232
1400	1508	17	-1336
1500	1640	20	-1450

Table 33. Box Beam Load vs. Deflection

Load (lbs)	Position "A" Deflection (in)	Position "B" Deflection (in)
20	0.025	0.024
40	.048	.0495
60	.071	.0735
80	.092	.0965
100	.114	.120
120	--	.144
140	.157	0.167
180	0.199	--

Table 34. Box Beam Strains, Position "A"

Load (lbs)	Strain ( $\mu \epsilon$ )					
	Gage #1	Gage #3	Gage #4	Gage #5	Gage #6	Gage #8
20	-250	-334	-265	245	195	138
40	-480	-664	-524	490	370	266
60	-710	-975	-782	738	548	400
80	-950	-1278	-1042	998	730	550
100	-1185	-1570	-1300	1250	915	690
140	-1665	-2135	-1800	1762	1280	970
180	-2140	-2700	-2290	2268	1640	1250

Table 35. Box Beam Strains, Position "B"

Load (lbs)	Strain ( $\mu \epsilon$ )					
	Gage #1	Gage #3	Gage #4	Gage #5	Gage #6	Gage #8
20	272	320	278	-268	-178	-150
40	539	616	550	-520	-362	-290
60	785	895	802	-754	-538	-420
80	1035	1180	1070	-992	-718	-552
100	1295	1474	1338	-1225	-900	-690
120	1545	1764	1610	-1460	-1080	-825
140	1800	2056	1890	-1692	-1270	-962
160	2062	2352	2168	-1925	-1455	-1100
180	2320	2650	2448	-2154	-1638	-1235

Table 36. Test Specimen Dimensions

Test Specimen No.	L (in)	w (in)	t (in)
1	9.0	0.756	0.151
2	9.0	.760	.153
3	9.0	.760	.152
4	6.550	1.237	.159
5	6.542	1.235	.158
6	6.565	1.233	.158
7	6.965	.980	.154
8	6.938	.974	.157
9	6.935	.982	.162
10	6.930	.978	.159
11	6.930	.978	.156
12	7.011	1.222	.156
13	7.070	.982	.166
14	7.065	.978	.166
15	0.610	.519	.154
16	.608	.529	.157
17	.586	.532	.156
18	.636	.512	.157
19	.603	.526	.158
20	.670	.503	.157
21	.649	.475	.154
22	.651	.489	.157
23	.648	.503	.156
24	0.645	0.505	.155
On-axis Shear	5.946	3.02	.158
Off-axis Shear	6.000	3.05	0.156

COMPARISON OF A THEORETICAL ANALYSIS WITH AN  
EXPERIMENTAL STRESS ANALYSIS OF AN FRP  
THIN-WALL COMPOSITE BOX BEAM

by

CLARK TIMOTHY HARBAUGH

B.S., Kansas State University, 1972

AN ABSTRACT OF A THESIS

submitted in partial fulfillment of the  
requirements for the degree

MASTER OF SCIENCE

Department of Mechanical Engineering

KANSAS STATE UNIVERSITY  
Manhattan, Kansas

1989

## ABSTRACT

The analysis of stress and strain in box beams composed of an isotropic material is a relatively elementary exercise. However, when the box beam is fabricated from a nonisotropic composite material, the analysis is not so simple.

In this study, a thin-wall box beam and a test specimen plate were hand fabricated of a nonisotropic composite material known as fiberglass reinforced plastic (FRP). For the box beam, the primary axis of the fiberglass reinforcing material was rotated  $+10^{\circ}$  for half of the wall thickness, and  $-10^{\circ}$  for the other half of the wall thickness. The test specimen plate consisted of 16 layers of fiberglass reinforcing cloth in which each layer's X and Y axes were collinear. Both the box beam and the test specimen plate utilized a modified plain weave fiberglass material as the reinforcement and a polyester resin as the matrix.

The elastic constants of the FRP were determined experimentally utilizing test specimens cut from the test specimen plate. The elastic constants determined by tension test methods included the moduli of elasticity, poisson's ratios, and the shear moduli.

The elastic constants found by compression test methods were to be determined experimentally also, but were deemed to be invalid. The modulus of elasticity in compression was found, however, by using an equilibrium equation.

The on-axis elastic constants thus found were then transformed to off-axis constants by using the compliance method of Tsai and Hahn<sup>1</sup>. These transformed elastic constants were then used to calculate the theoretical stresses and strains in the box beam subjected to a simple load. The actual strains in the box beam were found by loading the beam, after strain gages had been installed.

Since the box beam's walls contained some irregularities, a brittle coating analysis was used to provide additional qualitative information in analyzing the strain gage data. Moreover, the effects of shear lag were evaluated with the resultant isostatic lines.

There was considerable scatter in the strain gage data, but the overall average experimentally determined strain was within 6% of the theoretical strain in three out of four comparisons (the fourth was in error by 16%). The brittle coating analysis did provide useful information for use in evaluating the experimental strain gage data. Overall, the results

indicate the importance of using experimental methods when evaluating stress and strain in a material with unknown physical properties and which may contain irregularities or other anomalies due to imprecise fabrication techniques. In spite of the problems encountered, the theoretical and experimental stress analyses were found to be in generally good agreement.

<sup>1</sup>Tsai, S.W., and Hahn, H.T., Introduction to Composite Materials, Westport, Connecticut, 1980, pp. 88-91.

VITA

Clark Timothy Harbaugh

Candidate for the Degree of

Master of Science

Thesis:       COMPARISON OF A THEORETICAL ANALYSIS WITH AN  
                  EXPERIMENTAL STRESS ANALYSIS OF AN FRP THIN-  
                  WALL COMPOSITE BOX BEAM

Major Field:   Mechanical Engineering

Biographical:

Personal Data:   Born at Great Bend, Kansas,  
                  December 11, 1947, son of Ralph R. and  
                  Virginia L. Harbaugh.

Education:       After graduation from Russell High  
                  School in Russell, Kansas, attended Fort Hays  
                  State University, and then Kansas State Uni-  
                  versity, where a Bachelor of Science in Mech-  
                  anical Engineering was received in May, 1972.

Professional Organizations:   Associate member of  
                  the American Society of Mechanical Engineers  
                  since 1972.

Professional Experience:       Have held a number of  
                  positions since 1972, the longest and most  
                  noteworthy being a contract assignment for  
                  Northern Natural Gas Company as both a  
                  project Mechanical Engineer and a Project  
                  Manager.

Professional Qualifications:   Passed the Funda-  
                  mentals of Engineering (EIT) and the Prin-  
                  ciples and Practices of Engineering (P.E.)  
                  Examinations in 1988. Became a licensed  
                  Professional Engineer in the State of Kansas,  
                  effective January 31, 1989.

